

UNIVERSIDADE FEDERAL DO ABC
PROGRAMA DE POS-GRADUAÇÃO EM NANOCIÊNCIAS E
MATERIAES AVANÇADOS

“PLATAFORMAS TRIDIMENSIONAIS COM FIBROÍNA DE
SEDA PARA A ENTREGA DE FOTOSSENSIBILIZADORES NA
TERAPIA FOTODINÂMICA”

“THREE-DIMENSIONAL PLATFORMS WITH SILK FIBROIN
FOR THE DELIVERY OF PHOTSENSITIZERS IN
PHOTODYNAMIC THERAPY”

Doutorando: Jose Eduardo Ulloa Rojas

Orientador: Wendel A. Alves

Universidade Federal do ABC

Santo André / Maio/2023

JOSE EDUARDO ULLOA ROJAS

**“PLATAFORMAS TRIDIMENSIONAIS COM FIBROÍNA DE
SEDA PARA A ENTREGA DE FOTOSSENSIBILIZADORES NA
TERAPIA FOTODINÂMICA”**

**“THREE-DIMENSIONAL PLATFORMS WITH SILK FIBROIN
FOR THE DELIVERY OF PHOTSENSITIZERS IN
PHOTODYNAMIC THERAPY”**

**Tese apresentada para o curso de pós-
graduação em nanociências e materiais
avançados da Universidade Federal do
ABC como requisito parcial para a
obtenção do título de Doutor em
nanociências e materiais avançados.**

**Orientador: Prof.Dr. Wendell Andrade
Alves**

Santo Andre

2023

Sistema de Bibliotecas da Universidade Federal do ABC
Elaborada pelo Sistema de Geração de Ficha Catalográfica da UFABC
com os dados fornecidos pelo(a) autor(a).

Ulloa Rojas, Jose Eduardo

Plataformas tridimensionais com fibroína de seda para a entrega de fotossensibilizadores na terapia fotodinâmica. Three-dimensional platforms with silk fibroin for the delivery of photosensitizers in photodynamic therapy / Jose Eduardo Ulloa Rojas. — 2023.

121 fls.

Orientador: Wendell Andrade Alves

Tese (Doutorado) — Universidade Federal do ABC, Programa de Pós-Graduação em Nanociências e Materiais Avançados, Santo André, 2023.

1. Entrega de Fármacos. 2. Microagulhas. 3. Polímeros. 4. Terapia fotodinâmica. 5. Fibroína. I. Andrade Alves, Wendell. II. Programa de Pós-Graduação em Nanociências e Materiais Avançados, 2023. III. Título.

Este exemplar foi revisado e alterado em relação à versão original, de acordo com as observações levantadas pela banca examinadora no dia da defesa, sob responsabilidade única do(a) autor(a) e com a anuência do(a) (co)orientador(a).

Santo André , 23 de Junho de 2023 .



Documento assinado digitalmente

JOSE EDUARDO ULLOA ROJAS

Data: 10/07/2023 15:33:37-0300

Verifique em <https://validar.iti.gov.br>

Nome completo e Assinatura do(a) autor(a)



Documento assinado digitalmente

WENDEL ANDRADE ALVES

Data: 04/07/2023 09:13:22-0300

Verifique em <https://validar.iti.gov.br>

Nome completo e Assinatura do(a) (co)orientador(a)



MINISTÉRIO DA EDUCAÇÃO

Fundação Universidade Federal do ABC

Avenida dos Estados, 5001 – Bairro Santa Terezinha – Santo André – SP
CEP 09210-580 - Fone: (11) 4996-0017

FOLHA DE ASSINATURAS

Assinaturas dos membros da Banca Examinadora que avaliou e aprovou a Defesa de Tese de Doutorado do candidato, JOSE EDUARDO ULLOA ROJAS realizada em 18 de Maio de 2023:

Prof.(a) ANDERSON ORZARI RIBEIRO
UNIVERSIDADE FEDERAL DO ABC



Documento assinado digitalmente
ANDERSON ORZARI RIBEIRO
Data: 19/05/2023 12:14:25-0300
Verifique em <https://validar.iti.gov.br>

Prof.(a) FABIO FURLAN FERREIRA
UNIVERSIDADE FEDERAL DO ABC

Documento assinado digitalmente
gov.br **FERNANDO CARLOS GIACOMELLI**
Data: 19/05/2023 17:54:46-0300
Verifique em <https://validar.iti.gov.br>

Prof.(a) FERNANDO CARLOS GIACOMELLI
UNIVERSIDADE FEDERAL DO ABC

Prof.(a) FRANCESCA GIUNTINI

Prof.(a) DERVAL DOS SANTOS ROSA
UNIVERSIDADE FEDERAL DO ABC

Prof.(a) HERCULANO DA SILVA MARTINHO
UNIVERSIDADE FEDERAL DO ABC

Prof.(a) MARCELA SORELLI CARNEIRO RAMOS
UNIVERSIDADE FEDERAL DO ABC

Prof.(a) WATSON LOH
UNIVERSIDADE ESTADUAL DE CAMPINAS

Documento assinado digitalmente
gov.br **WENDEL ANDRADE ALVES**
Data: 19/05/2023 11:52:09-0300
Verifique em <https://validar.iti.gov.br>

Prof.(a) WENDEL ANDRADE ALVES
UNIVERSIDADE FEDERAL DO ABC - Presidente

* Por ausência do membro titular, foi substituído pelo membro suplente descrito acima: nome completo, instituição e assinatura



Universidade Federal do ABC

"O presente trabalho foi realizado com apoio da Coordenação de Aperfeiçoamento de Pessoal de Nível Superior - Brasil (CAPES) - Código de Financiamento 001"

"This study was financed in part by the Coordenação de Aperfeiçoamento de Pessoal de Nível Superior - Brasil (CAPES) - Finance Code 001"

Dedico esta tese de doutorado aos meus amados pais, cujo amor, apoio e sacrifícios tornaram possível esta conquista. Vocês são minha fonte constante de inspiração. Com todo o meu amor e gratidão. Sem o apoio incondicional que sempre me deram, essa jornada acadêmica teria sido impossível. Vocês foram os pilares que me sustentaram durante os desafios, as longas horas de estudo e as incertezas que surgiram ao longo do caminho.

Agradecimentos

Gostaria de expressar meus sinceros agradecimentos às pessoas que foram fundamentais na orientação e apoio ao longo da minha jornada de doutorado.

Primeiramente, ao Professor Orientador Wendel Andrade Alves, que guiou meus passos e compartilhou seu profundo conhecimento. Sua orientação especializada, dedicação e paciência foram essenciais para o sucesso desta pesquisa.

Agradeço também à Francesca Giuntini, cujas contribuições valiosas ajudaram a enriquecer o conteúdo desta tese. Sua expertise e visão crítica foram de imensa importância para o desenvolvimento do trabalho.

Expresso minha gratidão à Vivian Oliveira por sua orientação e suporte contínuo. Suas sugestões e conselhos foram inestimáveis, contribuindo para aprimorar a qualidade desta tese.

Agradeço a Gabriela Nunez e a todos os que dedicarem seu tempo, conhecimento e energia para me ajudar a alcançar esse marco em minha carreira acadêmica. Sou verdadeiramente grato pela confiança, incentivo e apoio que recebi de cada um de vocês.

"Todos nós mudamos. Quando você pensa sobre isso, somos todos diferentes de quem éramos ontem. No entanto, ainda podemos nos surpreender com quem nos tornamos." - Doctor Who

"Existência Perfeita", não é mesmo? A perfeição não existe neste mundo, pode parecer clichê, mas é a verdade. Certamente, sempre haverá tolos que anseiam pela perfeição e tentam alcançá-la. No entanto, qual é o significado da perfeição? Nenhum, além disso... a perfeição me desagrada. Depois da perfeição, não há nada superior. Não há espaço para a criação, o que significa que também não há espaço para a sabedoria ou o talento. Agora você entende? Para cientistas como nós, a perfeição é "desesperante". - Mayuri Kurotsuchi

Resumo

A terapia fotodinâmica (PDT) é um tratamento médico no qual uma combinação de um medicamento fotossensibilizante e luz visível produz espécies reativas de oxigênio (ROS) altamente citotóxicas que levam à morte celular. Uma das principais desvantagens da PDT para tratamentos tópicos é a penetração limitada na pele de alguns fotossensibilizadores comumente usados nesta terapia. Nesta pesquisa, desenvolvemos hidrogéis preparados pela impressão 3D e microagulhas com concentrações variadas de fibroína de seda derivada de fibras de seda, que foram utilizados como uma matriz para incorporar moléculas fotossensíveis com o objetivo de melhorar e facilitar a entrega para a terapia fotodinâmica. Empregamos técnicas de reologia, espectrofotometria e espalhamento para analisar as propriedades dos hidrogéis e das microagulhas resultantes, a fim de elucidar os fatores subjacentes envolvidos em sua formação, bem como investigar o comportamento da fibroína de seda após a incorporação da porfirina na matriz.

Palavras chave: Microagulhas, Entrega de Farmacos, Fibroína de Seda, Fotosensibilizadores, Impressão 3D, Polímeros naturais.

Abstract

Photodynamic therapy (PDT) is a medical treatment that utilizes a photosensitizing drug and visible light to produce highly cytotoxic reactive oxygen species (ROS), leading to cell death. However, the limited skin penetration of some commonly used photosensitizers in PDT is a major drawback for topical treatments. In this study, we developed 3D hydrogels and microneedles with varying concentrations of silk fibroin derived from raw silk fibers, which served as a matrix to incorporate photosensitive molecules, aiming to improve and facilitate their delivery for photodynamic therapy. We employed rheology, spectro-photometry, and scattering techniques to analyze the properties of the resulting hydrogel and microneedle scaffolds, elucidate the underlying factors involved in their formation, and investigate the behavior of silk fibroin following the incorporation of the porphyrin into the matrix.

Key Words: Drug delivery, Microneedles, Silk Fibroin, Photosensitizer, 3-D printing, Natural Polymers.

Figure summary

Figure 1- Diagram of transdermal drug delivery methods.....	9
Figure 2-Figure Comparison of Different Techniques for 3D Printed Hydrogels. A) Extrusion-based Printing ,B) Stereolithography(SLA) ,C) Two-photon polymerization and D) Ink-jet bioprinting.....	12
Figure 3- Representation of microneedles for drug delivery of molecules through the skin layers	15
Figure 4- The scheme represents the different microneedles used for drug delivery of molecules through the skin layers.....	16
Figure 5- Scheme representing the swelling process of a polymer swelling microneedles	19
Figure 6- Schematic representation of Bombyx mori silk fibroin structure.	23
Figure 7- Different materials formats fabricated from silk fibroin	28
Figure 8- Micromolding techniques for silk fibroin microneedles fabrication.....	32
Figure 9- Silk fibroin microneedles for insulin delivery. A) Silk Fibroin microneedles; B) Insulin release from silk fibroin microneedles.	34
Figure 10-Schematic diagram of the minimally invasive glucose electrochemical biosensor based on a silk/D-sorbitol microneedle electrode and the bio catalyzed reaction cycle involved in the detection of glucose using GOD.....	35
Figure 11- Schematic of the silk fibroin extraction procedure, from raw silk fibers to silk fibroin solution.	38
Figure 12-Scaffold design for 3D printed hydrogels. The 3D scaffold will have a square form with a 10 mm length, and each filament will have a thickness of 1 mm	39
Figure 13- The 3D printing process is used to prepare the 3D scaffolds using different polymer formulations.	40
Figure 14- Schematic representation of microneedle preparation. PDMS molds were filled with the polymer solution and centrifuged to force material into the mold voids. Subsequently, the additional polymer solution was added for the robust backing and then peeled after overnight drying under ambient conditions.	44
Figure 15- Temperature ramp of gelatin (15%)/ sodium alginate (2%) and silk fibroin hydrogels for 3D printed scaffolds.....	49
Figure 16- Temperature ramp of Pluronic F127 (30%)/ sodium alginate (2%) and silk fibroin hydrogels for 3D printed scaffolds	51
Figure 17- Frequency sweep curves of gelatin (15%)/ sodium alginate (2%) and silk fibroin hydrogels for 3D printed scaffolds	52
Figure 18- Frequency sweep curves of Pluronic (30%)/ sodium alginate (2%) and silk fibroin hydrogels for 3D printed scaffolds	54
Figure 19- Gelatin (15%)/ alginate (2%) inks with different concentrations of silk fibroin printability. A) filament uniformity, B) Structure uniformity	56
Figure 20- Pluronic (30%)/ alginate (2%) inks with different concentrations of silk fibroin printability. A) filament uniformity, B) Structure uniformity	57
Figure 21- Gelatin 3D printed hydrogels with different concentrations of silk fibroin and containing two other photosensitive molecules. A) Gelatin hydrogels containing a tetra sulfonate porphyrin, B) Gelatin hydrogels containing phenalenone.....	57

Figure 22- Pluronic F127 3D printed hydrogels with different concentrations of silk fibroin and containing two other photosensitive molecules. A) Pluronic F127 hydrogels containing a tetra sulfonate porphyrin, B) Pluronic F127 hydrogels containing phenalenone	58
Figure 23- FTIR spectra of 3D scaffolds containing gelatin (15%)/ alginate (2%) and different concentrations of silk fibroin	59
Figure 24-FTIR spectra of 3D scaffolds containing Pluronic F127 (30%)/ alginate (2%) and different concentrations of silk fibroin	60
Figure 25- Gelatin (15%)/ alginate (2%) and different concentrations of silk fibroin 3D printed scaffolds SEM micrographs	61
Figure 26- Gelatin 3D printed scaffolds. A) 3D hydrogels porosity and pore diameter, B) Fiber diameter, * denotes a p-value less than 0.05.....	61
Figure 27- Pluronic F127 (30%)/ alginate (2%) and different concentrations of silk fibroin 3D printed scaffolds SEM micrographs	62
Figure 28- Pluronic 3D printed scaffolds. A) 3D hydrogels porosity and pore diameter, B) Fiber diameter, * denotes a p-value less than 0.05.....	63
Figure 29- Gelatin (15%) /Alginate (2%) 3D scaffolds containing different silk fibroin compression analysis concentrations. A) 3D scaffolds strain/stress curve. B) 3D scaffolds Young's modulus	64
Figure 30- Pluronic F127 (30%)/Alginate (2%) 3D scaffolds containing different silk fibroin compression analysis concentrations. A) 3D scaffolds strain/stress curve. B) 3D scaffolds Young's modulus.....	65
Figure 31- Gelatin (15%)/alginate (2%) hydrogels scaffolds containing different concentration of fibroin swelling a loss mass analysis, * denotes a p-value less than 0.05,**denotes p-values less than 0.01 and *** p-value less than 0.001.....	66
Figure 32- Pluronic F127 (30%)/alginate (2%) hydrogels scaffolds containing different concentrations of fibroin swelling a loss mass analysis, * denotes a p-value less than 0.05 and *** p-value less than 0.00167	
Figure 33- Total amount of a tetra sulfonate porphyrin (A) and a phenalenone (B) released from the gelatin (15%)/Alginate (2%)/ SF(6%) scaffold in PBS buffer at 0.5,1,2,3,4,5,6,7,8,24,48 and 72 hours	68
Figure 34- The total amount of a tetra sulfonate porphyrin (A) and a phenalenone (B) released from the Pluronic F127 (30%)/Alginate (2%)/ SF(6%) scaffold in PBS buffer at 0.5,1,2,3,4,5,6,7,8,24,48 and 72 hours	69
Figure 35- Physical and chemical characterizations of the microneedles obtained by mold casting and polymer solutions: (a) polymer solution viscosity studies, (b) the FTIR spectra of the microneedles, and (c) SEM micrograph images from the prepared polymer microneedles showing structures and sizes of the fibroin and PVA microneedle in different proportions: SF treated with methanol, SF, SF 7:3 PVA, SF 1:1 PVA, SF 3:7 PVA, and PVA	73
Figure 36- Silk fibroin and PVA microneedles stability and swelling analysis: (a) swelling of microneedles prepared with different proportions of silk fibroin and PVA after being submerged in PBS (pH 7.4) for 24 h at room temperature, (b) stability evaluation (mass loss) of microneedles prepared with different proportions of silk fibroin and PVA after being submerged in PBS (pH 7.4) for 24 h at room temperature, (c) the degradation ratio of SF and PVA microneedles submerged in protease XIV solution for 24 h, and (d) polymer microneedle SEM micrographs after being submerged in PBS buffer for 24 h. Data are shown as mean \pm SD, n = 3	75
Figure 37- Insertion studies of the SF and PVA microneedles: (a) DOP of the microneedles in Parafilm M as a skin model with different applied forces; data are shown as mean \pm SD, n = 10, (b) number of Parafilm M sheets performed on by the microneedles using a commercial applicator ****p < 0.0001, (c)	

2D cross-sectional OCT images to confirm the microneedle insertion, and (d) 3D OCT images to assess the pore length and area formed in Parafilm M after microneedle insertion	77
Figure 38- Mechanical property assessment of the prepared SF and PVA blend MN using a rheometer in compression mode to control the force and speed of compression or insertion: (a) the compression test using a rheometer to assess the failure forces of the prepared MN patches, (b) the insertion test to study the insertion force of the SF and PVA blend MN patches in porcine skin, (c) 2D cross-sectional OCT of microneedle arrays after their insertion in porcine skin, and (d) OCT images of the microneedle arrays for assessment of pore formation after microneedle insertion	79
Figure 39- Effect of the MNs with a variable proportion of SF and PVA on (A) HaCaT keratinocytes and (B) 3 T3-fibroblasts viabilities after an incubation period of 24 h at 37 °C. Data are shown as mean ± SD, n = 4. *p < 0.05 (unpaired t test).....	80
Figure 40- Trans-epidermal water loss (TEWL) percentages and porphyrin permeation analyses. (a) Porcine skin TEWL before and after MN treatment and porphyrin permeation in untreated and treated full-thickness pork skin. Data were expressed as mean ± SD (n = 6/formulation). Statistical differences were a, intact skin vs SF methanol or SF, and b, intact skin vs SF 7:3 PVA. **p < 0.01 and *p < 0.05. (b) Porphyrin cumulative permeation through full-thickness porcine skin after being treated with microneedle patches with different proportions of SF and PVA for 30 s. (c) Total amount of porphyrin permeated through pork skin at 24 h after being treated with microneedle patches with different proportions of SF and PVA	82

Table summary

Table 1- Silk sericin and fibroin amino acid composition.....	24
Table 2- Printing parameters for 3D hydrogels prepared with Gelatin (15%)/Alginate(2%) and Pluronic F127(30%)/ Alginate(2%) with different concentrations of silk fibroin.	39
Table 3- Coefficient of determination for the storage modulus (G'), gel strength (S), and viscoelastic exponent (n) of the hydrogels gelatin inks obtained with different concentrations of silk fibroin.....	53
Table 4- Coefficient of determination for the storage modulus (G'), gel strength (S), and viscoelastic exponent (n) of the hydrogels Pluronic inks obtained with different concentrations of silk fibroin	54
Table 5- Gelatin and Pluronic F127 3D scaffolds drug release models fit.....	70
Table 6- Pore Length and Area in Parafilm after SF and PVA MN Insertion Using a commercial Applicators at Different Pressures	77
Table 7-Porphyrin Permeation Parameters across Intact and Microneedles treated Porcine Skin	83

Abbreviations and acronyms List

Arg0: Argireline

BSA: Bovine serum albumin

CMC: carboxymethylcellulose

DOX: doxorubicin hydrochloride

FTIR: Fourier transform infrared spectroscopy

G': storage modulus

G'': release modulus

Gel-MA: methacrylamide-modified gelatin

GOD: Glucose oxidase

HA: hyaluronic acid

ICG: Indocyanine green

MNs : Microneedles

N: Viscoelastic exponent

PAA: polyacrylic acid

PDMS: polydimethylsiloxane

PDT: Photo dynamic Therapy

PEG: poly(ethylene glycol)

PLF127: Pluronic F127

PLLA: poly(L-lactic acid)

PVA: Poly vinyl alcohol

QD: Quantum Dots

RhB: Rhodamine B

ROS: Reactive oxygen species

S: Gel strength

SLA: Stereolithography

TDDS: Transdermal drug delivery systems

TEWL: Trans-epidermal water loss

SF: Silk Fibroin

SEM: Scanning electronic microscopy

TPP: Two-photon polymerization

ZnPCS4: phthalocyanine tetrasulfonic acid

Summary

1. Introduction	1
2. Literature review	4
2.1. Photodynamic Therapy	4
2.2. Transdermal drug delivery	6
2.3. Hydrogels for drug delivery	9
2.4. 3D printed hydrogel scaffolds for photodynamic therapy	11
2.5. Microneedles for drug delivery	14
2.6. Silk Fibroin	22
3. Objectives	36
3.1. General objectives	36
3.2. Specific objectives	36
3.2.1. Development of 3D hydrogels for photosensitive molecules delivery	36
3.2.2. Development of Silk Fibroin/PVA microneedles for porphyrin delivery through the skin layers	36
4. Methodology	37
4.1. Silk Fibroin solution preparation	37
4.2. Silk Fibroin 3D-printed hydrogels scaffolds	38
4.2.1. Ink preparation	38
4.2.2. 3D scaffold printing process and printability assessment	38
4.2.3. Hydrogels rheological properties	41
4.2.4. Hydrogels scaffold characterization	41
4.2.5. Swelling and degradation analyses	41
4.2.6. Compression analyses of the 3D-printed scaffolds	42
4.2.7. Photosensitizer cumulative release	42
4.3. Preparation and characterization of silk fibroin microneedles	43
4.3.1. PVA solutions preparation	43
4.3.2. Polymer Solutions Viscosity Measurements	43
4.3.3. Polymer microneedles preparation	43
4.3.4. Scanning electronic microscopy	45
4.3.5. Fourier transform infrared spectroscopy (FTIR)	45
4.3.6. Insertion Studies	45
4.3.7. Mechanical Characterization	45

4.3.8.	Dissolving and swellable capacity of modified SF MNS	46
4.3.9.	<i>In vitro</i> Cytotoxicity Evaluation of MN Patches	47
4.3.10.	Porphyrin Permeation Studies in Porcine Skin.	47
4.3.8.	Trans-Epidermal Water Loss (TEWL) for Skin Integrity Assessment.	48
4.4.	Statistical Analysis	48
5.	Results and discussion	49
5.1.	3D-printed hydrogels for photosensitizer delivery	49
5.1.2.	Hydrogels rheology analyses	49
5.1.4.	3D-printed hydrogels characterization	58
5.1.5.	Compression analysis	63
5.1.7.	Drug release analysis	67
5.2.	Silk fibroin Microneedles.....	71
5.2.1.	SF and PVA Solutions Rheological Characterization.....	71
5.2.3.	SF and PVA Microneedles Preparation and Characterization.....	71
5.2.4.	Stability Evaluation and Swelling Studies of SF and PVA Microneedles.	73
5.2.5.	Depth of Penetration (DOP)	75
5.2.6.	Mechanical Properties.....	78
5.2.7.	<i>In vitro</i> Cytotoxicity Evaluation of MN Patches	79
5.2.8.	Porphyrin Cumulative Permeation across Porcine Ear Skin Treated with MNs	81
6.	Conclusions	84
7.	References	85

1. Introduction

Photodynamic therapy (PDT) is a promising medical treatment that has gained increasing attention in recent years due to its potential to treat various medical conditions, including cancer, infections, and age-related macular degeneration (BARBUGLI *et al.*, 2015). PDT is a minimally invasive procedure that uses a photosensitizing agent and a specific light wavelength to destroy cancer and other targeted cells. This innovative therapy has several advantages over traditional cancer treatments, including fewer side effects and the ability to perform on an outpatient basis (SATRIALDI *et al.*, 2020).

Photosensitive molecules are an important compound class that has gained significant attention in photodynamic therapy (PDT). These molecules can absorb light energy and transfer it to oxygen molecules in their surroundings, generating reactive oxygen species (ROS) that can cause damage to cancerous or diseased cells (ROJAS *et al.*, 2019). PDT is a promising non-invasive therapeutic approach that utilizes these photosensitive molecules to selectively target and destroy cancerous or abnormal cells while leaving healthy tissues unharmed. As such, photosensitive molecules have emerged as promising candidates for developing new and effective cancer treatments. In this context, understanding the mechanisms and properties of these molecules is crucial to developing effective PDT strategies for a range of cancers and diseases (IOELE *et al.*, 2017).

Overall, the delivery of photosensitive molecules through the skin presents significant challenges that require careful consideration of the properties of the molecules, the formulation and delivery system, and the specific application of PDT. The skin is a highly effective barrier that protects against environmental stresses and external threats, including toxins and pathogens. Moreover, the “*stratum corneum*”, the outermost layer of the skin, has a dense and impenetrable structure that restricts the entry of molecules with high molecular weight or hydrophilic properties, limiting the penetration of therapeutic

agents, including photosensitive molecules, into the skin and deeper tissues. One of the main challenges in delivering photosensitive molecules through the skin is their hydrophobicity (ZHAO, Xueze *et al.*, 2021). These molecules are typically lipophilic, meaning they have a strong affinity for fats and oils, making it difficult for them to dissolve in water-based formulations commonly used in topical delivery systems (CHEN, Huabing *et al.*, 2014). Also, photosensitive molecules can become activated upon exposure to light, generating reactive oxygen species and potentially damaging surrounding tissues. Therefore, it is crucial to carefully control the timing and dosage of light exposure during PDT to minimize the risk of adverse effects (ABRAHAMSE; HAMBLIN, 2017). However, to enhance the solubility and penetration of photosensitive molecules into the skin, alternative delivery approaches are often required, such as micellar systems or lipid-based formulations, hydrogels, transdermal drug delivery systems, and physical or mechanical methods like microneedles, ultrasound, or electroporation (CORREIA *et al.*, 2021; KEARNEY *et al.*, 2014; LI, Yijie *et al.*, 2022).

New drug delivery routes have been recently explored to overcome the disadvantages presented by the oral parental way, one of which is the transdermal route, which consists of formulating drugs and devices capable of delivering compounds through the skin layers. Transdermal drug delivery systems (TDDS) have generated extensive interest as a preferred alternative to oral drug delivery and hypodermic injections ever since the first scopolamine transdermal patch for motion sickness was approved by the US Food and Drug Administration (WANG, Min *et al.*, 2016). The Transdermal route provides many advantages over other routes of administration. It is a non-invasive delivery system that maintains the steady plasma level of the drug level in the systemic circulation within the therapeutic window for prolonged periods. The drug remains within its therapeutic grade, avoids peaks and valleys in plasma level by providing steady blood concentration, avoids degradation of the drug in the gastrointestinal tract, eliminates the first-pass effect, and improves patient compliance and acceptability of drug therapy (INDERMUN *et al.*, 2014).

The major problem with transdermal technology is that many drugs cannot cross the skin at the required rate necessary for therapeutic action (BORA; KUMAR; BANSAL, 2008).

Enormous efforts have been focusing on developing new materials, formulations, and devices capable of improving and increasing the efficacy of transdermal drug delivery. One of the most promising devices is microneedles patches. The development of this transdermal system has allowed modern treatments to bypass the limitations traditionally associated with conventional routes mentioned (ANDRONESCU; GRUMEZESCU, 2017; RAJA et al., 2013a). Microneedle patches and 3D hydrogel scaffolds have been developed as a platform technology for delivering high molecular weight and hydrophilic compounds through the skin barrier. The first-ever study of transdermal drug delivery by microarray technology demonstrated increased skin permeability to a model compound calcine using microarray technology (HENRY et al., 1998). Since then, this technology has undergone many changes and advances to improve efficiency. For example, the types of materials used to manufacture microneedles have been diversified, using different polymers, metals, or ceramics to modify their properties such as penetration capacity, immediate and controlled delivery, as well as improvements in their mechanical properties and dimensions (BARIYA et al., 2012; RAJA et al., 2013b).

Among the most promising materials for producing microneedles and hydrogels for the delivery of drugs through the skin, we have polymers. Due to their various properties, we can simultaneously vary each of these systems' properties using one or more polymers (WANG, Qi Lei *et al.*, 2016). Recently, microneedles have been fabricated from various polymers, including biocompatible, biodegradable, and water-soluble polymers. Polymer microneedles offer the advantages of ease of fabrication, cost-effectiveness, and mass production, as well as controlled drug release by utilizing the water solubility and degradation properties of the polymer (LEE, Jeong Woo; HAN; PARK, 2013). This work aims to prepare and develop 3D-printed scaffolds and microneedle patches from natural and synthetic polymers to obtain a device capable of delivering drugs through the skin quickly and efficiently.

2. Literature review

2.1. Photodynamic Therapy

Photodynamic therapy (PDT) is an up-and-coming treatment method that is being used all over the world to treat cancer. PDT offers several advantages over traditional therapies because it is minimally invasive, selective, and can be administered to patients with multiple doses without inducing resistance or exceeding total dose limitations. This therapy combines the effects of visible light, molecular oxygen, and a photosensitizing drug to achieve therapeutic results (SHARMAN; ALLEN; VAN LIER, 1999).

Ideally, a photosensitizing agent should be a single pure compound that can undergo quality control analysis, have low manufacturing costs, and be stable in storage. When the photosensitizer is exposed to specific wavelengths of light, it becomes activated from a “ground state” to an “excited state”. The released energy from the photosensitizer can cause cell death by two mechanisms: reacting with the substrate to form radicals or directly transferring energy to oxygen to form singlet oxygen, leading to selective cell killing (KWIATKOWSKI et al., 2018).

The reactive oxygen species (ROS) formed may induce oxidative damage to cellular proteins, lipids, and nucleic acids, leading to direct tumor and vascular cell death inside the treated tumor, which further leads to an activation of an immune response. Tumor destruction from PDT can occur by both programmed (apoptotic) and non-programmed (necrosis) pathways. This is advantageous because some tumors have developed genetic mutations that eliminate or minimize apoptosis (GUNAYDIN; GEDIK; AYAN, 2021).

In 1900, Raab et al. reported the first observation of tissue sensitization by light. However, it was not until the early 1980s that the first-generation photosensitizer, an active component of hematoporphyrin derivative (HpD), was isolated and partially identified. This photosensitizer consists of porphyrin dimers and higher oligomers. While it is effective for treating various types of cancer, it has several limitations, such as skin photosensitivity and

weak absorption of long wavelengths, which limits its light penetration depth (PHAM *et al.*, 2021).

To overcome these limitations, a second generation of photosensitizers has been developed that meets several requirements. These include efficient production of singlet oxygen, high absorption coefficient in the long wavelength region, no dark toxicity, stability, selective accumulation in a target tissue, the short time interval between the administration and maximum accumulation in tissue, and rapid clearance from the body after therapy. Porphyrins, chlorins, bacteriochlorins, and phthalocyanines are the most commonly used photosensitizers for cancer treatment using photodynamic therapy. (GHORBANI *et al.*, 2018).

Third-generation photosensitizers are distinguished by attaching targeting entities or moieties such as antibodies, carbohydrates, amino acids, or peptides to second-generation photosensitizers (MFOUO-TYNGA *et al.*, 2021). These modifications are intended to improve the accumulation of photosensitizers at the targeted tumor sites and to reduce adverse effects on surrounding cells. These compounds are further developed to sustain their functionality and enhance their delivery, especially towards specific sites targeted for treatment (AIRES-FERNANDES *et al.*, 2022). Alternatively, they can be encapsulated within carriers such as liposomes, micelles, nanoparticles, hydrogels, and other transdermal drug delivery systems to improve their diffusion through the skin layers and stability.

2.2. Transdermal drug delivery

Transdermal drug delivery systems (TDDS) are defined as self-contained, discrete dosage forms that, when applied to the intact skin, deliver the drug(s) through the skin at controlled rates to the systemic circulation. Transdermal drug products are intended to provide therapeutic quantities of drugs systemically to treat or prevent disorders at locations distant from the site of topical application. They have numerous merits over conventional drug delivery systems, including avoidance of hepatic first-pass metabolism, reduction of pain, reduction in fluctuations in plasma drug levels, reduction of dosing frequency, ease of termination of therapy, and sustained release of drugs (SHABBIR *et al.*, 2018).

Although the first commercially available prescription patch that administered scopolamine for motion sickness wasn't approved until 1979 by the US Food and Drug Administration (FDA) (CAO, Shi Lei; ZHANG; JIANG, 2007; SHAOUL *et al.*, 2012), the history of skin application of therapeutic substances goes back to ancient times. Transdermal delivery, or delivery of active ingredients across the skin, was prototyped in ancient China, Greece, and Egypt through certain plasters and ointments and are the early predecessors of today's transdermal patches (*emplastra transcutanea*). These early plasters generally contained multiple ingredients of herbal drugs dispersed into an adhesive natural gum rubber base applied to backing support made of fabric or paper (PASTORE *et al.*, 2015). Numerous carriers, including conventional semisolid bases (creams, gels, ointments), matrix systems (clays, polymers), and liquid systems (solutions, emulsions, suspensions), have been used for cutaneous application of therapeutics for centuries.

The first transdermal blockbuster was the nicotine patches, raising the profile of transdermal delivery in medicine and for the public in general. There are 19 transdermal delivery systems for drugs such as estradiol, fentanyl, lidocaine, and testosterone; combination patches containing more than one drug for contraception and hormone replacement; and iontophoretic and ultrasonic delivery systems for analgesia. It is

estimated that more than one billion transdermal patches are manufactured yearly (THONG; ZHAI; MAIBACH, 2007).

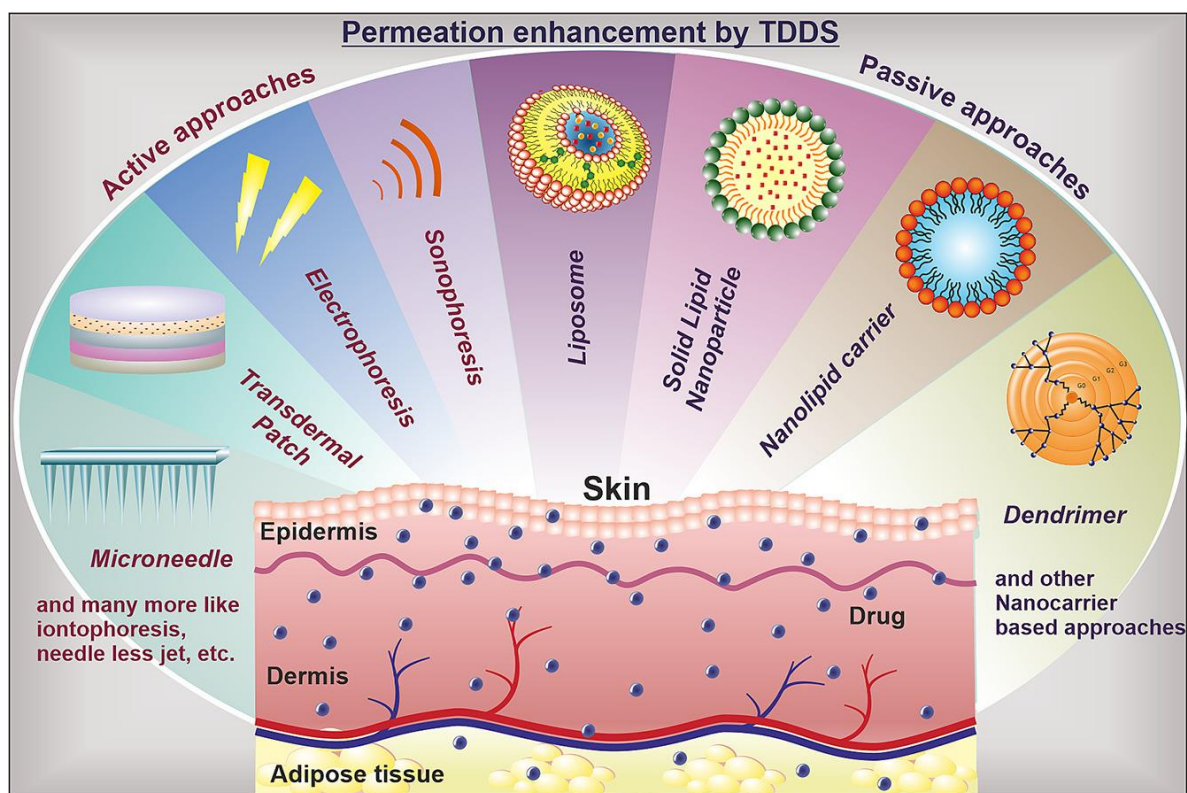
Compared to oral or systemic dosage systems, TDDS can provide a controlled release of drugs through the skin to the patient, which can reduce first-pass metabolism effects, minimize systemic side effects, improve dosage efficacy by enabling steady blood drug profiles throughout treatment, and enhance patient compliance. Transdermal delivery also has advantages over hypodermic injections, which are painful, generate dangerous medical waste, and pose the risk of disease transmission by needle reuse, especially in developing countries. These systems are noninvasive and can be self-administered. They can provide a release for extended periods (up to one week). They also improve patient compliance, and the systems are generally inexpensive. However, the greatest challenge for extensive applications of transdermal delivery is that only a limited number of drugs can be administered through this route due to the excellent barrier function of the skin, especially the stratum corneum, which is a stratified organ that prevents the invasion of external molecules, limiting the penetration of drugs (LANGER, 2008; SARAVANAKUMAR et al., 2015).

Like other lipid bilayer systems, solute transport in stratum corneum lipid bilayers is highly anisotropic and size-dependent. Specifically, lipid bilayers exhibit strong structural heterogeneity that results in spatial variations in solute partition and diffusion coefficients. As a result, molecules are believed to diffuse across skin following a tortuous pathway within either the tail-group (for hydrophobic molecules) or head-group (for hydrophilic molecules) regions, in which transport between bilayers can occur at bilayer–bilayer interfaces or other sites of structural disorganization (BARRY, 2001). Only a few drugs can passively penetrate through the skin to reach an effective concentration in the blood to treat diseases. Usually, these drugs are expected to be highly potent, lipophilic, and have a low molecular mass (<600 Da). The relatively lower permeability of the layer presents many problems in designing topical formulation. (WAGHULE et al., 2019)

Recently, numerous methods of overcoming the skin barrier to increase the efficiency of transdermal drug delivery have been developed. They can broadly be divided into two main categories: passive, active, or physical methods (PETRILLI; LOPEZ, 2018; VITORINO et al., 2014). The passive techniques involved using lipophilic carriers to increase drug permeation through the skin barrier, and chemical enhancers were used to improve this strategy. For example, metallic, organic, inorganic, and polymeric nanostructures, including dendrimers, micelles, and liposomes, are frequently considered when designing target-specific drug delivery systems for drugs with poor solubility and less absorption ability (PATRA et al., 2018). One example of passive methods is the strategies adopted to enhance the delivery of Argireline (Arg0) through the skin. Arg0 is a topical mimetic of Botox, which is effective in reducing wrinkles, with efficacies up to 48% upon four weeks of twice-daily treatment. However, the permeation of Arg0 through the skin is poor. To overcome the problem, several research groups have attempted to enhance the transdermal delivery of Arg0 by optimizing the formulations and structural modification of the amino acid side chains (LIM et al., 2018).

Active enhancement methods involve using external energy to act as a driving force and/or reduce the stratum corneum's barrier nature to enhance drug permeation. In contrast to passive methods, they are capable of delivering therapeutically active large molecular weight (> 500 Da) and also hydrophilic molecules (e.g., peptides and proteins) into and through the skin (Figure 1). Active enhancement methods can be divided into three major classes: electrical methods (iontophoresis, electroporation, radiofrequency, magnetophoresis), mechanical methods (microneedles, abrasion, skin stretching, skin puncture, and perforation), and other physical methods (laser radiation, ultrasound, thermophoresis) (DUNN et al., 2011; ZOREC et al., 2013).

Figure 1- Diagram of transdermal drug delivery methods.



Source: PHATALE *et al.*, 2022

2.3. Hydrogels for drug delivery

Hydrogels have emerged as a versatile class of materials with numerous applications in various fields due to their unique properties. They comprise hydrophilic polymer networks that can swell and retain large amounts of water or biological fluids without dissolving. The ability of hydrogels to mimic the properties of natural tissues, such as softness and biocompatibility, has led to their extensive use in biomedicine, including drug delivery, tissue engineering, and wound healing (CALÓ; KHUTORYANSKIY, 2015). Furthermore, hydrogels have also found applications in environmental sciences, such as wastewater treatment, soil remediation, and pollutant adsorption. Hydrogel scaffolds can also provide a protective environment for photosensitizers, shielding them from degradation, aggregation, and premature activation (ROJAS *et al.*, 2019). This can help maintain the photosensitizers' stability and efficacy, ensuring that they remain active until they are exposed to light during PDT treatment.

Hydrogels are also soft and flexible, which allows them to be easily manipulated and shaped into different forms, making them suitable for applications that require conformability, such as tissue engineering scaffolds (LI, Xiaomeng et al., 2018). The mechanical properties of hydrogels, such as elasticity and toughness, can be tuned by adjusting the composition and crosslinking density of the polymer network, making them highly customizable for specific applications (HO *et al.*, 2022). Additionally, hydrogels are biocompatible, meaning they are generally well-tolerated by living tissues and do not cause significant immune responses or toxicities. This biocompatibility makes hydrogels ideal for biomedical applications, such as drug delivery and tissue engineering (SAROIA *et al.*, 2018).

Hydrogels can be synthesized using various methods, including chemical crosslinking, physical entanglement, and self-assembly (MOHANKUMAR et al., 2022). Chemical crosslinking involves chemical reactions to create covalent bonds between polymer chains, resulting in a stable and permanent hydrogel network, common chemical crosslinking methods include free radical polymerization, Michael addition, and click chemistry (MADDUMA-BANDARAGE; MADIHALLY, 2021). Physical entanglement involves the use of physical interactions, such as hydrogen bonding, ionic interactions, and van der Waals forces, to hold polymer chains together, resulting in a reversible and temporary hydrogel network (PUZA et al., 2020). Physical entanglement methods include thermal gelation, pH-induced gelation, and solvent-induced gelation (WISOTZKI et al., 2017). Self-assembly involves the spontaneous organization of amphiphilic polymers into a hydrogel network through non-covalent interactions, such as hydrophobic interactions and hydrogen bonding (NORIOKA et al., 2021). Self-assembly methods include peptide-based hydrogels and supramolecular hydrogels (CHIVERS; SMITH, 2019).

Hydrogels can also be obtained from natural, synthetic polymers or a mixture. Natural hydrogels are derived from biological sources, such as proteins, polysaccharides, and extracellular matrix components. Examples of natural hydrogels include collagen, alginate, chitosan, silk fibroin, and hyaluronic acid (CALIARI; BURDICK, 2016; CATOIRA *et al.*, 2019; KUO; MA, 2001; NOGUEIRA *et al.*, 2011). Natural hydrogels are biocompatible and biodegradable and often exhibit excellent cell adhesion and tissue integration properties,

making them suitable for various biomedical applications (GYLES *et al.*, 2017; KAPUSTA *et al.*, 2023). Synthetic hydrogels are chemically synthesized from monomers using polymerization techniques, such as radical polymerization, ring-opening polymerization, or step-growth polymerization (RAPE *et al.*, 2015). Examples of synthetic hydrogels include polyacrylates, polyacrylamides, polyvinyl alcohols, and polyethylene glycols (ZHANG, Junmei *et al.*, 2019). Synthetic hydrogels offer precise control over their properties, such as mechanical strength, porosity, and degradation rate, making them highly tunable for specific applications.

2.4. 3D printed hydrogel scaffolds for photodynamic therapy

Hydrogel scaffolds fabricated using 3D printing, also known as additive manufacturing, have gained significant attention in various fields due to their unique properties and potential applications, allowing precise control over their shape, size, and internal architecture of the printed hydrogel scaffolds. Several 3D printing techniques have been employed for hydrogel scaffold fabrication, including stereolithography (SLA), extrusion-based printing, inkjet printing, and laser-assisted printing (Figure 2). These techniques differ in their principles of operation, material requirements, and fabrication resolutions, providing a wide range of options for designing hydrogel scaffolds. The image showcases a comparison of different techniques used for the 3D printing of hydrogels.

Stereolithography (SLA) is a layer-by-layer technique that uses a laser to selectively cure a liquid resin into a solid hydrogel, resulting in high-resolution structures with smooth surfaces. This technique is ideal for creating complex geometries and specific features in hydrogel scaffolds. Extrusion-based Printing shows a more porous and rough structure. Extrusion-based printing is a commonly used technique that involves the deposition of hydrogel material in a layer-by-layer using a syringe or nozzle. Inkjet printing is a droplet-based technique that uses a print head to deposit small droplets of hydrogel material onto a substrate, forming the scaffold layer by layer. This technique offers precise control over

Hydrogels have emerged as promising materials for delivering photosensitive molecules in various biomedical applications, including photodynamic therapy (PDT). The success of PDT relies on the precise delivery of photosensitizers to the targeted site and their controlled release upon activation by light (SUN, Lixin *et al.*, 2021). Hydrogels, with their tunable properties and ability to encapsulate photosensitive molecules, offer unique advantages for the efficient and controlled delivery of these molecules in PDT. For example, Pu *et al.* designed and synthesized the supramolecular gelator containing thioketal substituent, which can form injectable supramolecular gels with ROS-responsive properties. A chemo-photodynamic therapy system was developed by loading anticancer drug, doxorubicin hydrochloride (DOX), and photosensitizer, Zn(II) phthalocyanine tetrasulfonic acid (ZnPCS4) in the hydrogel structure, exhibiting excellent antitumor efficacy by a synergistic therapy (XU, Long *et al.*, 2017).

3D-printed hydrogel scaffolds for PDT can be tailored to possess specific properties to enhance their therapeutic efficacy. Also, 3D-printed hydrogels can be designed to encapsulate photosensitizers, which are crucial for PDT. The hydrogel scaffold should be able to effectively load and encapsulate photosensitizers and provide controlled release of the photosensitizers during PDT to ensure their optimal therapeutic effect (MALEKMOHAMMADI *et al.*, 2021). Some efforts have been made to design and prepare 3D-printed hydrogels containing photosensitive molecules for PDT and other applications. For example, Nisihigushi *et al.* showed an in situ 3D-printing technique based on multiphoton lithography using a biocompatible photoresist composed of protein–photosensitizer conjugates can cause singlet oxygen and cross-linking reaction to fabricate protein gels with submicrometer-scale precision. These conjugates substantially improve the cytocompatibility and the efficiency of gelation due to the stealth effect of rose bengal (RB) and the efficient transfer of singlet oxygen to bovine serum albumin (BSA) (NISHIGUCHI *et al.*, 2020).

2.5. Microneedles for drug delivery

Developing functional drug delivery systems through the skin is challenging, and specific physicochemical properties are needed in drug candidates for transdermal administration due to the resistance to drug transport offered by the stratum corneum, which can be solved by developing needles that measure a few microns and transport the active compound painlessly throughout the body, bypassing the stratum corneum (LARRAÑETA; RAGHU; SINGH, 2018). Microneedles can be defined as solid or hollow systems with an approximate length of 50 to 900 μm and an external diameter not exceeding 300 μm . Using microneedles to deliver drugs through the skin gives us a minimally invasive, simple, attractive, and commercially viable option (RZHEVSKIY et al., 2018).

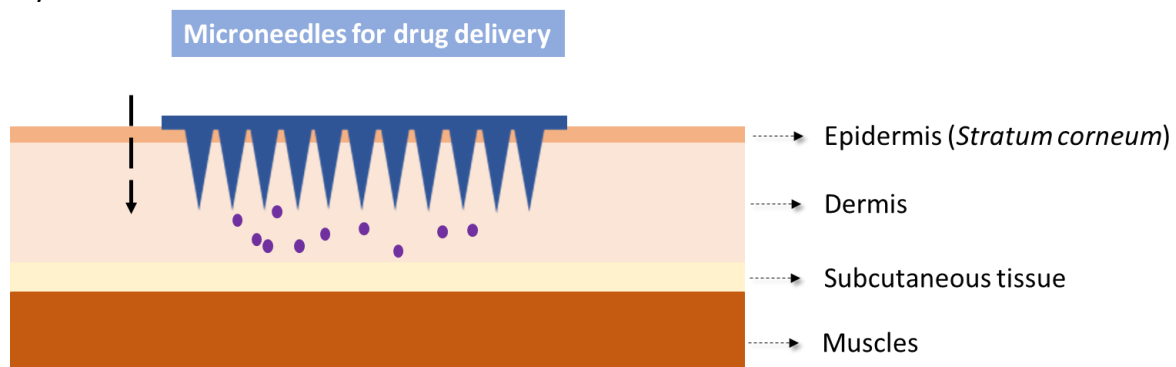
Microneedles were conceived as a means of delivering drugs through the skin for the first time around the 1970s as an alternative to intravenous drug delivery using hypodermic needles (YANG, Sixing et al., 2012). Gerstel and Martin from Alza Corporation first raised the concept of “microneedles” in 1976 to conquer the pain issue in drug administration. It was undoubtedly an extremely forward-looking sketch that laid the foundation for the initial goal of microneedle development as a solution to the pain problem. But its use in research was only possible in the 90's, when the new microfabrication processes allowed the development of these devices more cheaply and efficiently (KIM, Yeu-chun; PARK; PRAUSNITZ, 2012; LANDA, *et al.*, 2016). Thanks to the technological advances and research in microneedle technologies, MNs have been developed with various materials, for example, silicon, glass, ceramic, metal, polymers, and carbohydrates. We also have been capable of customized structure design, enabling MNs to be suitable for specific applications. Over the last decade, MNs have been extensively applied to the transdermal delivery of therapeutic compounds such as insulin, proteins, DNA, vaccines, and cells. However, in recent years, more studies have been reported to use MNs for transdermal diagnostic applications.

Microneedles represent a current paradigm in systems for administering injectable drugs, particularly in helping vaccines and molecules through the skin (DONNELLY et al.,

2014). Applying microneedle arrays to biological membranes creates transport paths of micrometer dimensions (

Figure 3). Once created, these micropores or "paths" are orders of magnitude larger than the molecular dimensions and, therefore, should allow for the transport of macromolecules easily. They can also be used for sampling body fluids (CAFFAREL-SALVADOR et al., 2015). The primary function of microneedles is to create a series of transient pores in the outermost layer of the epidermis, "*Stratum corneum*", and to allow large molecules to be permeated through it (Figure 3).

Figure 3- Representation of microneedles for drug delivery of molecules through the skin layers

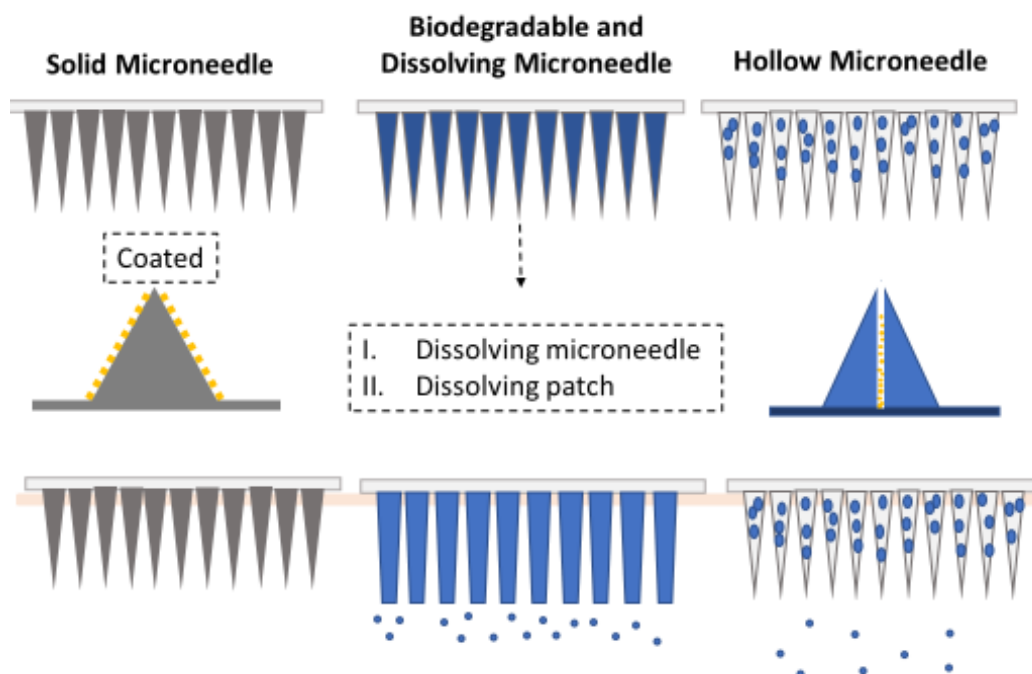


Source: The Autor

The microneedles must be long enough to pierce the "*Stratum corneum*" and short enough not to reach the capillary blood vessels and nerves. Thus the pores are generated, the medication is administered, and the drug molecules will diffuse to the underlying subcutaneous tissues and, eventually, will be absorbed and distributed systemically (ILIESCU, 2014).

Microneedles can be classified depending on the application method, material type, and structure. They can be metallic, ceramic, or polymeric (MORE; GHADGE; DHOLE, 2013). Depending on the material, the manufacturing process can also vary; for example, metallic microneedles are generally prepared by lithography and polymeric metallic positive molds and, more recently, by 3D printing (KOCHHAR et al., 2013). As for the strategies to deliver the drug through the skin, the microneedles can be classified into two large groups. Those with the drug inside their structure can be organized as hollow, soluble, and absorbent. These generally are prepared from polymers, and those with their surface are covered with a thin layer of the drug called coated microneedles, such as solid metal and polymeric microneedles (Figure 4) .

Figure 4- The scheme represents the different microneedles used for drug delivery of molecules through the skin layers



Source: Author

In the recent decade, synthetic and natural polymers have emerged as promising materials for preparing microneedles with different applications. Polymers microneedles

have advantageous properties that make them ideal for medical applications. One of these characteristics is their biocompatibility with biological systems, which prevents any undesired reaction caused by the material. Also, Polymer microneedles have the mechanical advantage of improved resistance to shear-induced breakage. Its viscoelastic property makes them strong enough to break through the *stratum corneum* skin barrier. In addition, polymer microneedles can be prepared in a reusable mold, providing an economic advantage in production(NGWULUKA et al., 2014).

Solid polymeric microneedles are prepared from biocompatible polymers and effectively generate holes through the stratum corneum. Because the drug is not encapsulated in solid microneedles, two processes are required to penetrate the skin and apply it to the medicine. It is inconvenient for users and is also susceptible to misuse. On the other hand, solid biodegradable polymer microneedles provide biological safety in case microneedle tips are broken while inserted in the skin (YANG, Sixing *et al.*, 2012). In contrast to solid polymeric MNs, biodegradable MNs are designed to dissolve into the skin, creating channels for drugs and other compounds to pass into the skin and interstitial fluid out of the skin. They can also typically be molded into the desired shape before insertion. One significant advantage of using this MN type is the biodegradable property of the material upon contact with the skin's interstitial fluid. This process allows the drug to be released from its matrix and subsequently introduced for local or systemic delivery (OGUNDELE; OKAFOR, 2017).

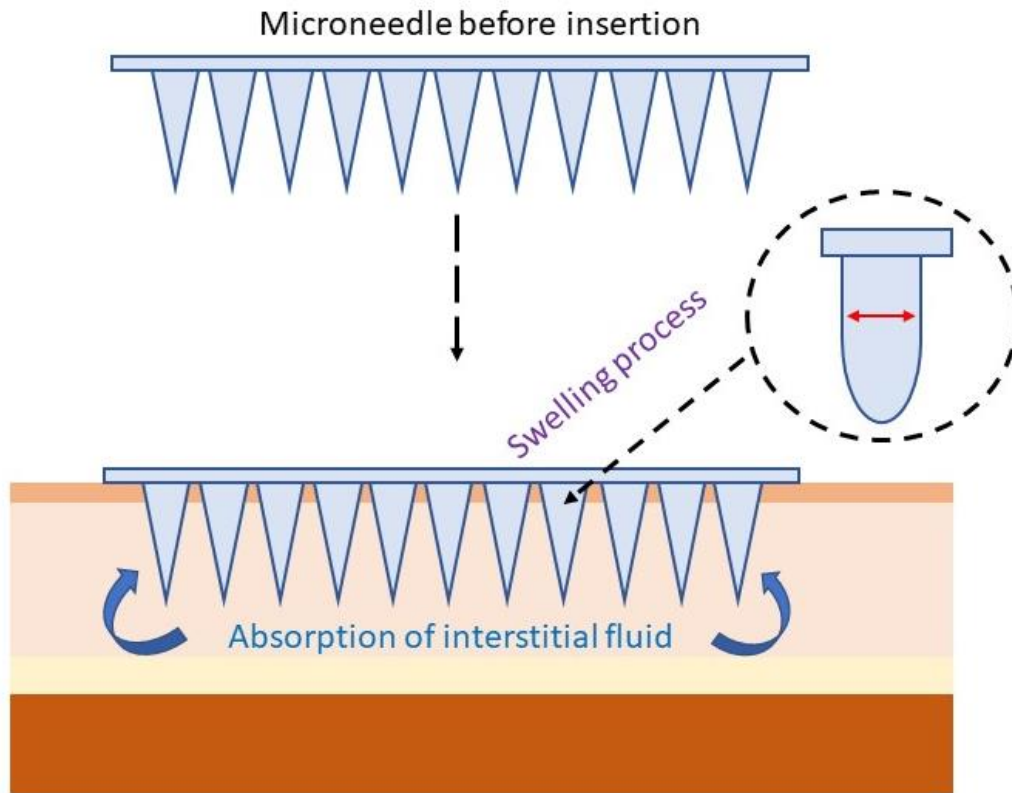
The most attractive characteristic of biodegradable polymeric MNs is to allow long-term drug-release post-skin insertion. The choice of materials is crucial, not only to fulfill various physical parameters such as mechanical strength and toughness but also for bio-friendliness – the tips of the needle will dissolve, circulate and metabolize in the human body(DILLON et al., 2017). Another type of microneedles that is often confused with biodegradable is dissolving microneedles. Usually, these two terms are interchangeable. The main difference between these two types of microneedles is that biodegradable MNs permit sustained drug release, and dissolving MNs offer a burst release profile. Dissolving MNs are often made from water-soluble polymers. The representative polymers are

hyaluronic acid (HA), carboxymethylcellulose (CMC), polyacrylic acid (PAA), PVA, PVP, sucrose, starch, trehalose, DNA, and their mixtures (CHANG, Hao et al., 2020).

Another fascinating approach is hollow microneedles, consisting of a vacant space filled with the drug dispersion or solution. They have holes at the tips. On inserted into the skin, the drug is directly deposited into the epidermis or the upper dermis layer. Mainly it is used for high molecular weight compounds such as proteins, vaccines, and oligonucleotides. These microneedles can administer a large drug dose as more drugs can be accommodated inside the needle's empty space (DU et al., 2017; VAN DER MAADEN et al., 2018).

Thanks to the advances in the formation of hydrogels and their properties for the efficient delivery of drugs, it has been possible to develop a new type of microneedles that combines the characteristics of both technologies. These are the so-called hydrogel-forming microneedles or swelling microneedles. These microneedles are prepared from polymers constituting the hydrophilic structure, making them capable of taking up a large amount of water in their three-dimensional polymeric network. These polymers swell when inserted into the skin due to interstitial fluid (Figure 5). It leads to channels between the capillary circulation and the drug patch. Before needling, these microneedles are just used to disrupt the skin barrier. On swelling, they behave as a rate-controlling membrane. Also, they have flexibility in size and shape with easy sterilization, and intact removal from the skin are unique properties (LEE, I. Chi *et al.*, 2015).

Figure 5- Scheme representing the swelling process of a polymer swelling microneedles



Source: Author

Microneedles can be widely applied in various areas of biomedicine, from drug delivery to sample collection. The application that a microneedle will have is determined by the type of material and the format in which it is made. For example, due to their beneficial properties, such as biodegradability and high ability to dissolve in water and other solvents, dissolvable polymeric microneedles are widely used to deliver drugs in a short period of minutes up to a few hours. For example, a hybrid PVP and PMVE/MA dissolving microneedle platform for transdermal delivery of a fixed-dose combination of cardiovascular drugs proved to be dissolved after 5 min of insertion into and removal from excised neonatal porcine skin (QUINN et al., 2015). Microneedles have been widely used to deliver macromolecules, such as vaccines, peptides, proteins, and hormones, including insulin, for treating diabetes organic molecules (AKHTAR, 2014). Most of the functions of MNs have emphasized the pretreatment of the skin to enhance the permeability of low molecular

weight drugs. The preparation of a pathway on the skin layer through SMN was helpful for the skin delivery of various medications to overcome the systematic barrier of the SC layer.

Regarding microneedles for macromolecule delivery, MNs have been used for transdermal gene delivery for genetic and other skin disorders. RNA therapy is a potential tool for treating skin conditions, e.g., allergies, hyperpigmentation, psoriasis, and skin cancer caused by aberrant gene expression. Yang Deng *et al.* evaluated for the first time the ability of the solid silicon microneedle array for punching holes to deliver cholesterol-modified housekeeping gene (Gapdh) siRNA to the mouse ear skin. Treating the ear with microneedles showed permeation of siRNA in the skin and could reduce Gapdh gene expression up to 66% in the skin without accumulation in the major organs. These results indicated that microneedle arrays could effectively deliver siRNA to relevant regions of the skin noninvasively (DENG *et al.*, 2016). Also, dissolvable polyethylene MNs have been used to deliver STAT3 siRNA for melanoma treatment. An *in vivo* experiment showed that MNs effectively suppressed melanoma development by silencing the STAT3 gene and the dose-dependent inhibition effect. Similarly, Lara *et al.* fabricated dissolvable PVA-PMMA MNs to inhibit CD44 gene expression through siRNA. This *in vivo* study showed that siRNA MNs could be used to treat several skin disorders by receptor inhibition (SINGH *et al.*, 2019).

Microneedle patches for transdermal drug delivery have been applied in the treatment of diseases like Alzheimer's disease, diabetes, obesity, and cancer (CHEN, Wei *et al.*, 2017; MOREIRA *et al.*, 2019). Dong *et al.* developed hyaluronic acid dissolving microneedle arrays containing the chemotherapeutic drug doxorubicin (DOX) and gold nanocages to combine chemotherapy with photothermal therapy for treating superficial tumors synergistically (YANG, Jian *et al.*, 2019). Yu *et al.* showed that a single removable transdermal patch bearing microneedles loaded with insulin and a non-degradable glucose-responsive polymeric matrix, and fabricated via *in situ* photopolymerizations, regulated blood glucose in insulin-deficient diabetic mice and minipigs (for minipigs >25 kg, glucose regulation lasted >20 h with patches of ~5 cm²). Under hyper-glycaemic conditions, phenylboronic acid units within the polymeric matrix reversibly form glucose boronate complexes owing to their increased negative charge, induce the swelling of the polymeric

matrix and weaken the electrostatic interactions between the negatively charged insulin and polymers, promoting the rapid release of insulin (YU, Jicheng *et al.*, 2020).

Regarding cancer therapies, Naguib *et al.* reported in 2014 the applicability of MNs as a 5-FU carrier for transdermal delivery across the skin layers for treating skin carcinomas. The *ex vivo* permeation experiments on mouse skin showed a 4.5-fold increased flux of 5-FU through the skin when the skin was pretreated with MNs. The *in vivo* experiments on a xenograft model using B16-F10 mouse melanoma cells had higher permeation when pretreated with MNs compared with the commercial 5-FU topical cream (5%) alone. 5-FU, proving that microneedle technologies could be used to improve the efficiency of cancer therapies (REJINOLD *et al.*, 2016).

Among the most promising microneedles applications, we deliver live-attenuated, inactivated, subunit, and virus-like particles vaccines, DNA vaccines, and antibodies (PRAUSNITZ; AVENUE; VIEW, 2009). Microneedles have been used to successfully deliver vaccines against influenza, *Clostridium difficile*, *Shigella*, measles, flavivirus, rabies, Ebola, and malaria (ERIN C. DOWD, M.D.A, MICHAEL J. FRANK, PH.D.B, ANNE COLLINS, PH.D.C, JAMES M. GOLDD, AND DEANNA M. BARCH, 2017; PEARSON *et al.*, 2015; SHIN *et al.*, 2017).

Microneedles patches have been gaining popularity in cosmetics over the past few decades. The main objectives for microneedle application in cosmetics are lie in stimulating the healing of the skin from micro-injuries created by the microneedles (skin-needling) and enhancing the skin permeation and delivery of cosmeceutical products (HAN *et al.*, 2012; HARRIS; NAIDOO; MURRELL, 2015; LANGER, 2008; YOU, Sung Kyun *et al.*, 2010). Patches, applicators, microneedles-rollers, and treatments related to the application of microneedles have been available in the market for professional or self-administration (TEO *et al.*, 2006). MN therapy for skin is also known as collagen induction therapy (CIT) or percutaneous collagen induction. Regarding the use of microneedles for enhancing the skin permeation and delivery of cosmeceutical products, molecules like collagen, bioactive compounds, hyaluronic acid, triamcinolone acetonide, and adenosine have been used. It

helps rapid recovery from skin injuries and dermatological treatments for wrinkle anti-aging and acne therapies (AVCIL *et al.*, 2020; HONG *et al.*, 2018; JANG *et al.*, 2020; LIN *et al.*, 2019).

As the research in microneedles increases, so do new areas and applications for these devices. One of these applications is microneedles as a biosensor for transdermal monitoring. Transdermal monitoring most commonly targets the ISF residing in the dermis. However, peripheral blood can also be transdermally sampled from the deeper layers of the skin, and microneedles devices can be used for ISF extraction and subsequent offline analysis or by direct transdermal monitoring using (DERVISEVIC *et al.*, 2020). Many biosensors with different properties and applications have been developed recently for detecting and monitoring various molecules such as glucose, cholesterol, ISF proteins, K⁺, ascorbic acid, lactate, H₂O₂, urea, and levodopa (GAO, Jie *et al.*, 2019; GOUD *et al.*, 2019; MILLER; NARAYAN; POLSKY, 2016; PARRILLA *et al.*, 2019; SENEL; DERVISEVIC; VOELCKER, 2019; SHARMA *et al.*, 2018).

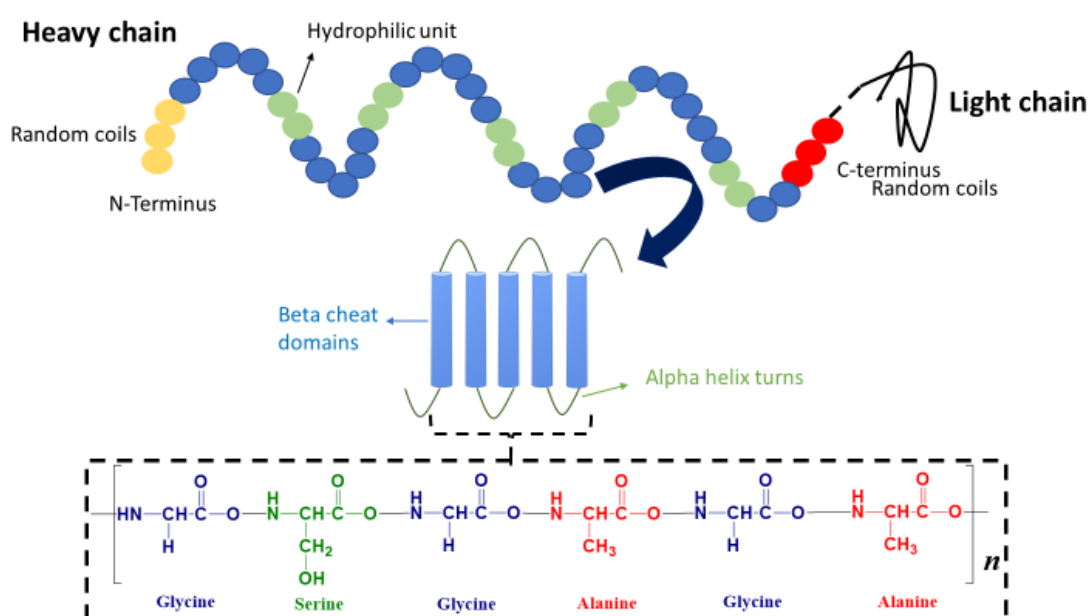
2.6. Silk Fibroin

Silk is a protein-based polymer composed of a filament core of two proteins, fibroin, and sericin, each one with a very different nature and composition. Silks are produced by members of the class Arachnida and by several worms of the order Lepidoptera, including mites, butterflies, moths, and bivalves. Silk fibrous proteins are synthesized in specialized epithelial cells lining these organisms' glands. For example, Mussel silk is obtained from bivalves such as *Pinna squamosa* and *Mytilus spp*, found in the shallow waters along the Italian and Dalmatian shores of the Adriatic (PASCHE *et al.*, 2019). These bivalves produce a strong brown filament or combed and spun into silk, popularly known as 'fish wool'. These silk threads anchor mussels in aquatic habitats helping to survive strong marine currents and resist predation (PASCHE *et al.*, 2018).

Silk fibroin comprises microfibrils, constituting 70% of the weight of silk fiber, and functions as a structural component. Silk fibroin is a block copolymer rich in hydrophobic β -sheet-forming blocks linked by small hydrophilic linker segments or spacers. The crystalline

regions primarily comprise glycine-X repeats, where X is alanine, serine, threonine, or valine. Within these domains lie subdomains rich in glycine, alanine, serine, and tyrosine. The result is a hydrophobic protein that self-assembles to form strong and resilient materials. The dominance of the β -sheet-forming regimes within the fibroin structure imparts the protein-based materials with high mechanical strength and toughness (MEINEL, L. et al., 2003) (Figure 6).

Figure 6- Schematic representation of *Bombyx mory* silk fibroin structure.



Source: Autor

Silk fibroin comprises two subunits of 370 equimolar protein (heavy chain) and 25 kDa light chain covalently linked by disulfide bonds and P25 (KIM, Hyun Ju *et al.*, 2017). The light chain is connected to the heavy chain by a single disulfide bond near the C-terminal region (KHAN; TSUKADA, 2014). The light chain has a non-repetitive sequence and only plays a marginal role in the fiber. On the contrary, the heavy chain is highly periodic, as the highly repetitive sections are composed of glycine (45%), alanine (30%), and serine (12%) in a proportion of 3: 2: 1 (FEDIČ; ŽUROVEC; SEHNAL, 2003) (Table 1). Four repetitive sequences are mainly found in the heavy-chain silk fibroin, GAGAGS, GAGAGY, and GAGAGVGY, forming hydrophobic domains, and eleven repetitive sequences

GTGSSGFGPYVA(N/H)GGYSGYEYAWSSSEDFGT forming relatively conserved hydrophilic spacers. The amino acid composition of silk fibroins may vary from species to species and differ depending on the worm species used to extract the fibroin. Some solvents explicitly used to dissolve the material may not act effectively (CHENG, Yuan et al., 2014).

Table 1- Silk sericin and fibroin amino acid composition.

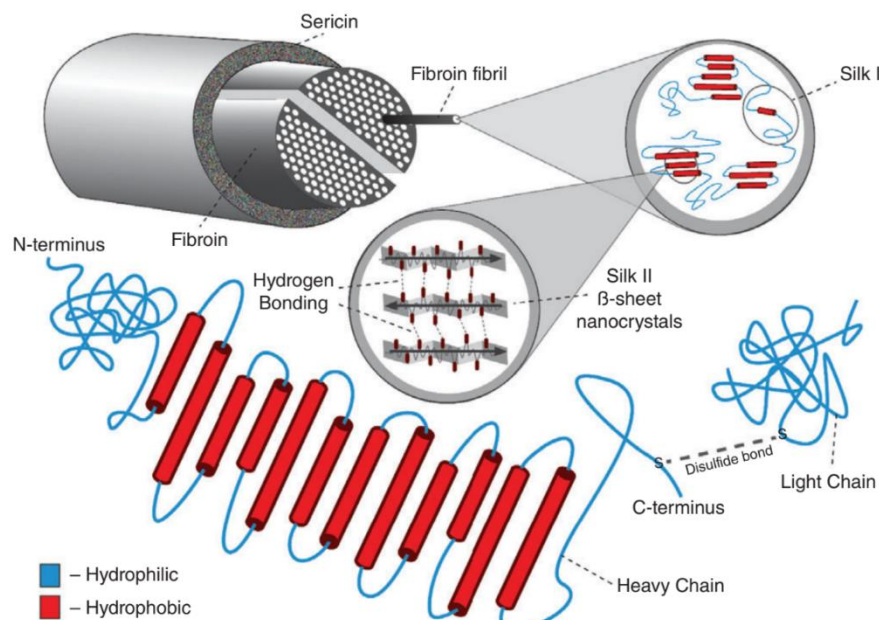
Amino acid	Type	Sericin (mol%)	Fibroin (mol%)
Alanine	Non-polar	15.2	31.6
Valine	Non-polar	3.34	2.04
Glycine	Non-polar	24.2	46.4
Leucine	Non-polar	1.99	0.22
Isoleucine	Non-polar	1.82	0.28
Methionine	Non-polar	0.11	0.00
Tyrosine	Aromatic	4.10	4.98
Phenylamine	Aromatic	0.69	0.00
Threonine	Polar	5.21	1.17
Serine	Polar	18.9	9.48
Proline	Polar	0.69	0.2
Histidine	Positive charged	0.98	0.08
Arginine	Positive charged	3.02	0.29
Lysine	Positive charged	2.07	0.58
Aspartic acid	Negatively charged	12.9	1.68
Glutaminic acid	Negatively charged	4.5	0.96

Source: Autor

The crystalline and semi-crystalline domains present two primary conformational states, an unstable glandular state called silk I (α -helix) before crystallization. They are stored in the middle silk glands after drying without external forces. Silk I is a soluble form that remains stable and not viscous up to high concentration without precipitating, presumably essential for the secretion of mature silk fibers. In contrast to liquid silk, Silk I contain random coil regions, together with regions with a well-defined ordered structure

(ASAKURA; OKUSHITA; WILLIAMSON, 2015). Conversely, Silk II can be easily defined as silk fibroin fiber after spinning. Silk II is also a mixture of crystalline and nanocrystalline domains consisting of the secondary structure of the β Silk II leaf (JIANG; ZHOU, 2011). The third polymorphism of silk has been previously reported in the literature. This third state is an air/silk interface mounted on water, called Silk III (CHENG, Yuan et al., 2014). This state might be a transitional state from Silk I to Silk II. In the spinning process, the Silk I conformation is transited to the Silk III conformation, then to the Silk II conformation (WILSON; VALLUZZI; KAPLAN, 2000) (Figure 7).

Figure 7 - Schematic representation of silk fibroin domains and molecular structure



Source: DEBARI; ABBOTT, 2019

Knowing the structure of this protein is of utmost importance since it allows preparing materials with different properties by modifying the design of the protein with metal nanoparticles, inorganic nanoparticles, organic macro and macromolecules, amino acids, chemical or physical modification, and feeding modification (LIU, Li; ZHANG; HUANG, 2019). These modifications aim to increase or modify specific molecular interactions or add other functional groups that can add or improve the already beneficial properties of silk

fibroin. For example, Gotoh *et al.* were able to attach approximately 210 poly (- ethylene glycol) (PEG) molecules (MW 104 Da) to each silk molecule using chemical coupling. It corresponds to the modification of 75% of the tyrosine residues present in SF. The addition of PEG to SF was found to promote the β -sheet formation and increase the hydrophilicity, reducing the contact angle of SF (MURPHY; KAPLAN, 2009).

Fibroin is a natural block copolymer that contains hydrophobic and hydrophilic blocks. The hydrophobic blocks create the β -sheet conformation of the fiber through hydrogen bonding between the blocks. These regions are responsible for the high fiber strength, insolubility, and fibroin's thermal stability of fibroin (BAILEY, 2013). Silks usually are insoluble in most solvents, including water, dilute acids, and alkalis. Different processes involving high temperatures and great concentrations of salts are needed to obtain silk fibroin solutions. Silk fibers exhibit high tensile strength, flexibility, and resistance to compressive forces. The excellent mechanical properties of silk fibroin make it well-suited for load-bearing biomedical applications (KUNDU et al., 2012).

One of the most fascinating and remarkable properties of the SF is its biocompatibility and biodegradability *in vivo* through enzymatic degradation, which processes the silk into harmless products that can be metabolized by the cell without causing any unwanted reaction due to the low foreign body response and inflammatory cell adhesion to fibroin (PHILIPP SEIB, 2017). The inflammatory response from degummed silk fibroin *in vitro* compared with other polymers typically used for biomedical applications, such as polystyrene and poly(2-hydroxyethyl methacrylate), showed less adhesion of immuno-competent cells. It has been demonstrated that silk films implanted *in vivo* induced a lower inflammatory response than collagen films and PLA films (MEINEL, Lorenz et al., 2005). Silk fibroin non-woven mats implanted subcutaneously in rats caused a weak foreign body response and no occurrence of fibrosis. There was minor upregulation of inflammatory pathways at the implantation site and no lymphocyte invasion after six months *in vivo* (CHARU VEPARI; DAVID L. KAPLAN, 2007).

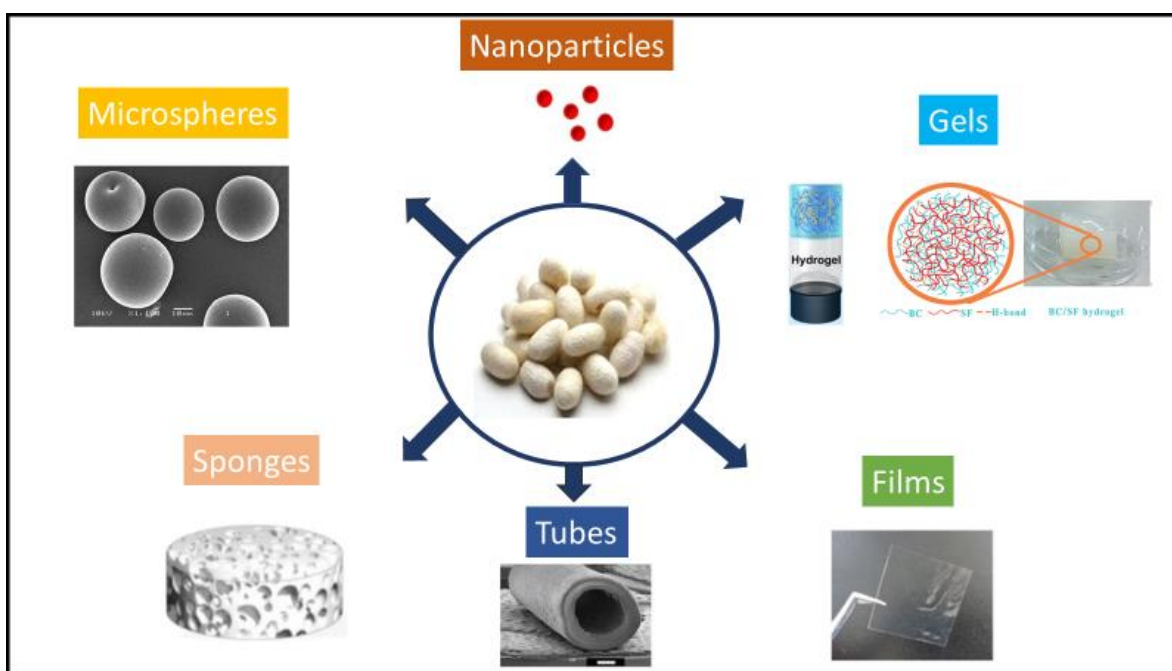
Regarding the mechanical properties of silk fibroin, it displays high tensile strength and extensibility, rendering it more rigid than almost all other natural or manufactured synthetic materials (YOU, Zhengying *et al.*, 2018). Naturally produced silk fibroin fiber from *Bombyx mori* has a high ultimate tensile strength of 300–740 MPa. It also has a considerable breaking strain and high toughness exceeding synthetic fibers such as Kevlar. Hence, the strength-to-density ratio of silk is very high, which renders silk suitable for applications that require a combination of high strength and low density. It could be attributed to the high volume of highly organized β -sheet crystallites responsible for silk's high tensile strength and modulus. The supporting amorphous bridges provide lateral strength and elasticity (PORTER; VOLLRATH, 2009). The environment can modify the mechanical properties of silk. For example, immersion of spider silk in water or methanol induces super-contraction, a specific state when fibers shrink by approximately 40–50%. The initial stiffness drops by three orders of magnitude, and the material becomes rubber-like in its behavior (JAUZEIN; COLOMBAN, 2009).

SF possesses excellent processability, and various SF-based biomaterials can be fabricated using different treatments. For the use of FS to produce biomaterials, the first step is to separate it from sericin by degumming. This step is routinely performed using a simple alkaloid, such as Na_2CO_3 or an enzyme, through a procedure called enzymatic degumming, producing silk-based biomaterials free from sericin (NULTSCH *et al.*, 2018). The degumming process is a crucial step in producing biocompatible silk for biomaterials. This knowledge comes from the historical use of silk as a material for sutures since adverse effects caused by sericin residues in silk sutures have been reported and attributed to inflammatory reactions (WRAY *et al.*, 2011). The final molecular weight, mechanical properties, and cellular function of pure silk protein depend on the degumming process, as demonstrated by Wray *et al.* in 2011, who found that exposing silk cocoons to varying degumming times affected these properties. After being degummed, fibroin can be implemented as a suture in the biomedical area, but if the objective is to develop other biomaterials such as films, hydrogels, and sponges, the fibroin must also be dissolved in water or through organic solvents (WENK; MERKLE; MEINEL, 2011). It is accomplished by

dissolving the silk fibroin in water, using a concentration of salts called “salting in” (WRAY *et al.*, 2011).

Raw and regenerated versions of SF obtained from silkworm has been widely used commercially in textile production and the biomedical field for sutures, coatings for cell culture, drug delivery matrices, and 3D scaffolds for ligament, bone, cartilage, fat, and vasculature engineering (DEBARI *et al.*, 2021) . Due to its remarkable properties, fibroin can be processed into films, sponges, hydrogels, microparticles, and many more (Figure 7) (LAWRENCE *et al.*, 2010; LIU, Qiang; LIU; FAN, 2017; SILVA *et al.*, 2016; TAVSANLI; OKAY, 2019; XU, Zongpu *et al.*, 2019).

Figure 7- Different materials formats fabricated from silk fibroin



Source: CHENG, Baochang *et al.*, 2018; KIM, Min Hee *et al.*, 2017; SRIHANAM *et al.*, 2011; TSUCHIYA; MASUNAGA; NUMATA, 2017

These materials have applications in many areas, including the textile industry, surgical sutures, tissue engineering, therapeutic agent delivery, and optical sensing. Fibroin

films have been used to coat surfaces, resulting in improved cell adhesion for anchorage-dependent cells comparable to collagen substrates. Fibroin films have also been shown to induce bone tissue growth *in vitro* when seeded with osteoblasts. Small silk fibroin fragments can increase osteoclastogenic gene expression, and DNA microarray results showed (ZAHARIA et al., 2012). The SF extracted from *Bombyx mori* has been used for the wound healing process, matrix for tissue cell growth, ligament tissue engineering applications, dental applications, nerve regeneration techniques, and others (JEON et al., 2019). SF hydrogels and films have been widely used as the substrate for the culture of animal cells in place of collagen. For example, cell culture has studied the attachment and growth of L-929 cells by using silk proteins. Films of pure component proteins exhibited a high cell attachment and development, as in collagen (JOSEPH; RAJ, 2013).

Silk fibroin can also be incorporated into other materials to increase biocompatibility and improve their properties. For example, silk nanoparticles incorporate into poly(L-lactic acid) (PLLA) to prepare composite scaffolds via a phase-inversion technique using supercritical carbon dioxide (SC-CO₂). Due to its properties, the silk nanoparticles SF nanoparticle core increased the surface roughness and hydrophilicity of the PLLA scaffolds, leading to a high affinity for albumin attachment (CHEN, Biao Qi et al., 2017). Silk fibroin has also been used to dope materials such as ceramics to improve their compressive strength and enhanced degradation for use as scaffolds for reconstructing cartilage and bone defects. Xie *et al.* evaluate the biocompatibility and safety of a ceramic composite doped with silk fibroin. The results of this study indicated that the SF/ceramic scaffold yielded better biocompatibility and safety performance than the ceramic scaffold *in vitro* and *in vivo*. Also, immunohistochemistry staining *in vivo* for OPN and OCN indicated that SF/Ceramic has the potential to promote the regeneration of critical-sized cranial defects, proving that the SF/Ceramic scaffold due to its biocompatibility serves as a potential effective bioceramic for a range of bone regeneration applications (XIE et al., 2017).

Silk hydrogels have also been widely used for delivering drugs through the skin barrier. Structural properties like crosslinking and water absorption can be modified to enhance the delivery of drugs and molecules. Wang *et al.* synthesized bacterial cellulose

(BC) and silk fibroin (SF) double-network hydrogel with high mechanical strength and biocompatibility for cartilage tissue engineering, revealing that the hydrogel, due to its highly interconnected open porous structure and improved biocompatibility with the modification of SF could be used as a cartilage repair material in a clinical application (WANG, Ke *et al.*, 2020). Silk nanoparticles and hydrogels composite materials are also excellent materials for drug delivery applications. Wu *et al.* prepared Ptx-loaded SF-NPs (Ptx- SF-NPs) and Sal-loaded SF-NPs (Sal-SF-NPs) and dispersed these drug-loaded SF-NPs system in an SF solution for gelification by ultrasound. The resulting SF hydrogel (Sal-Ptx-NP-Gel) retained its injectable properties, exhibited biodegradability, and demonstrated homogeneous drug distribution compared to the non-NP incorporated hydrogel. Sal-Ptx-NP-Gel showed superior tumor growth inhibition compared to single drug-loaded hydrogel and systemic dual drug administration in the murine hepatic carcinoma H22 subcutaneous tumor model, suggesting that SF-NPs incorporated SF hydrogel is a promising drug delivery platform (WU, Puyuan *et al.*, 2018).

Besides the applications of silk fibroin solution (SFS) and biomaterials in biomedicine regenerative medicine and drug delivery, recent work demonstrates the ability of silk films to serve as a platform for transistors and various classes of electronic and photonic devices. With its excellent mechanical, optical, and electronic properties, superior sustainability and biodegradability, and ease of fabrication, silk fibroin has emerged as an ideal material for designing and integrating high-performance flexible electronic devices for a wide range of applications (KOH *et al.*, 2018). Silk fibroin has been reinvented as a sustainable material for optics, photonics, and electronics applications. Silk fibroin has been applied to the material formats (e.g., fibers, foams, particles, films, hydrogels) (GODIYA *et al.*, 2019). The use of fibroin in optics and biosensing is particularly appealing for its biocompatibility and biostability. Fibroin has been imbued with dyes/probes or patterned to generate various optical and sensing dispositive, most notably fibroin has been developed as optical fibers, diffraction gratings, lens arrays, electrical sensors, oxygen sensors, pH sensors, glucose sensors, food sensors, etc. (KOH *et al.*, 2015). Using a similar approach, Zheng *et al.* incorporated Quantum dots (QD) into silk hydrogels for bioimaging applications. The

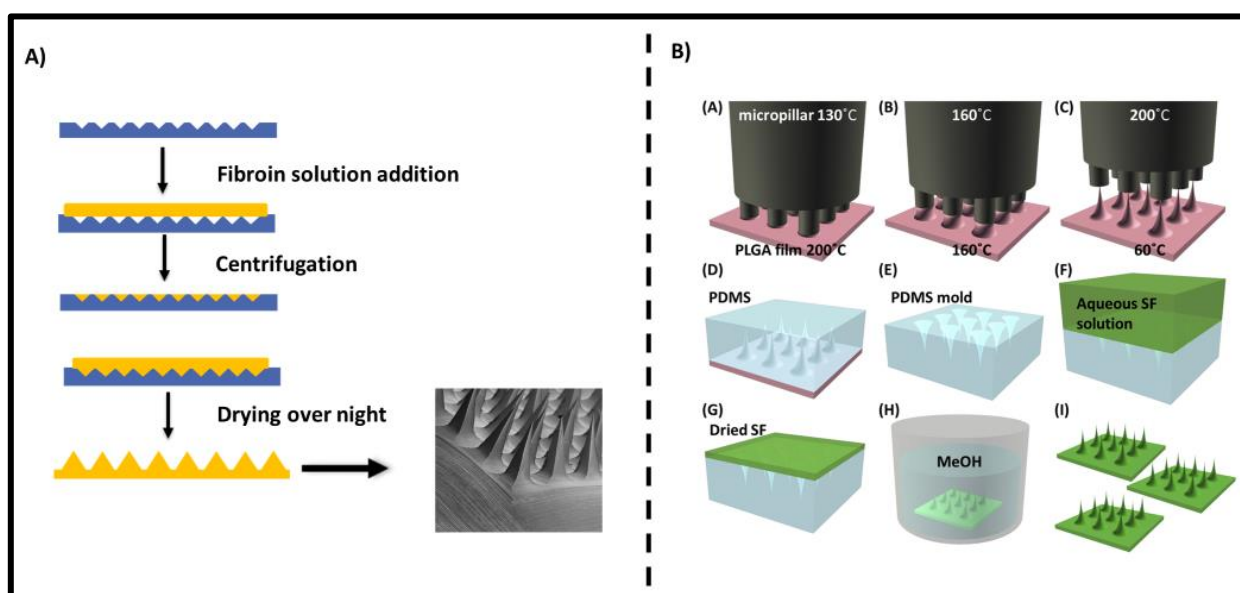
fluorescence of QD-incorporated silk hydrogels and microspheres remained stable in PBS pH 7.4 for more than four days. The amount of QDs released from the materials during incubation depended on loading. After subcutaneous injection into mice, the fluorescence of QD-incorporated silk microspheres was quenched within 24 h, similar to free QDs. In contrast, the QD-incorporated silk hydrogels fluoresced for more than four days *in vivo* (Z.Z. ZHENG, M. LI, S.Z. GUO, J.B. WU, D.S. LU, G. LI, S.S. LIU, X.Q. WANG, 2016).

The use of silk fibroin to prepare fibroin-based microneedles has been described in the literature since the beginning of this decade. You *et al.* described the manufacturing of a dissolving silk fibroin microneedle patch using a reverse polydimethylsiloxane (PDMS) mold to prepare the microneedle device. These fibroin microneedles serve as a matrix to incorporate drug molecules while maintaining drug activity. These fibroin matrix microneedles can dissolve within one minute under the skin to release the drug molecules. The dissolved fibroin in the skin generates non-inflammatory amino acid degradation products usable in cell metabolic functions. The fibroin microneedles containing methylene blue as a drug were fabricated, and their surface morphology, internal layered structure, mechanical property, and dissolving characteristics were examined. These rapidly dissolving fibroin microneedles provide more benefits than conventional syringes for painless transdermal drug delivery (YOU, Xueqiu; PAK; CHANG, 2010).

The molding method can easily prepare Silk fibroin microneedles by pouring a silk fibroin solution inside a PDMS-negative mold. The first step for silk fibroin microneedles manufacturing is to create an Al microneedle master to fabricate an elastomer-based microneedle negative mold using PDMS by using established soft lithography techniques. This soft elastomer material faithfully reproduces micron-scale features and easily detaches the silk structures, minimizing the probability of damaging the resulting devices (TSIORIS *et al.*, 2012). Another alternative to positive metal molds is the thermal drawing technique, which can be used to make high aspect ratio structures of any thermoplastic material much more easily than the micro molding technique typically used for positive mold fabrication. The shape of MN structures can be customized by simply adjusting the drawing temperatures, steps, and speeds. Since the geometry of microneedles can affect aspects

such as penetration depth, tissue healing, drug distribution, and mechanical properties, the ability to customize microneedle shapes using the thermal drawing technique is advantageous. This allows for the production of microneedles that are optimized for various tissue types and drug molecules (LEE, Ji Yong *et al.*, 2015). Lee *et al.* fabricated high aspect ratio microneedles with various body profiles by thermal drawing and replicated them multiple times onto silk fibroin MNs using micro molding, for drug delivery applications (Figure 8).

Figure 8- Micromolding techniques for silk fibroin microneedles fabrication

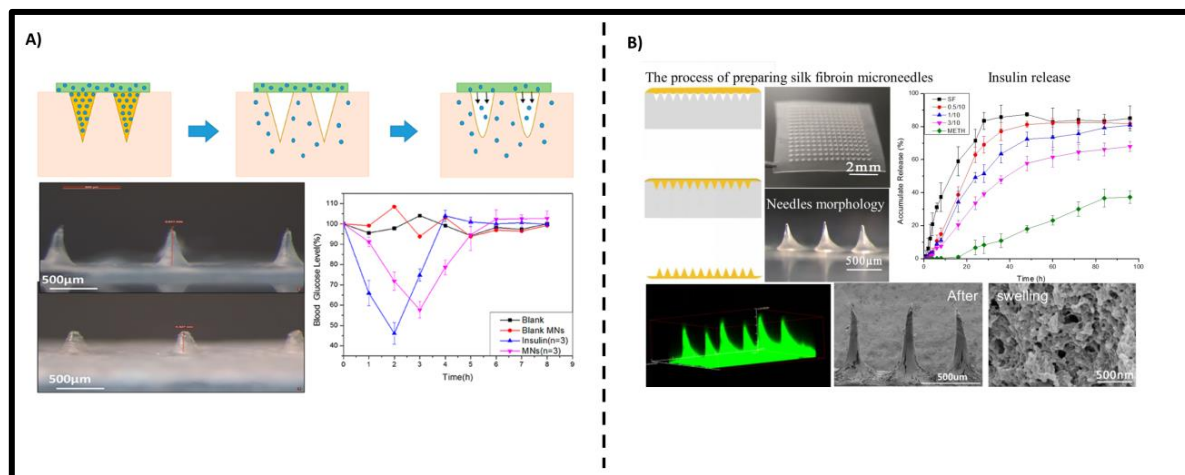


Source: Autor

Silk fibroin microneedles have been used to deliver different types of drugs through the skin layer, such as vaccines, proteins, fluorescent molecules, hormones, peptides, antigens, anti-cancer drugs, and active cosmetic agents (STINSON *et al.*, 2017). For instance, Stinson *et al.* developed a microneedle array from a silk fibroin protein solution for delivering vaccines against influenza, *Clostridium difficile*, and *Shigella*. The successful vaccination of mice against three separate antigens demonstrated that silk fibroin is well-suited for use as a solid-coated microneedle delivery system and offers long-term potential similar to that of leading microneedle biomaterials.

Fibroin microneedles have also been developed to combat and control diseases of such relevance and incidence in the world population as diabetes, a common metabolic disease characterized by high blood sugar. Long-term diabetes can cause other disorders, such as retinopathy, renal failure, neuropathy, and cardiovascular disease. Currently, insulin is the most used drug for the treatment of diabetes. Several attempts at insulin delivery using silk fibroin microneedles have been reported in the literature with successful results. Zu *et al.* fabricated a composite insulin-loaded microneedle patch with different properties at the patch's tip and base. The tip of the microneedle had suitable dissolving properties. It dissolved rapidly to promote insulin release, and the pedestal had the property of swelling without dissolving and was carrying insulin as a drug store. The insulin held by the pedestal could release continuously through the micropore channels created by the microneedles (ZHU et al., 2020). Other approaches have been taken to improve insulin-mediated delivery by fibroin microneedles. For example, adding amino acids like proline within the microneedle structure has improved the microneedle's water absorption capabilities, inducing the microneedle's secondary conformation to a Silk I-type structure. The needles have enough strength to pierce the stratum corneum of the skin. *In vitro* release experiments with insulin indicate that the release time from the microneedles is maintained up to 60 h. This delivery system may provide an easy and effective insulin intake route for treating diabetic patients(WANG, Shiyi et al., 2019)(Figure 9).

Figure 9- Silk fibroin microneedles for insulin delivery. A) Silk Fibroin microneedles; B) Insulin release from silk fibroin microneedles.



Source: WANG, Shiyi et al., 2019

It has also been possible to manufacture microneedles that not only contain fibroin but can also contain other polymers and compounds in their structure to take advantage of the properties of these compounds, such as the water absorption capacity and flexibility of PVA. For example, Gao *et al.* report the successful preparation of a novel polymeric microneedle comprising silk fibroin, poly-(ethylene glycol) diacrylate (PEGDA) primarily, and sucrose as the needle matrix. Fibroin scaffolds can instantly adsorb prepolymer solution due to capillary force and subsequently initiate the formation of microneedles via photoinduced polymerization. Based on three types of model drugs, including Rhodamine B (RhB), indocyanine green (ICG), and doxorubicin (DOX), the fabricated PEGDA/ sucrose microneedles can realize effective transdermal delivery and controllable release of therapeutic molecules by regulating the sucrose content. The presented method provides a simple strategy for quickly fabricating polymeric microneedles toward transdermal (GAO, Ya et al., 2019).

One of the least explored areas regarding the use of fibroin microneedles corresponds to the use of this type of device as a biosensor, among the only investigations that have been reported in recent years had described the use of this type of microneedle

3. Objectives

3.1. General objectives

Our project aims to use controlled release technology to develop an alternative cutaneous delivery method for active compounds. Specifically, we will use 3D-printed scaffolds made from different formulations of gelatin, alginate, Pluronic F127, and silk fibroin, as well as microneedles made from various formulations of silk fibroin and polyvinyl alcohol (PVA) to enhance the delivery of two different photosensitive molecules. The ultimate goal is to improve the effectiveness of photodynamic therapy for future applications.

3.2. Specific objectives

3.2.1. Development of 3D hydrogels for photosensitive molecules delivery

- Formulate and optimize hydrogel ink for 3D printing hydrogels, including the selection of appropriate materials, rheological properties, and printability parameters;
- Evaluate the printability of different formulations of 3D-printed hydrogels;
- Evaluate the mechanical properties of 3D-printed hydrogels, such as compression strength;
- Characterize the morphological features and microstructure of 3D-printed hydrogels and microneedles using advanced imaging techniques, such as scanning electron microscopy (SEM) and FTIR;
- Investigate the release properties of two photosensitive molecules from 3D-printed hydrogel scaffolds, including the influence of hydrogel composition.

3.2.2. Development of Silk Fibroin/PVA microneedles for porphyrin delivery through the skin layers

- Formulate and optimize silk fibroin/PVA microneedles;
- Evaluate the mechanical properties of silk fibroin/PVA microneedles, such as compression strength and insertion studies;
- Characterize the morphological features and microstructure of silk fibroin/PVA microneedles using advanced imaging techniques, such as scanning electron microscopy (SEM) and FTIR;

- Study the effect of different silk fibroin/PVA microneedle formulations on the penetration of a porphyrin across the skin layers;
- Evaluate the biocompatibility of silk fibroin/PVA microneedles using *in vitro* and *in vivo* studies;
- Propose potential applications of 3D-printed hydrogel and microneedles for photodynamic therapy.

4. Methodology

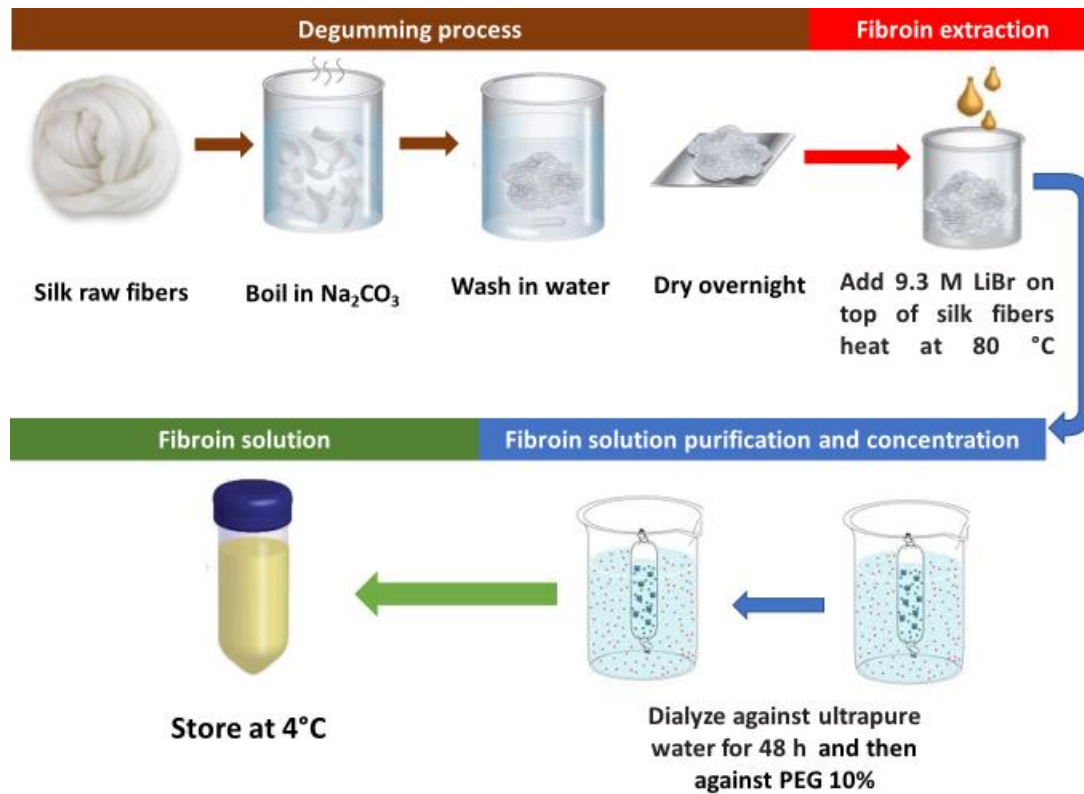
4.1. Silk Fibroin solution preparation

Fibroin from *Bombyx mori* was isolated from 10 g of raw silk and was degummed by soaking in aqueous 20 mM (1 L) Na_2CO_3 at 85°C for 60 minutes to remove the sericin from the fibers, followed by rinsing in deionized for 30. The fibers were then dried for 24 hours at 72°C. The degummed fibers were dissolved in 9.3 M aqueous LiBr solution by heating at 80°C–100°C on a hot plate with constant stirring to aid in the dispersion of the fibroin. The solutions obtained were purified by dialysis against water for 48 hours to eliminate the salts contained in the solutions and then were centrifuged to eliminate solid residues (Figure 11). Then the resulting fibroin solution was dialyzed against PEG (10%) to concentrate the solution. The fibroin concentration (70 mg/mL corresponding to 6.1% w/v) was determined by measuring the residual mass after drying at 37°C using Equation 1:

$$SFS \text{ concentration } \% = (W2 - W / W1 - W) \times 100 \quad (\text{Eq. 1})$$

where W and W1 represent the plate mass before and after adding 1 mL of silk fibroin solution, and W2 indicates the plate weight after the solution was dried at 60°C for 4 hours. The purified silk solution was stored at 4°C before use, and the solutions were stable in this condition.

Figure 11- Schematic of the silk fibroin extraction procedure, from raw silk fibers to silk fibroin solution.



Source: Adapted from ROCKWOOD et al., 2011

4.2. Silk Fibroin 3D-printed hydrogels scaffolds

4.2.1. Ink preparation

Two different bioinks were formulated using silk fibroin (7% w/v) (SF) and alginate as a base, and gelatin (15% w/v) or Pluronic® F-127 (30% w/v) were added to increase the viscosity of the inks and improve the mechanical properties of the hydrogels. To achieve 3D printed tough hydrogels, the SF/alginate mixture ink was first prepared, and then gelatin or Pluronic was added to the mixture at 40°C to keep the gelatin in a liquid state. For the SF/Alginate/Pluronic ink, the Pluronic solution was prepared at 4°C, and then the SF and alginate were added to the solution and mixed to form a uniform solution. Both inks were stored at 4°C until used.

4.2.2. 3D scaffold printing process and printability assessment

The hydrogel mixture was loaded into a 4 mL syringe and then inserted into the nozzle of a 3D printer. Alginate was prepared as the crosslinking agent. For the ink printability assessment, four different hydrogels were prepared with varying concentrations of SF (0%, 2%, 4%, 6%) to evaluate the effect of SF concentration on the printability of the 3D structures. The following parameters (Table 2) were used for the printing process.

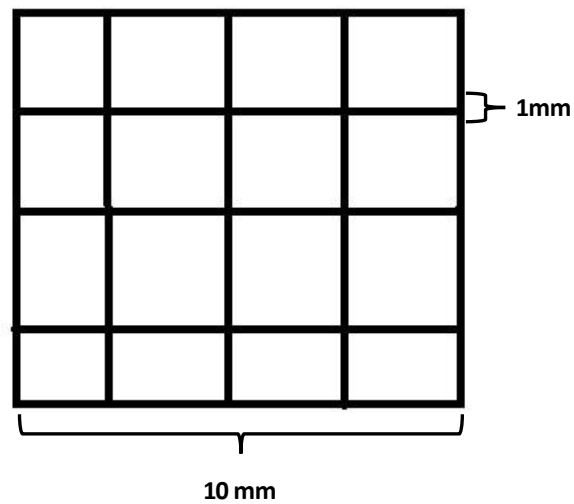
Table 2- Printing parameters for 3D hydrogels prepared with Gelatin (15%)/Alginate(2%) and Pluronic F127(30%)/ Alginate(2%) with different concentrations of silk fibroin.

Ink	Gauge (mm)	Pressure (Pa)	Speed (mm/s)	Temperature (°C)
PLF127	0.41	200	2	25
Gelatin	0.64	60-70	2	40

The design for the 3D scaffold was a square with a length of 10 mm and a filament thickness of 1 mm (

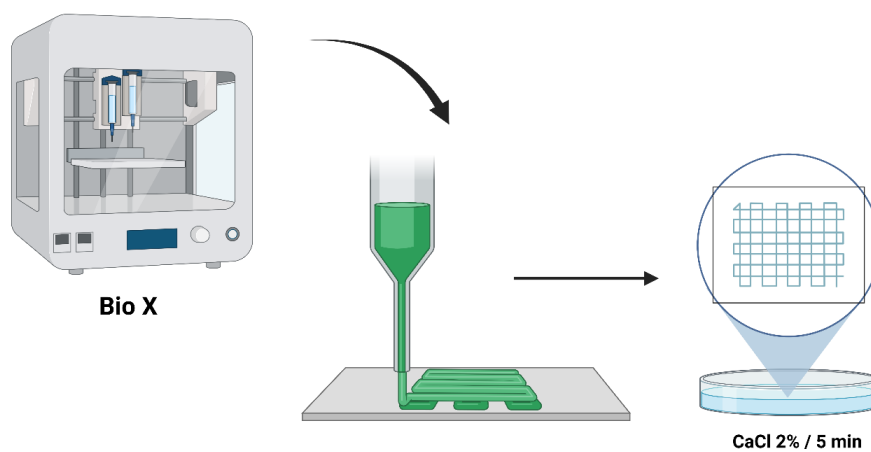
Figure 12). The square design was chosen because it is versatile and allows customization to meet specific application requirements. Additionally, the square form provides a regular and symmetrical geometry, which can result in a more uniform and consistent structure throughout the printed hydrogel. This can be advantageous in applications where precise control over shape and dimensions is important, such as tissue engineering scaffolds or drug delivery systems.

Figure 12-Scaffold design for 3D printed hydrogels. The 3D scaffold will have a square form with a 10 mm length, and each filament will have a thickness of 1 mm



For the Ink printability assessment, four different hydrogels were prepared with a variable concentration of SF (0%,2%,4%,6%) to assess the effect of SF concentration on the printability of the 3D structures After the printing was complete, the printed structure was removed from the printer and soaked in a 2% (w/v) calcium chloride solution for 5 minutes (Figure 13).

Figure 13- The 3D printing process is used to prepare the 3D scaffolds using different polymer formulations.



Source: Biorender

4.2.3. Hydrogels rheological properties

Viscoelastic properties of all hydrogels were analyzed using a controlled-stress Malvern rheometer (Ki nexus Lab +) equipped with a parallel plate geometry and a sample gap of 0.1 mm at room temperature. A constant shear stress of 1 Pa was selected to perform the frequency sweep from 0.1 to 20 Hz, and the storage(G') and loss (G'') moduli were recorded.

4.2.4. Hydrogels scaffold characterization

The FTIR spectra were recorded using a Spectrum Two FTIR spectrometer (PerkinElmer) by absorbance of the samples at 400–4000 cm^{-1} . The SEM images were acquired using an FEI Inspect F50 scanning electron microscope at John Moore Liverpool University (Liverpool, United Kingdom). Each scaffold was sputter-coated with 15 nm of gold, and the images were produced using secondary electrons, 10 kV voltage, and 4 mm spot size.

4.2.5. Swelling and degradation analyses

The stability and swelling properties of hydrogels were tested. Samples of each type of microneedle ($N = 3$ per group) were added to a PBS buffer solution (pH 7.4) and shaken in a constant temperature water bath at 37 °C for 24 h. The hydrogels were removed from the bath, rinsed with deionized water, and blotted dry with filter paper to remove surface moisture. The samples were then weighed to determine the swelling ratio (eq. 1). To calculate the degradation ratio (mass loss) (eq. 2), the samples were dried at 60°C overnight and weighed again.

$$\text{swelling ratio(Sr)} = \frac{w_1 - w}{w} \times 100\% \quad (1)$$

$$\text{degradation ratio(Dr)} = \frac{w_d - w}{w} \times 100\% \quad (2)$$

4.2.6. Compression analyses of the 3D-printed scaffolds

To understand the mechanical properties and behavior of the hydrogel under compressive forces, a compression test was performed on the printed scaffolds using a texture analyzer (TA.XTplusC Texture Analyzer, Stable Micro Systems). The compression speed was set to 0.1 mm/min with a fixed load cell capacity of 25 N. The compressive modulus of the hydrogel was calculated from the slope of the stress-strain curve in the linear region. This parameter represents the stiffness of the hydrogel under compressive forces.

4.2.7. Photosensitizer cumulative release

To evaluate the *in vitro* release profile of hydrogel formulations loaded with two different photosensitive molecules, a drug release assay was performed in phosphate-buffered saline solution (PBS) at 37°C and pH 7.4 to maintain sink conditions. At predetermined time points (0.5, 1, 2, 3, 4, 5, 6, 7, 24, 48, and 72 hours), a sample of 1 mL was taken from the PBS buffer, and an equal volume of fresh PBS buffer was replaced to maintain sink conditions. The concentration of the photosensitive molecules was assessed using a spectrophotometer (porphyrin $\lambda = 420$ nm and $\lambda = 360$ nm for the phenalenone). The resulting curves were fitted to four different drug release models to analyze the release behavior of the photosensitive molecules from the 3D-printed scaffolds.

4.3. Preparation and characterization of silk fibroin microneedles

4.3.1. PVA solutions preparation

The PVA solution was prepared by dissolving 3.5 g of PVA in 50 mL of deionized water to obtain a 7% weight/volume solution. The mixture was stirred and heated to 90 °C until a transparent gel was formed.

4.3.2. Polymer Solutions Viscosity Measurements

A rotational rheometer (Anton Paar, MCR 502) was used to analyze the viscosity of SF/PVA mixtures in different proportions (1:0, 7:3, 1:1, 3:7, and 0:1) at 25 °C. Parallel plate geometry was adopted for analysis with a 25 mm diameter and a 0.5 mm gap. The tests were carried out as a function of shear rate, ranging from 0.01 to 1000 s⁻¹.

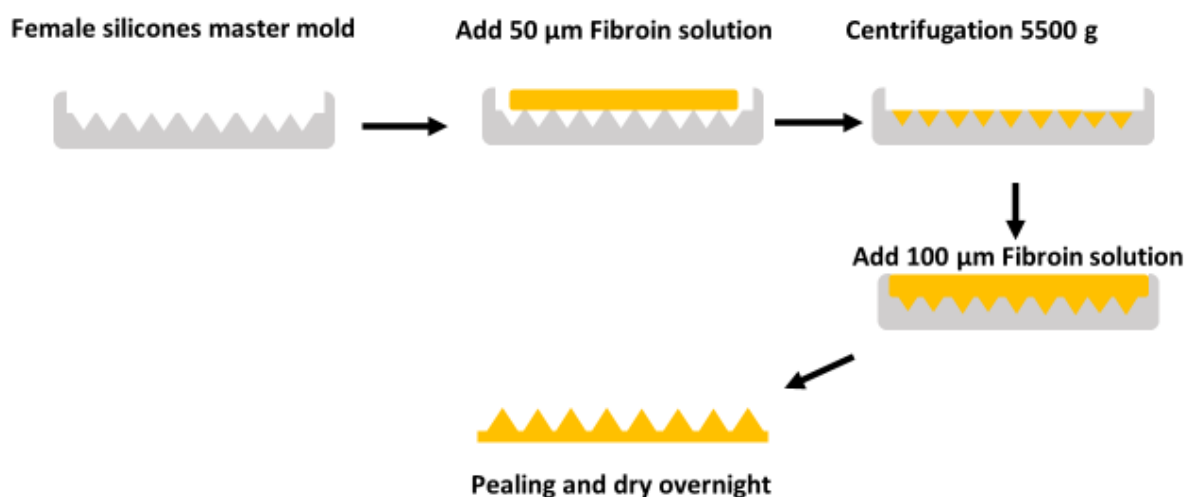
4.3.3. Polymer microneedles preparation

The process for fabricating polymer-based microneedles has been well-documented in literature. The first step involves creating molds, into which the polymer is poured and then dried to form microneedle structures. For silk microneedle fabrication in this study, negative poly-(dimethylsiloxane) (PDMS) molds (Sylgard 184, Dow Corning, Midland, MI) were used. These molds were made from pre-existing positive master molds whose creation has been previously described. The positive molds were created using computer numerical control machining to drill a chamber in a wax block, which was subsequently milled with drill bits to create an array of microneedle templates. A profile tool (Bits and Bits, Silverton, OR) was then used to smooth out any surface irregularities and create the final microneedle geometry. Epoxy (Araldite 502, Electron Microscopy Sciences, Hatfield, PA) was cast into the machined wax mold and cured for 48 hours at 80 °C. The master positive mold was then examined through SEM before undergoing further soft lithography to produce identical daughter molds. The PDMS was then poured around the master epoxy positive mold to form the negative mold from which silk microneedles were made. The final PDMS molds

had a 10 x 10 array of conical microneedles, each with the geometry of 700 μm height, 25 μm tip diameter, and 200 μm base diameter. The final microneedle array had an area of 1.5 cm by 1.5 cm.

To prepare the silk fibroin microneedles, 50 μL of prepared silk fibroin solution (~ 7 w/v%) was pipetted into the PDMS molds and centrifuged at 5,000 rpm for 20 minutes at 4 $^{\circ}\text{C}$ to force the solution into the needle cavities and eliminate any trapped air. After centrifugation, any remaining bubbles were removed with a pipet, and the mold trenches were filled with silk solution (total volume ~ 50 μL). Once 100 μL was added to the mold, the filled molds were left to dry under ambient temperature and humidity conditions for 24 hours. The dried silk microneedle devices were then removed from the molds and placed in a vacuum chamber to undergo water-vapor annealing for 24 hours at ambient temperature (as shown in Figure 14).

Figure 14- Schematic representation of microneedle preparation. PDMS molds were filled with the polymer solution and centrifuged to force material into the mold voids. Subsequently, the additional polymer solution was added for the robust backing and then peeled after overnight drying under ambient conditions.



Source: Autor

Microneedles were prepared using the method described above with different ratios of silk fibroin (7%) and PVA (7%) (SF, SF 7:3 PVA, SF 1:1 PVA, SF 3:7 PVA, PVA), as well as silk fibroin treated with methanol (90%) for 60 s.

4.3.4. Scanning electronic microscopy

Image acquisition was performed using an FEI Inspect F50 scanning electron microscope at the LNNano, Brazilian Nanotechnology National Laboratory (CNPEM, Campinas, Brazil). The images were produced using secondary electrons, a 5-kV voltage, a 3–3.5 mm spot size, a 10–12 mm working distance, and gold coating. For metallization, 60 seconds of deposition and 40 mA currents were used. The images were analyzed using the ImageJ program to measure fiber diameters. The porosity and fiber diameter of the hydrogels was analyzed using image J.

4.3.5. Fourier transform infrared spectroscopy (FTIR)

The fibroin MNs' internal structures were analyzed using Fourier transform infrared spectroscopy (FT-IR). Infrared spectra of hydrogels were obtained using Spectrum 1000 (PerkinElmer) spectrometer in the range of 400-4000 cm^{-1} .

4.3.6. Insertion Studies

Parafilm M (Bemis Company Inc., Soignies, Belgium) was used as a previously validated model system to determine the insertion properties of the microneedle arrays.⁴⁰ The microneedle arrangements were inserted into the Parafilm M sheet folded into an eight-layer film using different applying forces (10, 20, 30, and 40 N) using a commercial applicator (μ PRAX Micro solutions, Delft, the Netherlands) and removed after 30 s.

4.3.7. Mechanical Characterization

The mechanical properties of pure fibroin microneedles, methanol-treated insoluble fibroin microneedles, and PVA/fibroin composite microneedles were evaluated using an Anton Paar MCR 502 rheometer in compression mode with varying loading capacities, utilizing a 25 mm parallel plate geometry. To determine the microneedles' failure force, a microneedle array was secured to the test platform, and the geometry was set to move vertically against the needles at a rate of 0.035 mm/s until failure/fracture occurred. To measure the force required to penetrate full-thickness porcine skin, a porcine skin sample was fixed to the lower plate, and the microneedle was secured to the geometry, which moved vertically against the skin. The plate was set to move at a constant speed of 0.035 mm/s until the microneedle punctured the skin.

4.3.8. Dissolving and swellable capacity of modified SF MNS

To obtain the SF MNS with consistent and controllable transdermal delivery capacities, insolubility and swell ability characteristics within interstitial fluid after administration is essential. The modified SF MNS was immersed in PBS (pH 7.4) to evaluate its dissolving and swelling characteristics. The morphological dimensions of SF MNS before and after swelling were monitored by stereomicroscope and SEM. Dried SF microneedles weighed as m1 (0.1 g) were swollen in 10 mL PBS for 24 h at 37 °C and bath ratio of 1:100 (w/v), four parallel samples in each group. The percentage swelling and dissolving were calculated, respectively, by using the following Eqs (2) and (3):

$$(2) \quad \text{Swelling \%} = \frac{W_1 - W}{W} * 100$$

$$(3) \quad \text{Mass loss \%} = \frac{W_d - W}{W} * 100$$

where w is the initial dry mass of the needles, w_d is the mass of the needles after swelling, and w_d is the weight of the microneedle after drying overnight at 60 °C.

4.3.9. *In vitro* Cytotoxicity Evaluation of MN Patches

Microneedles for human or animal use must demonstrate low cytotoxicity or cytotoxicity compatible with the proposed final field of application. The SF and PVA microneedles were evaluated by MTT assay on HaCaT and 3 T3 cells. Cells were plated and incubated in a complete DMEM culture medium for 24 h at 37 °C with 5% CO₂. Then, the microneedles were immersed in the cell-containing medium for 24 h. The medium was then replaced with a solution of MTT (0.5 mg/mL) in DMEM. After 4 h, the supernatant was removed, DMSO was added (200 µL), and the sample was gently shaken for 15 min to allow the dissolution of formazan crystals. Optical absorbance was measured using a microplate reader (SPARK 10 M, TECAN) at 570 nm. The cell viability was calculated according to the following equation (4):

(4)

$$Cell\ viability = \frac{untreated\ cells\ (OD) - treated\ cells\ (OD)}{Treated\ cells\ (OD)} \times 100\%$$

To evaluate the potential inflammatory effects of microneedle formulations, IL1-β and TNF-α cytokine concentrations were determined in the 3 T3-fibroblasts cells medium by using commercially available kits (mouse IL1-β/IL-1F2 and TNF-α DuoSet ELISA, R&D systems, Techne Corporation, Minneapolis, MN, USA).

4.3.10. Porphyrin Permeation Studies in Porcine Skin

For ex vivo permeation tests, porcine ears were obtained from a slaughterhouse certified by the Federal Inspection Service (SIF N° 1762). All experiments were approved by the Ethics Committee on Animal Use of the Brazilian Federal University of ABC (CEUA/UFABC N° 2,693,041,219). Full-thickness skin was used for all the experiments, with

an approximate thickness of 850 μm measured by OCT. The outer part of the skin of the ear was separated from the cartilage; blood vessels and subcutaneous tissues were also removed. The skin samples were frozen until use and stored for 3 months. The *ex vivo* permeation tests were carried out in a vertical diffusion Franz cell presenting two compartments, donor (0.6 cm^2 permeation area) and receptor compartments filled with 4.5 mL of phosphate buffer (pH 7.4). The skin samples were thawed in PBS for 30 min, cut into small pieces, and treated with the microneedle patches before being fixed to the Franz-type diffusion cell between the donor and receptor compartments. Aliquots (1 mL) from the receptor compartment were withdrawn and analyzed by UV/vis spectrophotometry ($\lambda = 420 \text{ nm}$). The cumulative amounts of permeated porphyrin (5-[4-(2-carboxyethanoyl) aminophenyl]-10,15,20-tris-(4-sulphonatophenyl) porphyrin trisodium) were expressed as $\mu\text{g cm}^{-2}$, and the results were plotted as a function of time (h). Flux values were determined from linear regression in the interval from 4 to 6 h, following the equation (eq5):

$$(5) \quad J = P * C_d$$

where J is the drug flux across the skin, and C_d is the drug concentration in the donor compartment.

4.3.8. Trans-Epidermal Water Loss (TEWL) for Skin Integrity Assessment.

After treatment with MNs, the barrier function of porcine skin was examined as trans-epidermal water loss (TEWL) using a VapoMeter (Delfin Technologies Ltd., Kuopio, Finland). A commercial applicator applied microneedle samples to intact porcine skin for 30 s (N = 3 per MN type). After the application, the TEWL was measured. After the application, the TEWL was measured at least three times for each skin sample.

4.4. Statistical Analysis

The data were presented as means \pm S.D. of three independent experiments performed in triplicate. A standard significance level of $p < 0.05$ was used. The analyses were performed with GraphPad Prism 7.0 software (GraphPad Software, Inc., La Jolla, CA, USA) or Origin (Pro) (Version Number 2019, OriginLab Corporation, Northampton, MA, USA).

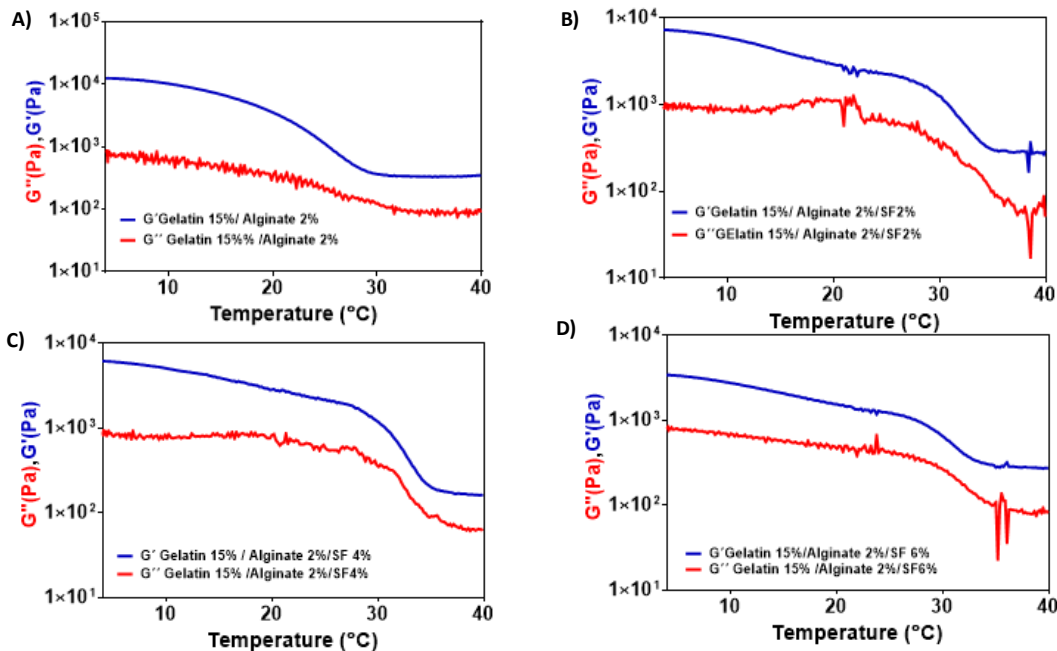
5. Results and discussion

5.1. 3D-printed hydrogels for photosensitizer delivery

5.1.2. Hydrogels rheology analyses

The viscoelastic properties of the resulting hydrogels were assessed by oscillatory rheology. First, we performed a temperature ramp to analyze the behavior of the inks through different temperatures. The rheological properties of gelatin and plutonic, including its gelation behavior, are influenced by various factors, such as concentration, pH, and temperature (GIOFFREDI et al., 2016). As it is possible to observe in Figure 15, gelatin is typically in a solid, glassy state at low temperatures, whereas at high temperatures, it is a viscous liquid. The temperature range between these two states is the gelation range, where the gelatin transforms from a liquid to a gel (KOKOL et al., 2021). For the temperature-sensitive gelatine used in 3D printing, the relationships between printing parameters and hydrogel consistency are critical and contribute to the gel's strength rate during printing, as well as the resolution and shape fidelity of the scaffold after printing (DONDERWINKEL; VAN HEST; CAMERON, 2017).

Figure 15- Temperature ramp of gelatin (15%)/ sodium alginate (2%) and silk fibroin hydrogels for 3D printed scaffolds

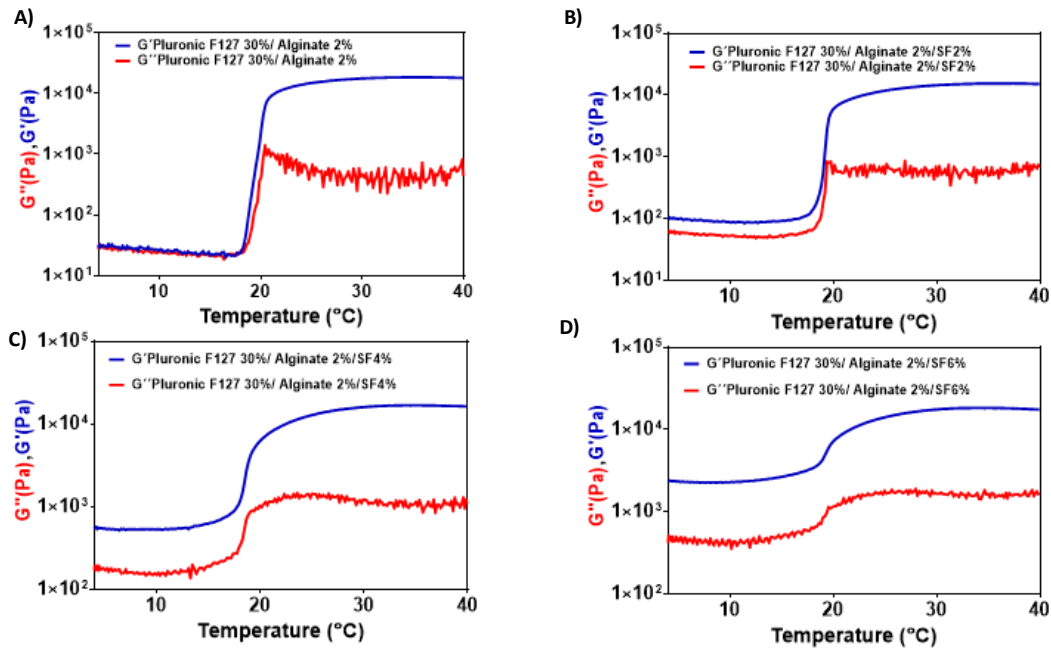


We can also observe the opposite behavior in the inks containing pluronic F127 (Figure 16). Pluronic F127 is a triblock copolymer composed of poly(ethylene oxide) (PEO) and poly(propylene oxide) (PPO) segments. Its behavior can vary depending on the temperature due to changes in the polymer structure and interactions between the polymer and the surrounding environment. Pluronic F127 can form a gel-like structure at high temperatures due to the aggregation of the PPO segments. This gel structure is thermally reversible, which can liquefy upon cooling and reform upon heating. Pluronic F127 exhibits thermogelling behavior at 20–30 °C *via* a micelle packing mechanism forming a physical crosslinking network that traps water and other components in a gel-like structure (DOU; ABDUL KARIM; LOH, 2016).

As the temperature increases, we can see the transition from a liquid-like structure to a gel-like one. This transition is often referred to as the sol-gel transition. The sol-gel transition temperature can be affected by factors such as polymer concentration, molecular weight, and the presence of other compounds in the surrounding environment (CHATTERJEE et al., 2019). Generally, the gelation temperature of Pluronic F127 is around 20-25°C at a concentration of 20% w/w in water. However, the gelation temperature can be adjusted by changing the concentration of Pluronic F127 as we can observe for a spot of

ink with 30% of pluronic F127. For example, at a concentration of 30% w/w in water, the gelation temperature may be around 10-20°C (SHRIKY et al., 2020).

Figure 16- Temperature ramp of Pluronic F127 (30%)/ sodium alginate (2%) and silk fibroin hydrogels for 3D printed scaffolds



Regarding the frequency sweep analysis, the resulting oscillatory rheology frequency sweep curves typically display two key parameters: storage modulus (G') and loss modulus (G''), which are plotted as a function of frequency. The storage modulus (G') represents the elastic or solid-like component of the material's response. In contrast, the loss modulus (G'') represents the viscous or liquid-like component of the material's response (RUBIO-HERNÁNDEZ et al., 2013). The shape of the oscillatory rheology frequency sweep curve can provide insight into the structural and dynamic properties of the material. For example, a material with a high crossover frequency and a broad plateau region in the G' curve indicates a highly crosslinked and structured material. In contrast, a material with a low crossover frequency and a steep slope in the G' curve shows a more liquid-like material.

Figure 17 shows the behavior of the gelatin (15%)/Alginate (2%) inks with different concentrations of silk fibroin at different shear rates. The inks present a shear thickening behavior, a non-Newtonian fluid behavior characterized by increased viscosity with increasing shear rate. In contrast to Newtonian fluids, which have a constant viscosity regardless of the shear rate, shear-thickening fluids exhibit a shear-dependent viscosity (KOKOL et al., 2021). Also, it is possible to observe that in all the inks G' value it is higher than the G'' value meaning that all the gelatin inks form hydrogel structures and that this value decreases every time we increase the silk fibroin concentration (SF). The n and S parameters yield a quantitative estimation of the strength of the hydrogel structures that can be related to the crosslinking density within the polymer network. With increasing concentrations of SF in the hydrogels, we observed decreasing values for G' and S and low n exponent values (Table 3), indicating a decreasing crosslinking density, resulting in weaker gel structures.

Figure 17- Frequency sweep curves of gelatin (15%)/ sodium alginate (2%) and silk fibroin hydrogels for 3D printed scaffolds

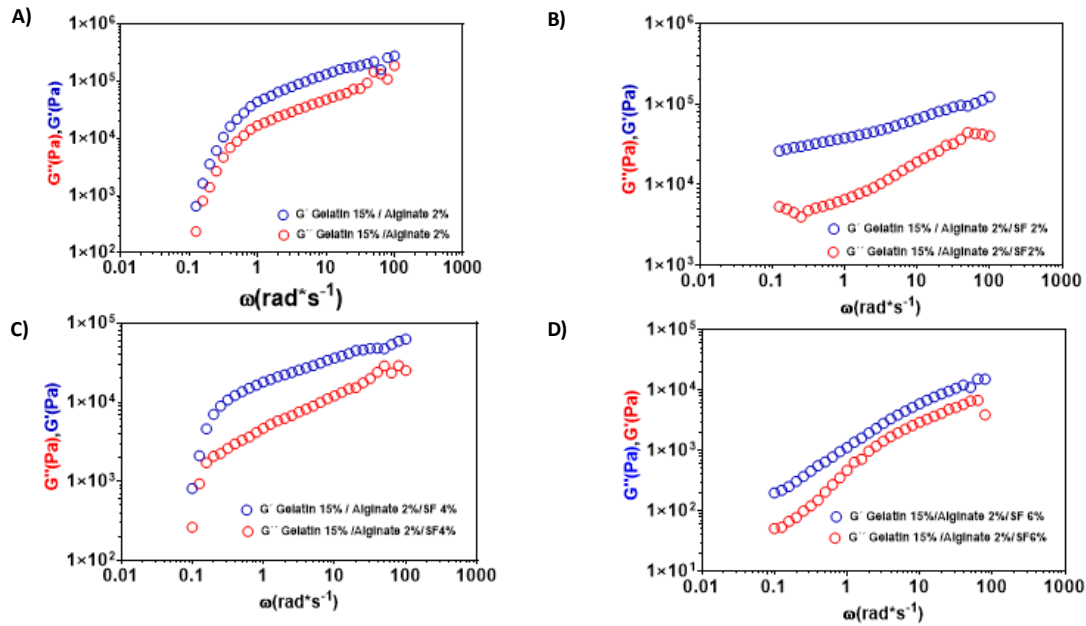


Table 3- Coefficient of determination for the storage modulus (G'), gel strength (S), and viscoelastic exponent (n) of the hydrogels gelatin inks obtained with different concentrations of silk fibroin.

SF concentration	G' (mPa)	S	n
SF0	95630.553±15118.926	47943.867 ± 2800.968	0.396 ± 0.016
SF2	57328.709±5219.963	37794.136 ± 681.604	0.249 ± 0.005
SF4	28097.709±3140.240	17305.525 ± 714.785	0.286 ± 0.012
SF6	4535.670±858.293	1655.061 ± 114.630	0.523 ± 0.018

Regarding the Pluronic F127 hydrogel's behavior under different frequencies (Figure 18 and Table 4), when subjected to a frequency sweep test, Pluronic 127 typically exhibits viscoelastic behavior. At low frequencies, the material behaves as a viscous liquid and shows little resistance to deformation. As the frequency increases, the material behaves more like an elastic solid and exhibits greater resistance to deformation (ROJAS et al., 2019; YEH et al., 2017). Observe the plateau formation for the frequencies used in this study, indicating that the inks' modulus was independent of the frequency variation. Also, we observed an increase in the G' of the hydrogels with higher SF concentrations. This indicated the formation of more elastic and crosslinked structures. Overall, the rheological behavior of silk fibroin and Pluronic hydrogels can be modulated by controlling the concentration, cross-linking density, and other factors such as pH and temperature. Understanding the rheological behavior of these hydrogels can help design and optimize their performance for various applications such as drug delivery, tissue engineering, and wound healing (LI, Qingtao et al., 2021; YOUN et al., 2021).

Figure 18- Frequency sweep curves of Pluronic (30%)/ sodium alginate (2%) and silk fibroin hydrogels for 3D printed scaffolds

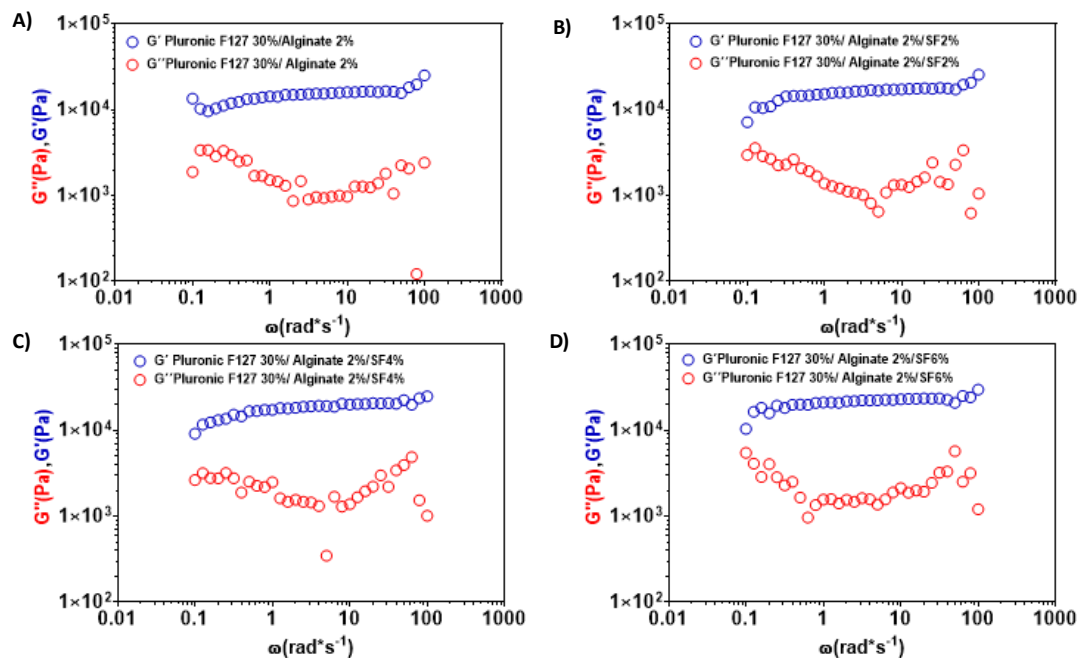


Table 4- Coefficient of determination for the storage modulus (G'), gel strength (S), and viscoelastic exponent (n) of the hydrogels Pluronic inks obtained with different concentrations of silk fibroin

SF concentration	G' (mPa)	S	n
SF0	15015.838±535.319	13457.965± 328.801	0.082 ± 0.009
SF2	16064.806±604.563	14305.810 ± 352.271	0.087 ± 0.009
SF4	18166.064±634.121	16267.626 ± 307.959	0.083 ± 0.006
SF6	21388.064±598.847	19797.085 ± 407.858	0.060 ± 0.007

5.1.3. Hydrogels printability

In this study, we used extrusion-based printing to prepare the 3D scaffolds. This is the most used technique, as it is relatively simple and can print a wide range of hydrogels with varying properties. The printability of a material refers to its ability to be used for 3D printing, considering factors such as its flow properties, curing behavior, and adhesion to the printing surface. The printability of hydrogels is influenced by several factors such as their rheological properties, crosslinking density, and swelling behavior (ASHAMMAKHI et al., 2019; NAGHIEH; CHEN, 2021).

For a hydrogel ink to be suitable for 3D printing, it must meet certain criteria for printability. The material must flow smoothly through the printing nozzle and be able to solidify or cure quickly enough to maintain the integrity of the printed scaffold (WANG, Yuzhen et al., 2022). The material must also adhere well to the printing surface and must be able to maintain its shape and structural integrity during the printing process (GU et al., 2020).

Our results regarding the filament uniformity and printing fidelity of the gelatin inks show that increasing the silk fibroin concentration increases both parameters (Figure 19 and Figure 20). As we observed previously, increasing the concentration of silk in the ink composition decreases the viscosity of the hydrogel and thus facilitates the extrusion of the ink through the nozzle, even though it wasn't possible to achieve the desired printability of these inks.

Figure 19- Gelatin (15%)/ alginate (2%) inks with different concentrations of silk fibroin printability. A) filament uniformity, B) Structure uniformity

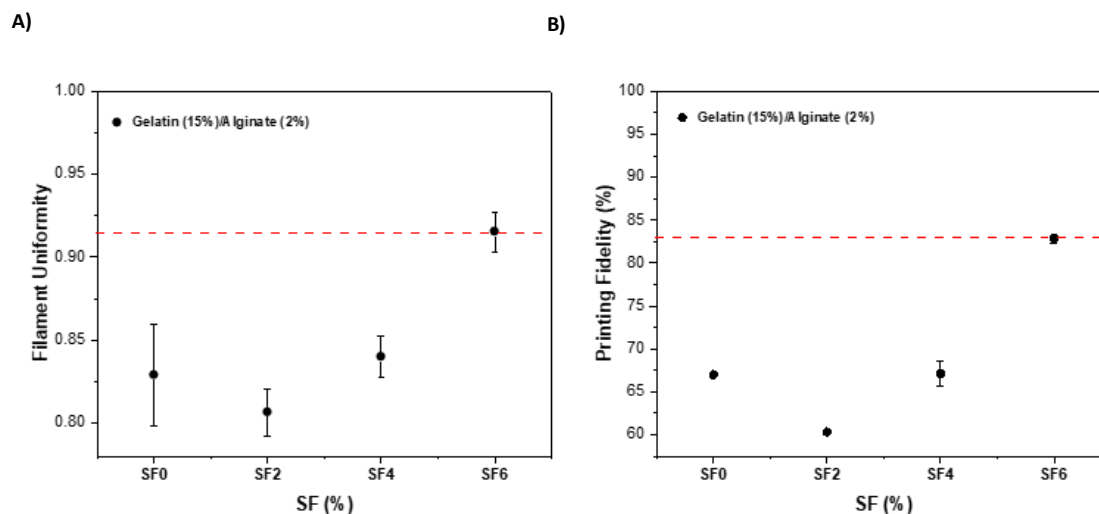
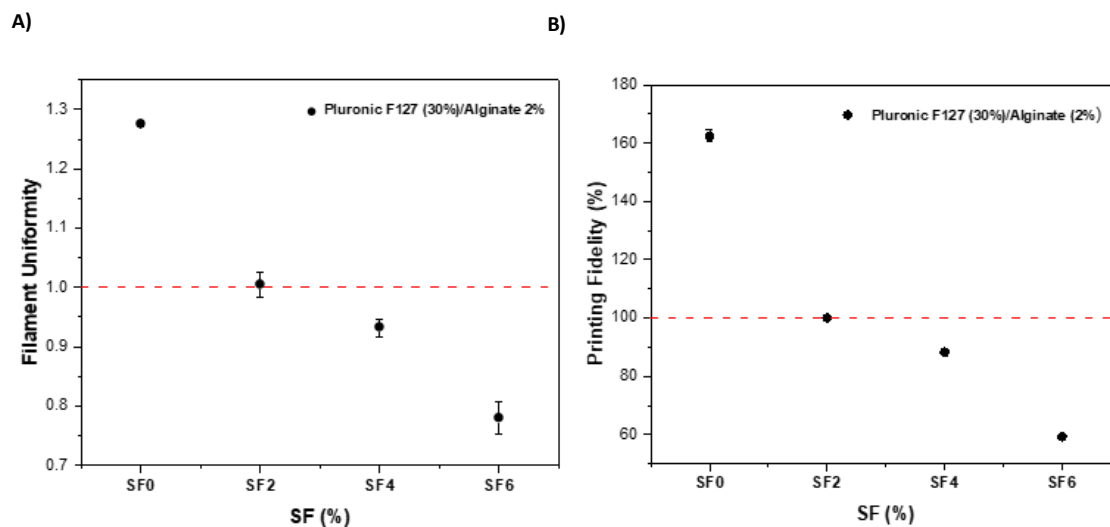


Figure 20 shows the calculated printability parameter for the Pluronic F127 (30%)/Alginate (2%) inks with different concentrations of silk fibroin. As discussed previously, adding fibroin to the hydrogels increases the viscosity of the inks, resulting in a more robust hydrogel and solid structure capable of running smoothly through the nozzle and maintaining its structure after the printing process. Fibroin can improve the shear thinning behavior and increase the viscosity of the hydrogel, which can facilitate extrusion through the printing nozzle (TRUCCO et al., 2021).

Figure 20- Pluronic (30%)/ alginate (2%) inks with different concentrations of silk fibroin printability. A) filament uniformity, B) Structure uniformity



In Figure 21 and Figure 22 we can observe the printed hydrogels using a extrusion 3D printer, it is possible to observe the differences in the uniformity and printability of the hydrogels dependin on the SF concecntraion containing whiting the inks structure.

Figure 21- Gelatin 3D printed hydrogels with different concentrations of silk fibroin and containing two other photosensitive molecules. A) Gelatin hydrogels containing a tetra sulfonate porphyrin, B) Gelatin hydrogels containing phenalene

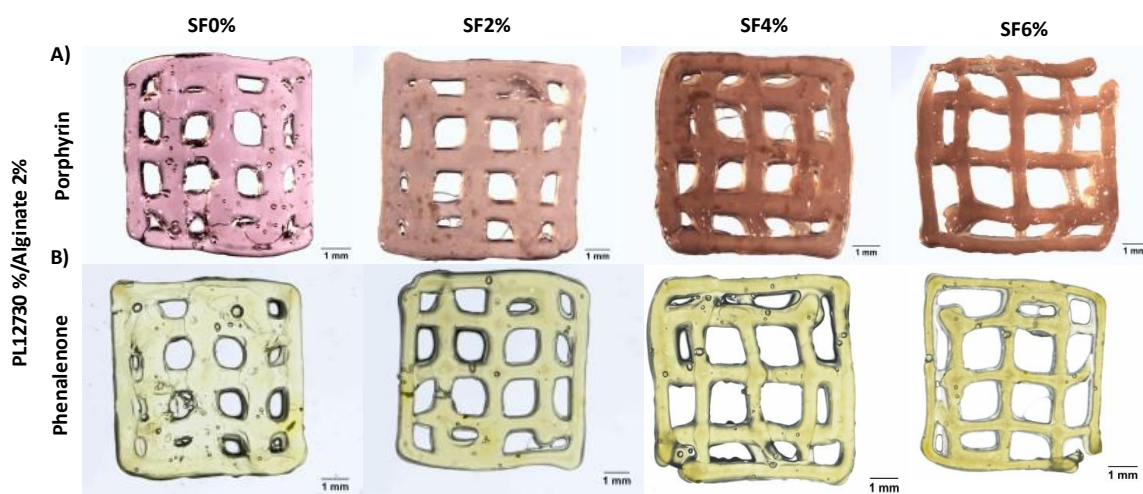
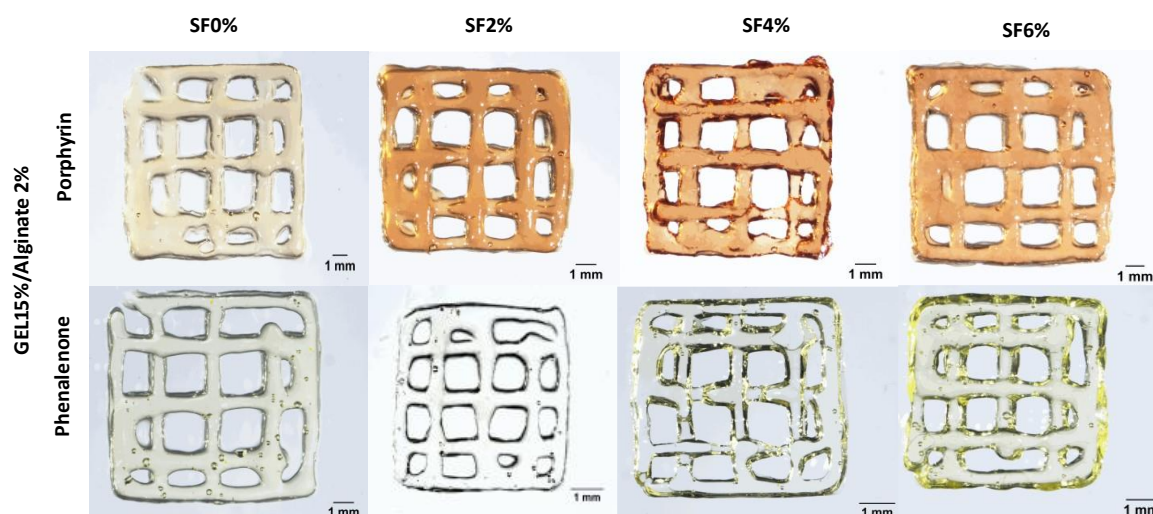


Figure 22- Pluronic F127 3D printed hydrogels with different concentrations of silk fibroin and containing two other photosensitive molecules. A) Pluronic F127 hydrogels containing a tetra sulfonate porphyrin, B) Pluronic F127 hydrogels containing phenalenone

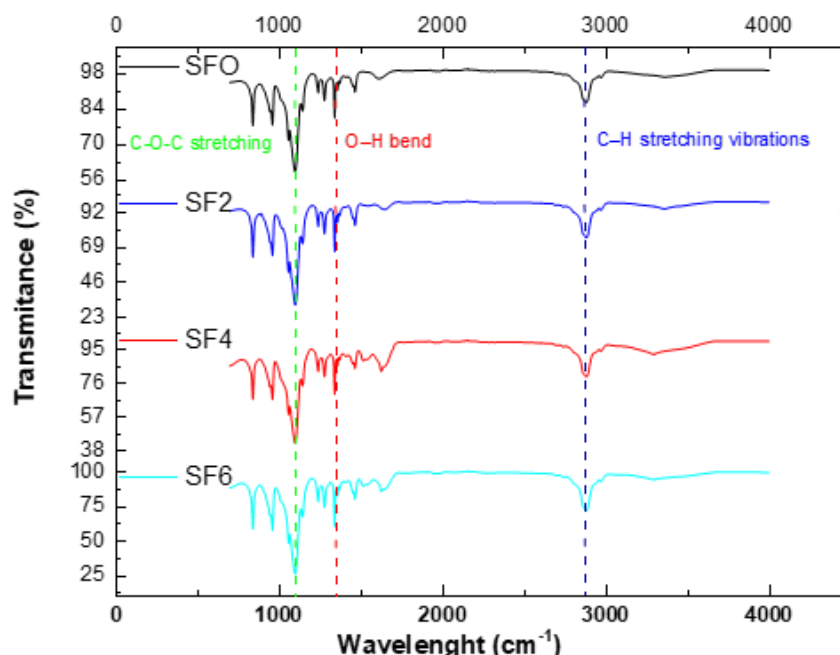


5.1.4. 3D-printed hydrogels characterization

All the 3D printed scaffolds were characterized using electronic scanning microscopy and Fourier transform infrared spectroscopy (FTIR). Figure 23 shows the representative peaks of the hydrogels containing gelatin (15%)/ Alginate (2%) and different concentrations of silk fibroin. It is possible to identify a series of peaks in the $4000\text{--}600\text{ cm}^{-1}$ range (DAS et al., 2017). The peaks in this region correspond to the different vibrational modes of the functional groups present in the gelatin molecule. Some of the prominent peaks in the gelatin FTIR spectrum include an amide A band (around 3300 cm^{-1}) due to the stretching vibrations of the N-H bonds in the amide groups and an amide B band (around 2925 cm^{-1}) due to the stretching vibrations of the C-H bonds in the amide groups (PENG; LI; SHEN, 2012; YU, Weijiang et al., 2017). The peak at around 1650 cm^{-1} is characteristic of the amide I band and arises from C=O stretching vibrations in the peptide backbone. This peak is sensitive to the protein's secondary structure and can provide information on whether the protein is in an alpha-helical or beta-sheet conformation. (MUYONGA; COLE; DUODU,

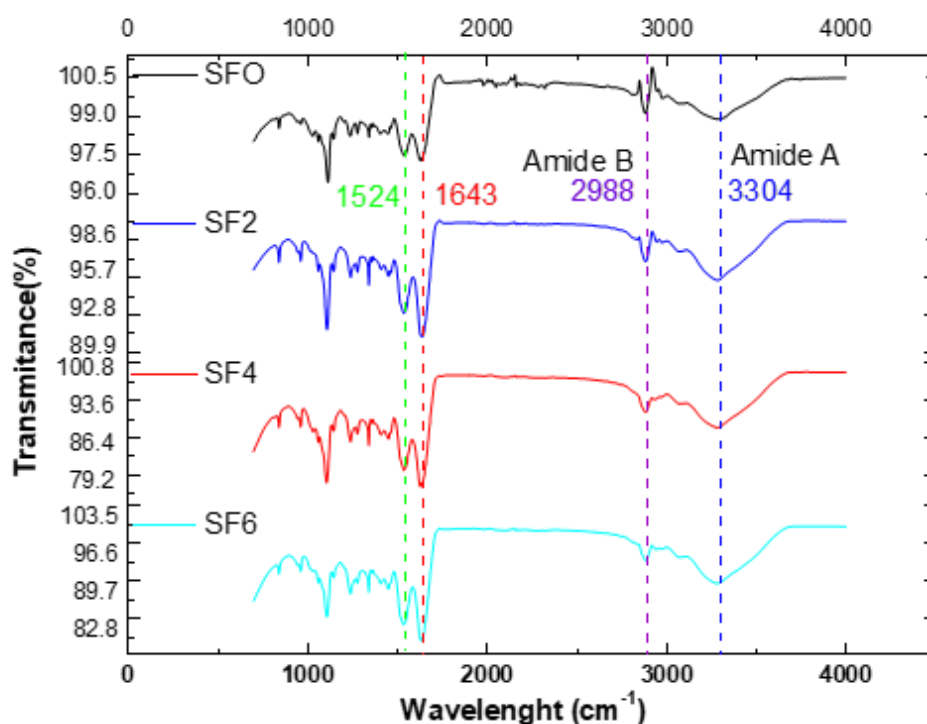
2004)n. Finally, the peaks around 1550 cm^{-1} are due to N-H bending and C-N stretching vibrations in the amide groups (POLYAK; REICH, 2019).

Figure 23- FTIR spectra of 3D scaffolds containing gelatin (15%)/ alginate (2%) and different concentrations of silk fibroin



Regarding the FTIR spectra of the 3D scaffolds containing Pluronic F127 (30%)/alginate (2%) and different concentrations of silk fibroin, peaks can be observed at around $2900\text{--}3000\text{ cm}^{-1}$, corresponding to the C-H stretching vibration of the EO and PO blocks of Pluronic F127 (FU; YU, 2017). The C-O stretching vibrations of the EO and PO blocks can also be observed in the spectra, with peaks typically appearing at around $1100\text{--}1300\text{ cm}^{-1}$. The PO block also shows a characteristic peak at about 900 cm^{-1} , corresponding to the vibration of the PO group. The absence of a significant shift in the observed peak positions suggests the lack of interactions between Pluronic F127 and the other polymers due to the high concentration of Pluronic within the scaffold (Figure 24).

Figure 24-FTIR spectra of 3D scaffolds containing Pluronic F127 (30%)/ alginate (2%) and different concentrations of silk fibroin



Regarding the SEM analysis of gelatin (30%)/alginate (2%) and different concentrations of silk fibroin is possible to identify pores and fibers within the 3D hydrogels structures (

Figure 25). SEM (Scanning Electron Microscopy) images of gelatin-fibroin hydrogels can provide insights into the structure and morphology of these materials (CHANG, Kai-Chi et al., 2019). In general, it is possible to observe a porous network of interconnected fibers or filaments (Figure 26). The fibers appear to be randomly oriented. The size and shape of the pores vary depending on factors such as the concentration of fibroin used to create the hydrogel (SUN, Mingyue et al., 2018).

Figure 25- Gelatin (15%)/ alginate (2%) and different concentrations of silk fibroin 3D printed scaffolds SEM micrographs

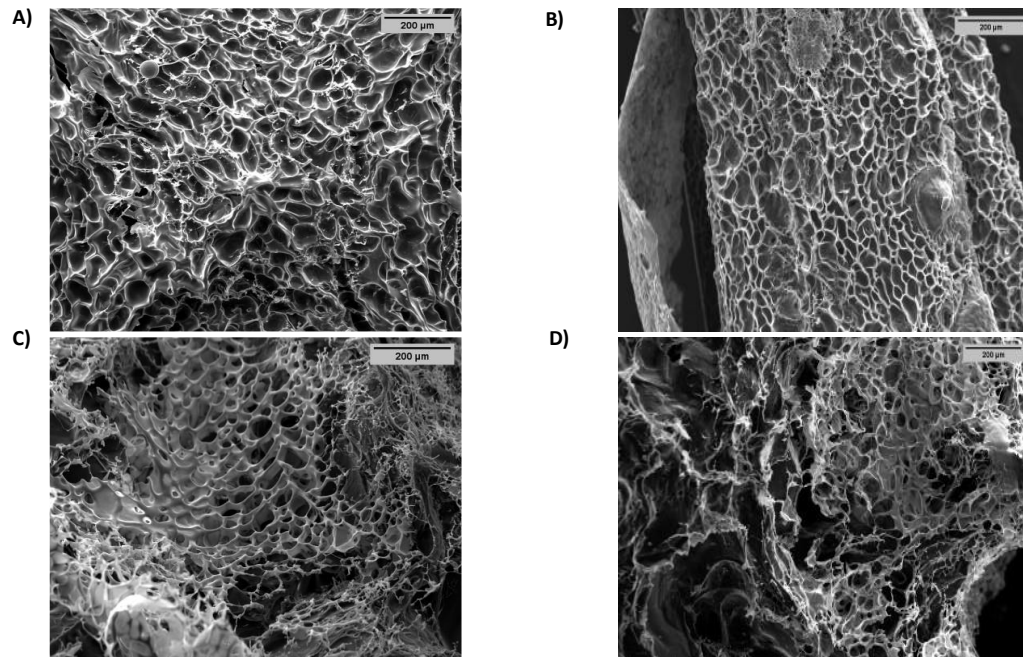
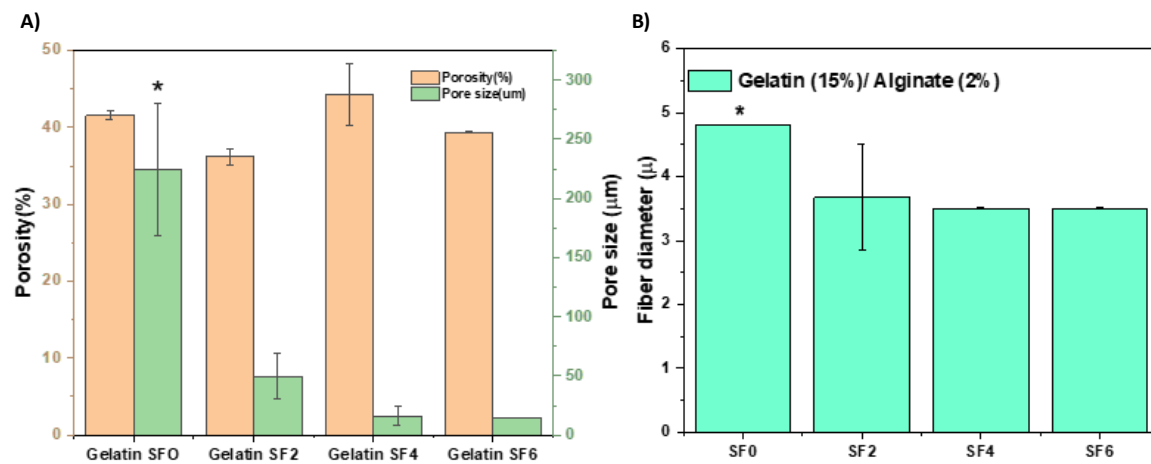


Figure 26- Gelatin 3D printed scaffolds. A) 3D hydrogels porosity and pore diameter, B) Fiber diameter, * denotes a p-value less than 0.05



SEM images of Pluronic F127 and SF hydrogels typically show a porous (Figure 27), sponge-like structure with interconnected channels or pores. The surface of the hydrogel also appears rough, with variations in pore size and shape. The exact appearance of the hydrogel depends on factors such as the concentration of SF used to make the hydrogel, the method of preparation, and the environmental conditions under which the hydrogel was formed, forming fibers with different diameters after adding SF to the structure (ROJAS et al., 2019). Increase the concentration of SF in the structures result in a increase in the porosity of the structure, giving us structures with more pores but smaller area and zero impact in the diameter of the fiber (Figure 28).

Figure 27- Pluronic F127 (30%)/ alginate (2%) and different concentrations of silk fibroin 3D printed scaffolds SEM micrographs

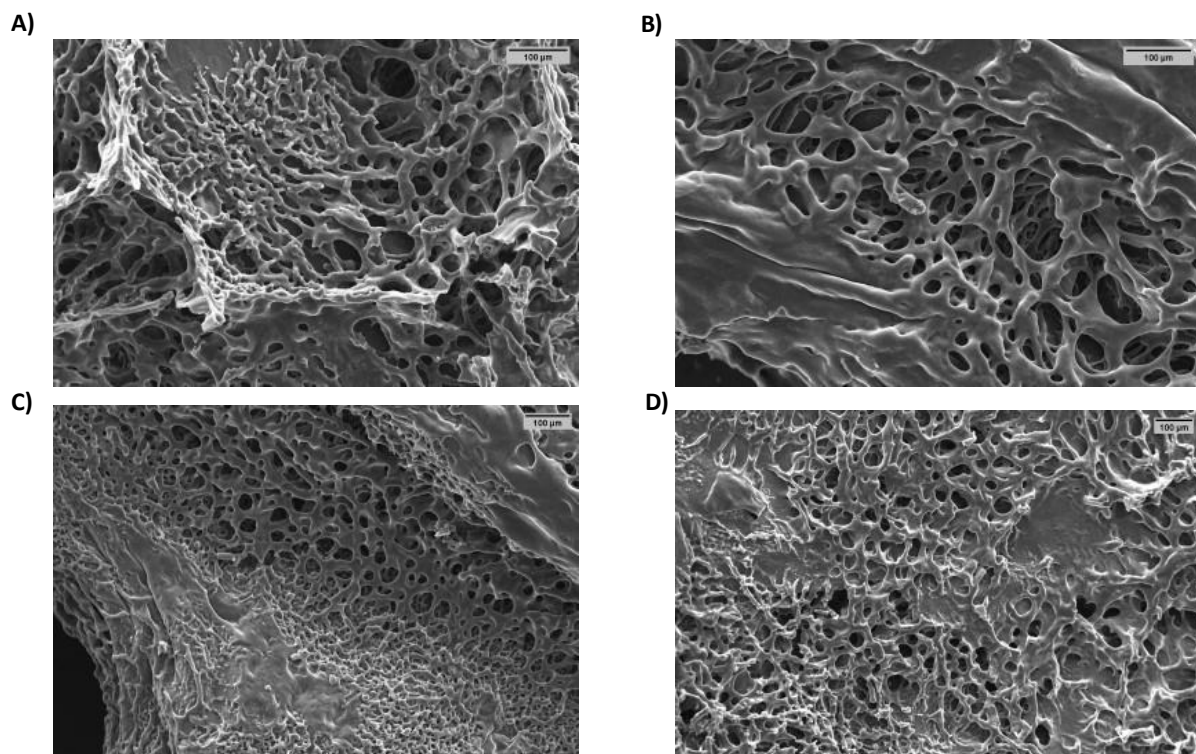
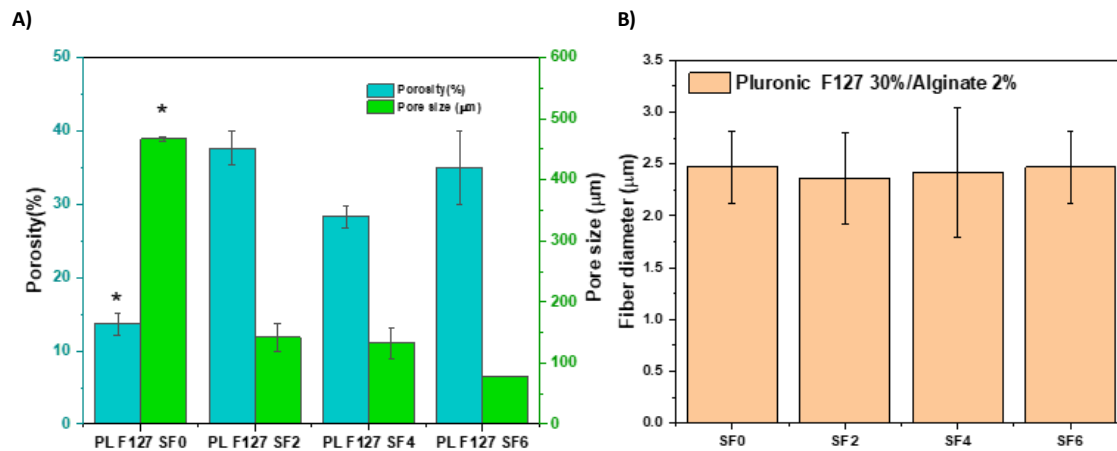


Figure 28- Pluronic 3D printed scaffolds. A) 3D hydrogels porosity and pore diameter, B) Fiber diameter, * denotes a p-value less than 0.05



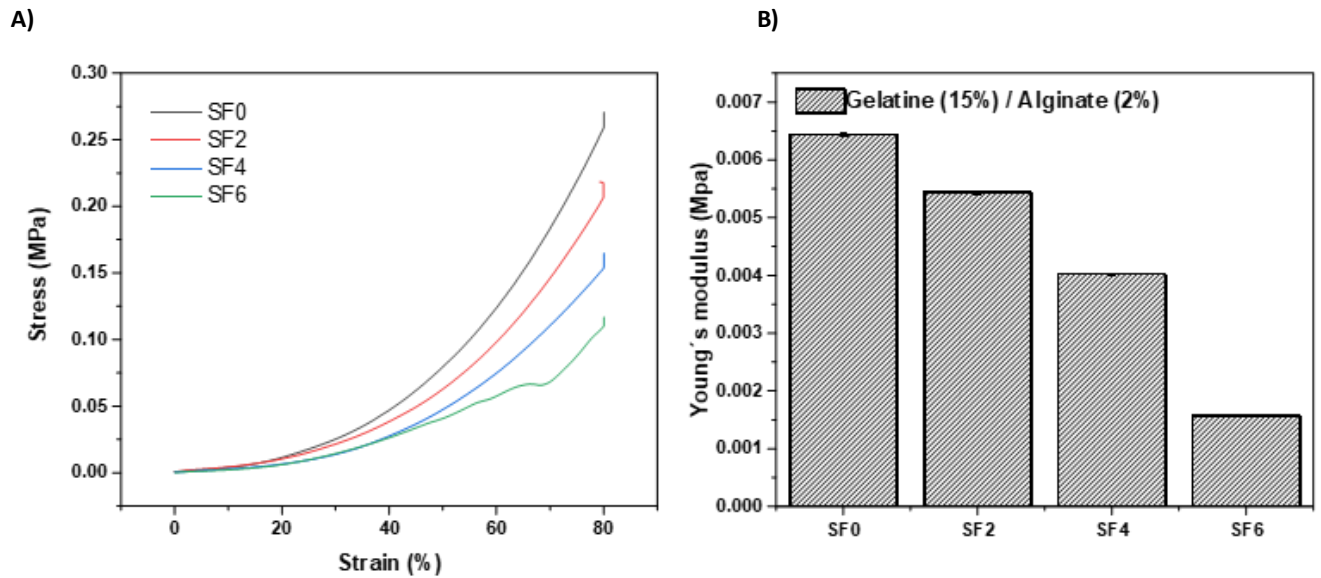
5.1.5. Compression analysis

A compression test involves applying a force to the sample and measuring the resulting deformation or displacement. The force-displacement data obtained from the test can be used to calculate several parameters, such as compressive strength, compressive modulus, and strain at failure (KIM, Soon Hee et al., 2021). In the case of a 3D-printed gel made from silk fibroin and gelatin, the compression behavior may depend on various factors such as the printing parameters, the composition of the gel, the printing pattern, and the post-printing treatment (WEI et al., 2019). The higher the compressive strength, the more resistant the gel is to compression.

The addition of silk fibroin hydrogels to the 3D matrix decreases the compression force of the scaffolds and results in lower Young's modulus for all the 3D printed hydrogels Figure 29 and Figure 30. In the case of the gelatin hydrogels, the addition of SF can affect the gelation process of gelatin due to its ability to form hydrogen bonds with water molecules. Silk fibroin has a high affinity for water, and this can cause water to be drawn away from the gelatin, leading to a delay or inhibition of the gelation process. This effect

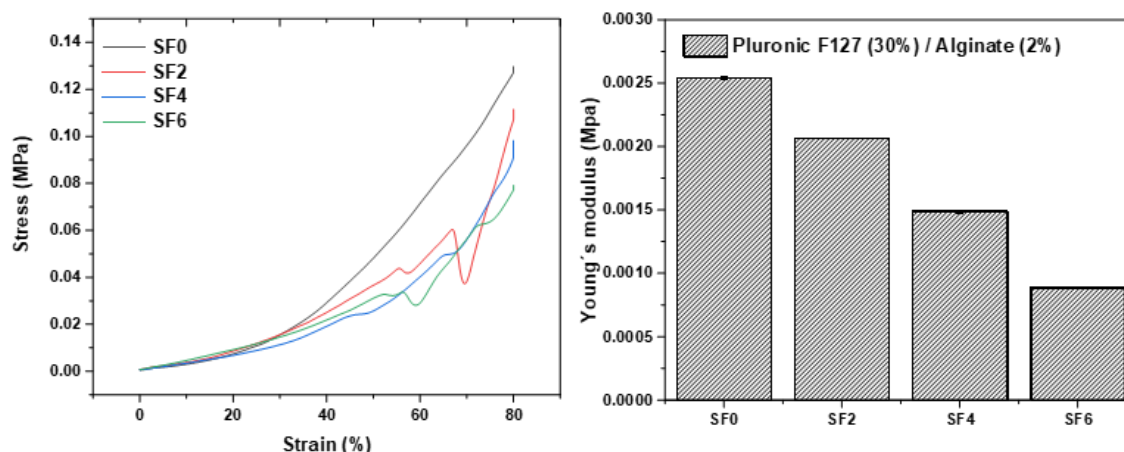
can be controlled by adjusting the ratio of silk fibroin to gelatin and the processing conditions, such as the temperature and time of gelation.

Figure 29- Gelatin (15%) /Alginate (2%) 3D scaffolds containing different silk fibroin compression analysis concentrations. A) 3D scaffolds strain/stress curve. B) 3D scaffolds Young's modulus



The same behavior can be observed in the 3D scaffolds containing Pluronic F127. Adding calcium chloride is critical for forming a stable hydrogel for these inks. The decrease in Young's modulus could be due to the effect of silk fibroin fibers on the diffusion of calcium chloride through the structure, which interferes with the gelation process of the hydrogel (Figure 30).

Figure 30- Pluronic F127 (30%)/Alginate (2%) 3D scaffolds containing different silk fibroin compression analysis concentrations. A) 3D scaffolds strain/stress curve. B) 3D scaffolds Young's modulus.

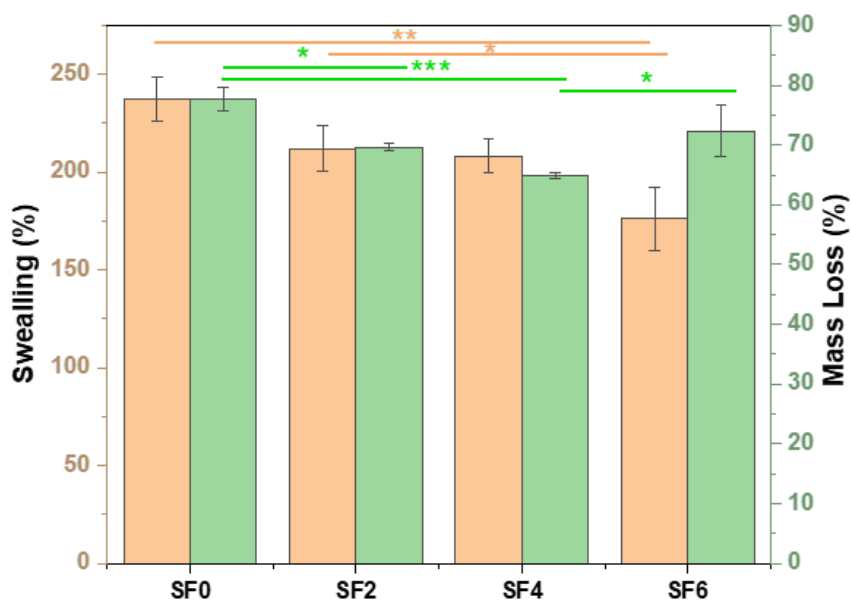


5.1.6. 3D hydrogel swelling and loss mass analysis

Hydrogels are three-dimensional networks of hydrophilic polymers that absorb and retain large amounts of water. Generally, the swelling behavior of hydrogels is characterized by their swelling ratio, which is defined as the ratio of the swollen volume to the dry volume (WANG, Hai Yan; ZHANG, 2015). The swelling properties of 3D-printed hydrogels can be optimized by carefully controlling the material composition, printing parameters, and post-processing conditions (BITTNER et al., 2021). This can help to ensure that the hydrogel retains its ability to absorb water and maintain its structural integrity, which is critical for many biomedical applications. For example, alginate hydrogels have high swelling ratios and can absorb up to several hundred times their own weight in water (DUTTA et al., 2021). Gelatin and silk fibroin hydrogels, on the other hand, have lower swelling ratios but can be modified to have tunable mechanical properties.

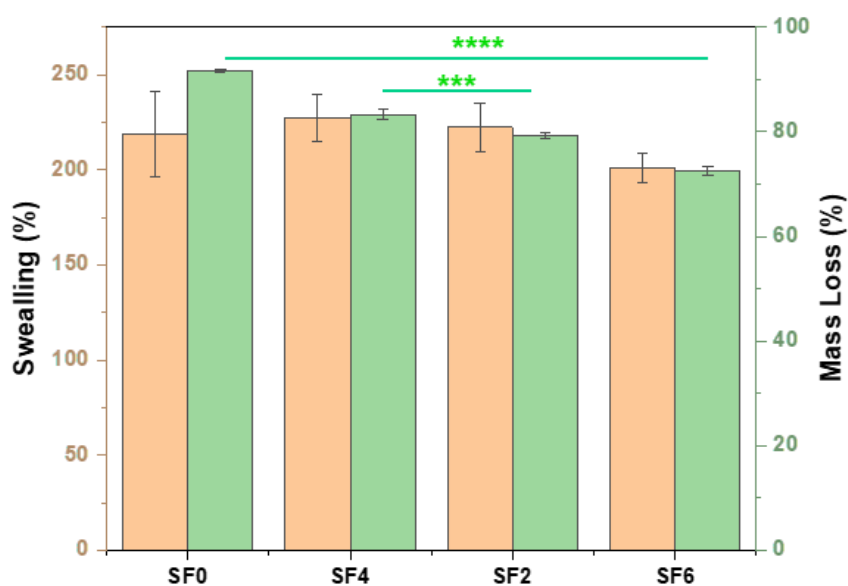
The 3D printed hydrogels prepared using the gelatin (15%)/alginate (2%) and variable concentrations of SF present a significant difference in the swelling ratio and mass loss of each treatment (Figure 31). It is possible to observe that the swelling behavior of the hydrogels decreases with the addition of silk fibroin. This could be due to a higher crosslinked structure (ESTER-BRIDGED et al., 2021). Usually, hydrogels with a high crosslink density present a lower swelling ratio than low crosslinked hydrogels due to the lower diffusion of the water through the structure. The swelling behavior of hydrogel scaffolds has been accepted as indicative of their crosslinking density (DUTTA et al., 2021).

Figure 31- Gelatin (15%)/alginate (2%) hydrogels scaffolds containing different concentration of fibroin swelling a loss mass analysis, * denotes a p-value less than 0.05, **denotes p-values less than 0.01 and *** p-value less than 0.001



On the other hand, Pluronic F127 (30%)/alginate (2%) inks with variable concentrations of fibroin exhibit different behavior than gelatin inks. The swelling behavior of the inks is variable and independent of the addition of silk fibroin due to the high concentration of Pluronic F127, but the degradation of the hydrogels decreases with an increase of SF concentrations within the structure (Figure 32).

Figure 32- Pluronic F127 (30%)/alginate (2%) hydrogels scaffolds containing different concentrations of fibroin swelling a loss mass analysis, * denotes a p-value less than 0.05 and *** p-value less than 0.001



5.1.7. Drug release analysis

Drug release from 3D-printed hydrogels can be influenced by several factors, such as the properties of the hydrogel and the type of drug being released. The properties of the hydrogel, such as porosity, stiffness, and swelling behavior, can also affect drug release. For

example, hydrogels with higher porosity, swelling, and degradation rate may release drugs faster due to increased diffusion (CARBINATTO et al., 2014). Hydrogels with higher stiffness may also release drugs slower due to reduced swelling and increased resistance to drug diffusion (ABBASI et al., 2020). As we can observe, all hydrogels prepared in this study were capable of a rapid release of both photosensitive molecules after 30 min. in variable concentrations depending on the properties of each of the principal components of each ink (Figure 33 and Figure 34). For the gelatin (15%) / alginate (2%) ink for the release studies, we used the one with a concentration of 6% silk fibroin due to better printability, and for the Pluronic (30%) alginate (2%) with choose the one with a 2% silk fibroin concentration as well for its better printability and mechanical properties.

Figure 33- Total amount of a tetra sulfonate porphyrin (A) and a phenalenone (B) released from the gelatin (15%)/Alginate (2%)/ SF(6%) scaffold in PBS buffer at 0.5,1,2,3,4,5,6,7,8,24,48 and 72 hours

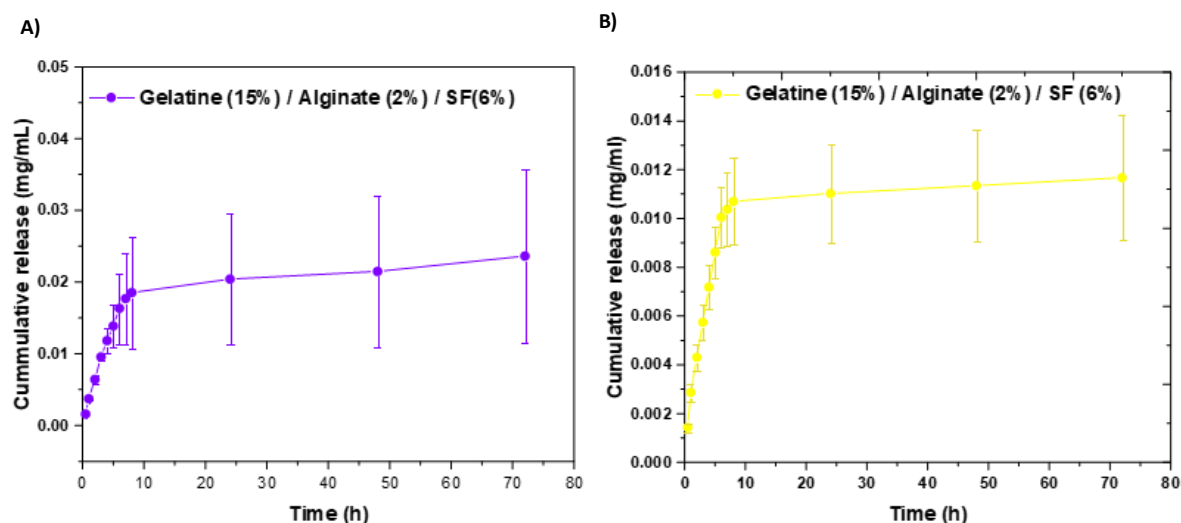
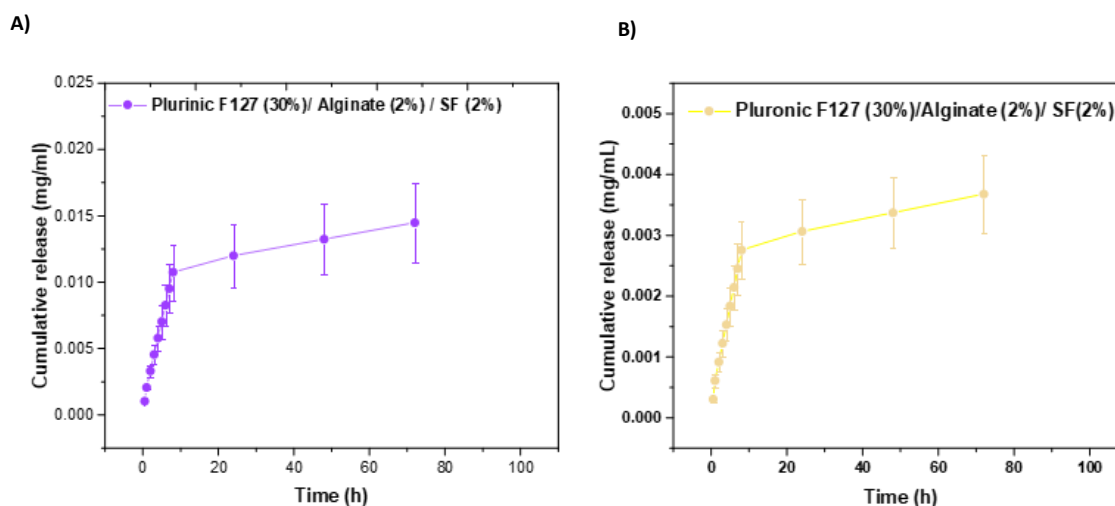


Figure 34- The total amount of a tetra sulfonate porphyrin (A) and a phenalenone (B) released from the Pluronic F127 (30%)/Alginate (2%)/ SF(6%) scaffold in PBS buffer at 0.5,1,2,3,4,5,6,7,8,24,48 and 72 hours



For a better understatement of the released behavior of the printed 3D scaffolds, we tested different drug-released models for each of the tested hydrogels (Table 5). Drug release models are mathematical models that describe drug release from various drug delivery systems, including 3D hydrogels scaffolds. These models can help predict drug release profiles under different conditions, which can be useful in developing new drug delivery systems (HEREDIA et al., 2022).

There are several drug release models, each based on different assumptions and mathematical principles. For this study, we chose the four models most used in the literature to describe drug release from hydrogel scaffolds (TRUCILLO, 2022). Zero-order assumes that drug release occurs at a constant rate, regardless of the drug concentration or other factors (VARELAS; DIXON; STEINER, 1995). The First-order release model assumes that drug release occurs at a rate proportional to the amount of drug remaining in the drug delivery system (HEREDIA et al., 2022). The third model used, the Higuchi model, assumes

that drug release occurs by diffusion through a matrix and that the drug release rate is proportional to the square root of time (PAARAKH et al., 2019).

One of the most used models to describe the drug release rate from the polymeric matrix, the Korsmeyer-Peppas model assumes that the rate of drug release is proportional to the fractional power of time (AHMED et al., 2019; WU, Iren Yeeling et al., 2019). And last the Hixson-Crowell cube root law, also known as the Hixson model, is a widely used drug release model that assumes that the rate of drug release from a solid matrix is proportional to the surface area of the matrix and the difference in drug concentration between the matrix surface and the bulk of the matrix (LISIK; MUSIAŁ, 2019).

Of the four models used in this study, the Higuchi model was the one that better adjusted to the obtained results for the hydrogels containing Pluronic F127 as the main component. This indicates that drug release occurs through diffusion through the hydrogel matrix based on the Fickian diffusion equation for these scaffolds. As for the drug release mechanism from the gelatin (15%)/Alginate(2%)/SF(6%) scaffold, the first-order model was the one that better explained the drug release rate for both molecules, where the release rate is concentration-dependent.

Table 5- Gelatin and Pluronic F127 3D scaffolds drug release models fit

	PLF127 (30%)/ Alginate (2%)/ (SF2%)		Gelatin (15%)/Alginate (2%)/SF (6%)	
	Tetrasulfonate porphyrin (R²)	Phenalenone (R²)	Tetrasulfonate porphyrin (R²)	Phenalenone (R²)
Zero order	0.619	0.9999	0.979	0.9211
First order	0.9868	0.9999	0.9868	0.9264
Huguchi model	0.9999	0.9999	0.979	0.9211
Hixson	0.9995	0.9952	0.9845	0.9041
Kor's peppas	0.8886	0.8423	0.7498	0.7345

5.2. Silk fibroin Microneedles

5.2.1. SF and PVA Solutions Rheological Characterization.

The viscosities of the SF and PVA aqueous solutions before microneedle casting were analyzed. Figure 20 shows the viscosity (η) of the solutions, and it is possible to observe that apart from the neat PVA solution, all samples present a shear thinning, non-Newtonian flow behavior. The neat SF solution displays the lowest viscosity values, and by increasing the PVA content, the viscosity tends to increase at any given shear rate. The hybrid polymer solutions with higher PVA proportions (SF 1:1 PVA and SF 3:7 PVA) present the highest viscosity values at low shear rates and the most pronounced shear thinning character. This behavior is typical for polymer solutions, as the initially coiled polymer molecules tend to align with the increasing shear rate. In particular, it is a characteristic and prevalent behavior of SF aqueous solutions.(TRUCCO et al., 2021) With rising shear rates, the shear-thinning became less pronounced. The dependence of viscosity on frequency dramatically decreases until the solutions display a Newtonian behavior in a high-shear rate regime, indicating a flowing alignment of the underlying microstructure.(YANG, Zhe et al., 2010) The rheological behavior of PVA aqueous solutions is determined by the concentration of PVA and the strength and number of hydrogen bonds, including intrachain, interchain, and PVA-H₂O hydrogen bonds.(ZHANG, Xin; PAN, 2020)

5.2.3. SF and PVA Microneedles Preparation and Characterization.

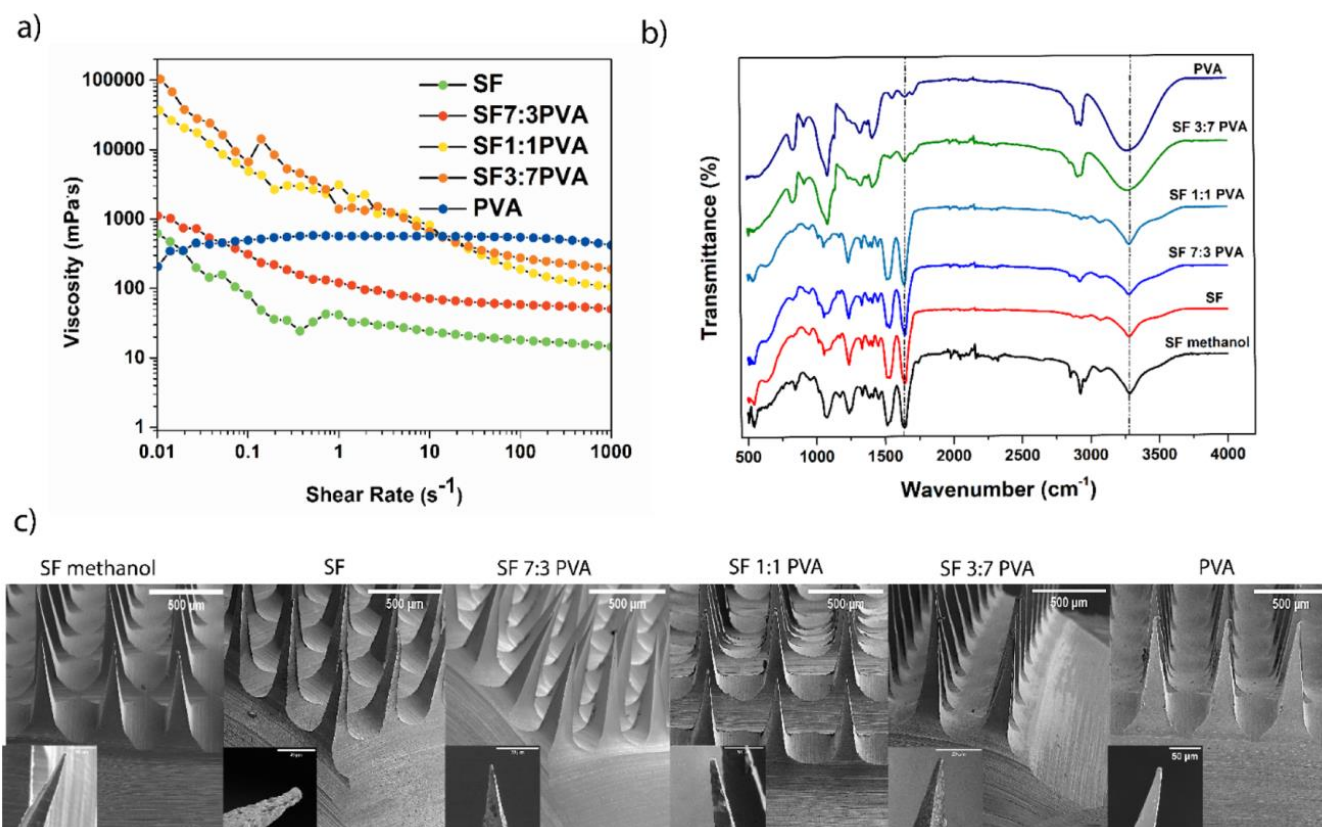
The microneedles obtained from PVA and SF blend solutions (SF methanol, SF, SF 7:3 PVA, SF 1:1 PVA, SF 3:7 PVA, and PVA) were prepared by a straightforward two-step casting method. In the first step, a given volume of the polymer solution was cast into the PDMS mold and centrifugated to fill the voids and form the tips. In the second step, an additional volume of the polymer solution has been added to the mold to form the backing layer. The FTIR spectra of SF microneedles (Figure 35) show intense absorption bands around 3200-3600, 2932, 1648 and 1535, and 1237-1444 cm⁻¹, which are characteristic of protein structures.(BADILLO-SANCHEZ et al., 2019; BOULET-AUDET; VOLLRATH; HOLLAND, 2015; LING et al., 2013) These peaks were assigned to the O-H stretching vibrations and symmetrical and asymmetrical stretching vibrations of the C-H, amide I (-C=O stretching),

amide II (-N-H bending), and amide III (-C-N stretching) bands, respectively. Accordingly, increasing PVA content in the microneedles results in a gradual decrease of these peaks and the appearance of characteristic vibrations of PVA at 3200–3400 cm^{-1} (-OH stretching), 2940 cm^{-1} (-C-H stretching), 1650–1750 cm^{-1} (-C=O and -C-O stretching from the acetate group remaining from PVA), 1640 cm^{-1} (absorbed water), 1435 cm^{-1} (-C-H bending), and 1095 cm^{-1} (-C-O stretching). (BLOUT; KARPLUS, 1948)

The FTIR spectra of SF 1:1 PVA and SF 3:7 PVA are different than the spectra of neat fibroin and PVA, as shown in Figure 35 2b. The -OH group of SF microneedles (3345 cm^{-1}) increases in height, and a broad absorption band was observed after incorporating PVA in the blend polymer systems. This change is caused by the strong interaction between carboxyl groups on SF and hydroxyl groups on PVA and the weakening of the hydrogen bonds between SF chains. The inter-polymer complexation was favored with an increasing PVA ratio, leading to a more effective mixing of both constituents, increasing the viscosity of the solution, as shown in Figure 35 2a. Particularly, the SF 3:7 PVA microneedles show a reduction of amide I band intensity (1650 cm^{-1}) and formation of a new bond at 1711 cm^{-1} , which is quite evident from the spectra as the PVA content is increased, which can be related to the intermolecular and intramolecular interactions between biopolymer chains. (SHAHBAZI et al., 2017)

Patches containing grids of 10 × 10 microneedles with a square-based pyramidal shape were successfully produced through this approach. The needles were 700 μm in length, 200 μm wide at the base, and 25 μm wide at the tip, as shown in Figure 35 2c. Also, we did not observe any significant changes in the morphological structure in general (independent of polymer composition). According to the literature, the microneedles presented excellent reproduction of the negative master mold used for their preparation and ideal proportions to pierce the stratum corneum. (LEE, I.-Chi et al., 2015; ZHU et al., 2020).

Figure 35- Physical and chemical characterizations of the microneedles obtained by mold casting and polymer solutions: (a) polymer solution viscosity studies, (b) the FTIR spectra of the microneedles, and (c) SEM micrograph images from the prepared polymer microneedles showing structures and sizes of the fibroin and PVA microneedle in different proportions: SF treated with methanol, SF, SF 7:3 PVA, SF 1:1 PVA, SF 3:7 PVA, and PVA



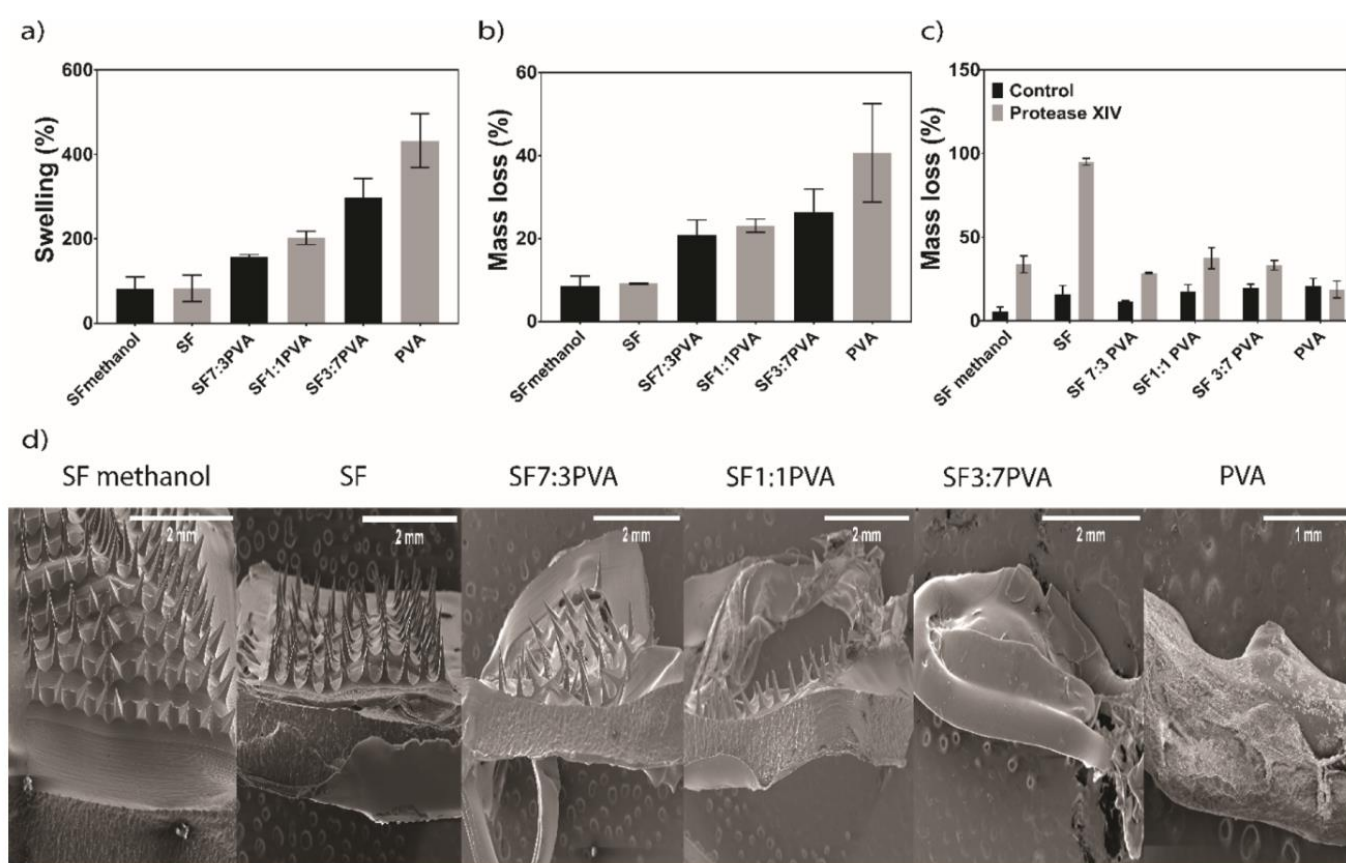
5.2.4. Stability Evaluation and Swelling Studies of SF and PVA Microneedles.

The control of the stability and water absorption of the microneedle devices is desired to tune the release of the active principle (TURNER et al., 2021). Microneedles obtained from pure SF treated or not treated with methanol present almost the same swelling and stability behavior; these microneedles show minor deformation compared to their initial structures following incubation in PBS for 24 h (Figure 36). The stability evaluation and water absorption behavior depend on the PVA amount present in the hybrid systems. The increase in the PVA polymer in the matrix favors water absorption due to the formation of strong hydrogen bonds (ABDULLAH; DONG, 2019; JAIN; SINGH; CHAUHAN,

2017) thereby enabling water to penetrate, dissolving the microneedles partially, as shown in Figure 21b. Conversely, the stability and swelling ratio are lower in the microneedles with a higher proportion of SF due to the poor solubility of this protein in most solvents. There was no significant difference in instability and the swelling ratio between the MNs prepared only with fibroin and fibroin treated with methanol. This behaviour was somewhat unexpected since methanol is known to favour the formation of intra- and intermolecular hydrogen bonds in SF and its crystallinity, possibly due to the formation of β -sheet secondary structures, which would have led to anticipate a lower solubility of the microneedles (JOHARI; MORONI; SAMADIKUCHAKSARAEI, 2020). In order to evaluate the resistance of the microneedles toward enzymatic degradation, the samples were treated with a solution of protease XIV, which cleaves amide bonds adjacent to aliphatic, aromatic, or hydrophobic residues (NAIDOO et al., 2015).

The degradation rate of the microneedles was affected by the SF content of each sample, and it increased for the higher protein content. Notably, in this case, we observed a significant decrease in the degradation rate of the SF methanol microneedles compared to non-treated SF ones, which can be ascribed to the stabilization of the secondary structure by methanol (MÜLLER-HERRMANN; SCHEIBEL, 2015). Treatment with methanol induces the formation of the β -sheet content in SF materials by helping the transition from α -helices/random coils (unfolded chains) to highly ordered chains containing oriented β -sheet crystals and decreasing the enzymatic degradation of the samples (LIU, Bin et al., 2015; UMUHOZA et al., 2020).

Figure 36- Silk fibroin and PVA microneedles stability and swelling analysis: (a) swelling of microneedles prepared with different proportions of silk fibroin and PVA after being submerged in PBS (pH 7.4) for 24 h at room temperature, (b) stability evaluation (mass loss) of microneedles prepared with different proportions of silk fibroin and PVA after being submerged in PBS (pH 7.4) for 24 h at room temperature, (c) the degradation ratio of SF and PVA microneedles submerged in protease XIV solution for 24 h, and (d) polymer microneedle SEM micrographs after being submerged in PBS buffer for 24 h. Data are shown as mean \pm SD, n = 3



5.2.5. Depth of Penetration (DOP)

One of the factors that determine the effectiveness of the delivery of an active molecule through the application of microneedles is the efficiency of penetration of the device through the skin. The microneedles prepared in this study display favourable

dimensions to penetrate the skin and act as drug delivery vehicles, as microneedles from 150 up to 700 μm in length have proven to be able to cross the stratum corneum and deliver active compounds to the dermis (MIGDADI et al., 2018; QUINN et al., 2015). For example, it has been reported that microneedle patches with 416, 500, and 600 μm lengths can successfully deliver magnesium ascorbic phosphate, insulin, deoxyribonucleic acid (DNA), and sulforhodamine B, respectively, into the skin (KIM, Yujin et al., 2019; WANG, Qi Lei et al., 2016). The penetration efficiency was evaluated using a polymer film Parafilm^M, a commercial hydrocarbon wax and polyolefin blend that provides a simple membrane model for microneedle insertion studies (RODGERS et al., 2018; TSIORIS et al., 2012). The microneedles were applied using an adjustable commercial applicator, with different application forces from 5 to 40 N (from 0.05 to 0.4 N per microneedle, respectively).

The DOP was evaluated using OCT to confirm the insertion of the microneedles in the Parafilm M membrane model in real time. Greater penetration of the microneedles results in deeper perforation pores. Our results show that the DOP is affected by the applied pressure rather than the composition of the microneedles, as shown in Figure 37 a,b. OCT images showed that although there is virtually no difference in the lengths of the pores formed by the different types of microneedles, it is possible to observe a difference in the area as the proportion of PVA increases independently of pressure on the surface. The pores formed in the parafilm become larger and more uniform when the contents of fibroin increase in the MNs, which is related to improving the mechanical properties of hybrid SF/PVA microneedles (Figure 37C. and Table 6).

Figure 37- Insertion studies of the SF and PVA microneedles: (a) DOP of the microneedles in Parafilm M as a skin model with different applied forces; data are shown as mean \pm SD, n = 10, (b) number of Parafilm M sheets performed on by the microneedles using a commercial applicator ****p < 0.0001, (c) 2D cross-sectional OCT images to confirm the microneedle insertion, and (d) 3D OCT images to assess the pore length and area formed in Parafilm M after microneedle insertion

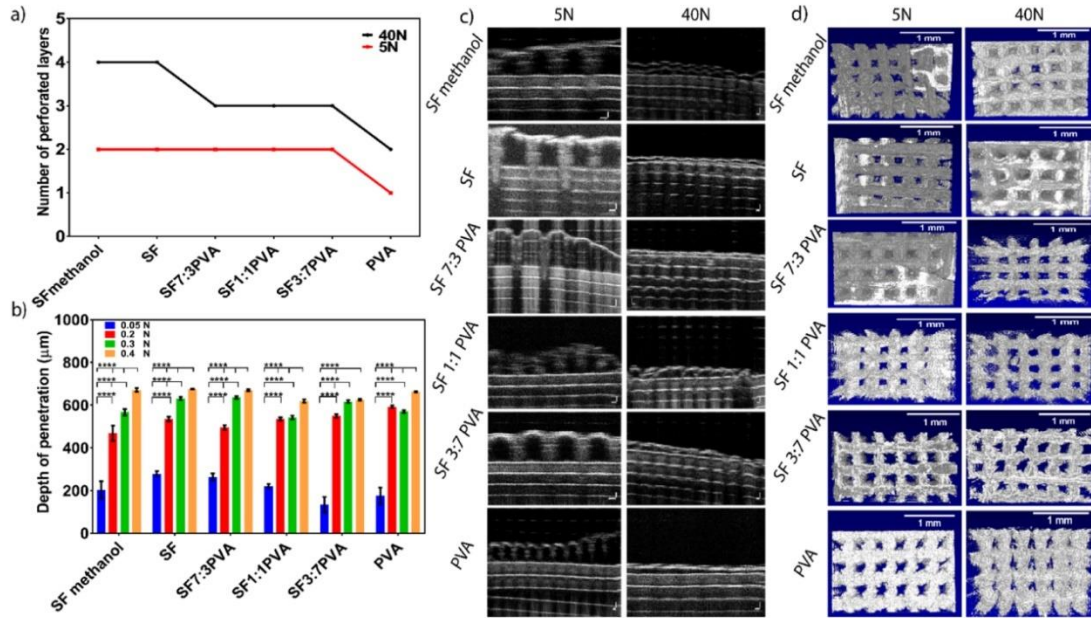


Table 6- Pore Length and Area in Parafilm after SF and PVA MN Insertion Using a commercial Applicators at Different Pressures

MN/force applied	5 N		40 N	
	pore length (μm)	area (μm)	pore length (μm)	area (μm)
SF methanol	0.152 \pm 0.017	0.021 \pm 0.007	0.177 \pm 0.024	0.025 \pm 0.003
SF	0.144 \pm 0.012	0.020 \pm 0.004	0.184 \pm 0.022	0.027 \pm 0.005
SF 7:3 PVA	0.159 \pm 0.023	0.022 \pm 0.006	0.149 \pm 0.011	0.018 \pm 0.005
SF 1:1 PVA	0.137 \pm 0.013	0.010 \pm 0.005	0.153 \pm 0.021	0.014 \pm 0.003
PVA 7:3 SF	0.143 \pm 0.028	0.014 \pm 0.05	0.140 \pm 0.026	0.015 \pm 0.004
PVA	0.135 \pm 0.021	0.012 \pm 0.003	0.113 \pm 0.018	0.009 \pm 0.003

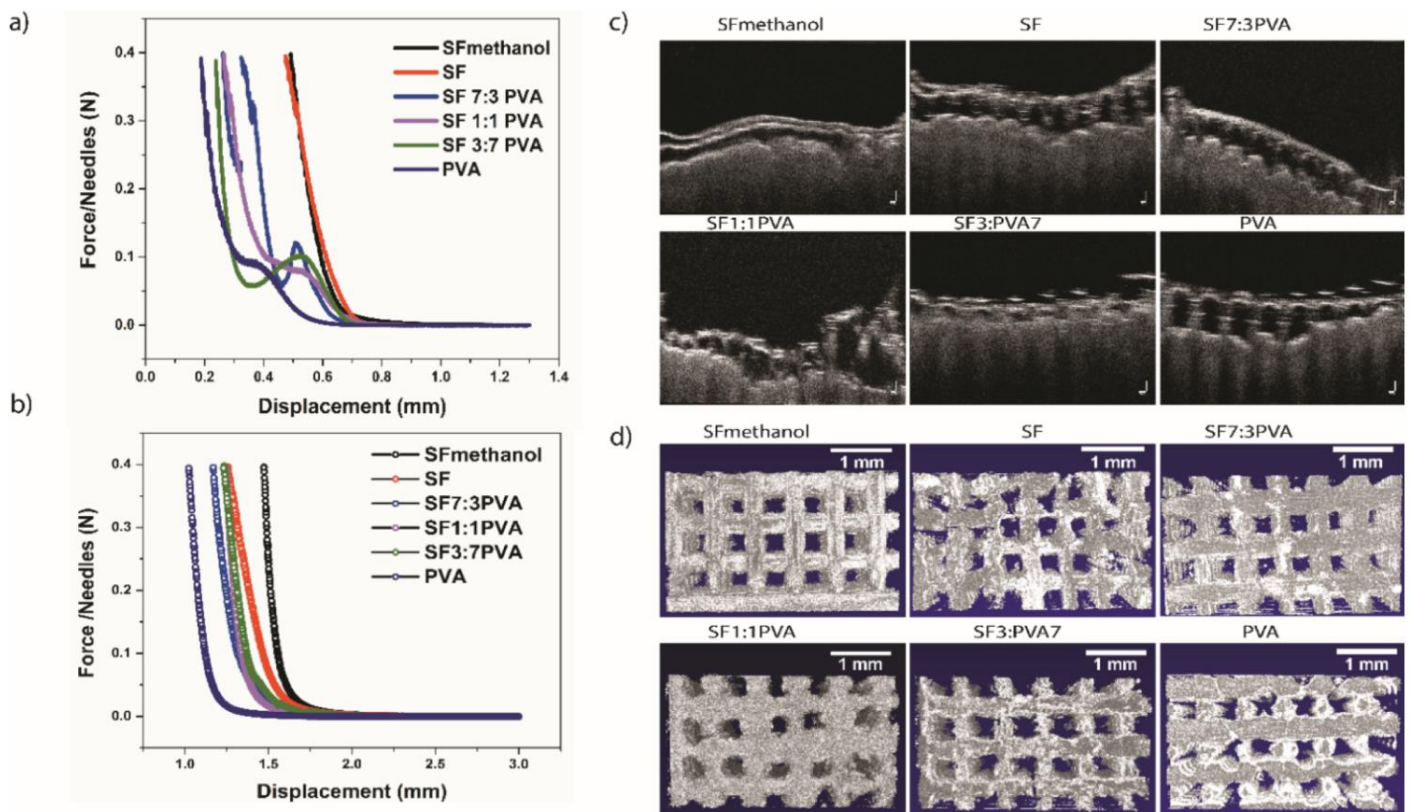
5.2.6. Mechanical Properties

The device needs to have enough mechanical strength to penetrate through the superficial layers of the epithelial tissue and maintain its shape and structure as much as possible to achieve an effective transdermal drug delivery. To assess the mechanical properties of the microneedles, we studied their failure force by applying a gradient of pressure to the patches. Figure 38a shows a diagram of the mechanical test setting and the failure forces measured for the different types of microneedles. The SF microneedles, both treated and non-treated with methanol, do not exhibit fracture/plastic failure on the tip of the needles. The crushing force only increases continuously as the compressive test proceeds, which is typical behaviour for bending failure.(GITTARD et al., 2013)

The micrographs for SF methanol show a slight/localized permanent deformation, consistent with bending fracture/ failure mode (Figure 38c), whereas as PVA content increases, the mechanical properties are highly affected. The force versus displacement curves exhibits a spike/plateau in intermediate force values, which indicates a plastic failure/fracture. The corresponding curves and highly deformed needle tips seen on the SEM micrographs corroborate these results.

According to previous studies, the applied pressure necessary to penetrate the skin is around 0.08 and 3.04 N per needle, which are values that allow insertion by hand; since the microneedles prepared in this study show a mechanical resistance to pressure up to 0.1 N, it is possible to affirm that all SF/MNs are adequate for use as transdermal drug delivery devices (CAO, Yunteng et al., 2020; LUTTON et al., 2015; MAKVANDI et al., 2021; PATRAVALE; DANDEKAR; JAIN, 2012; RIPOLIN et al., 2017). However, it is evident that the SF/PVA ratio choice influences the microneedle strength. Higher content of PVA proportion causes a decrease in mechanical strength (Figure 38B). Accordingly, the strongest MNs were obtained when using only pure SF in methanol.

Figure 38- Mechanical property assessment of the prepared SF and PVA blend MN using a rheometer in compression mode to control the force and speed of compression or insertion: (a) the compression test using a rheometer to assess the failure forces of the prepared MN patches, (b) the insertion test to study the insertion force of the SF and PVA blend MN patches in porcine skin, (c) 2D cross-sectional OCT of microneedle arrays after their insertion in porcine skin, and (d) OCT images of the microneedle arrays for assessment of pore formation after microneedle insertion



5.2.7. *In vitro* Cytotoxicity Evaluation of MN Patches

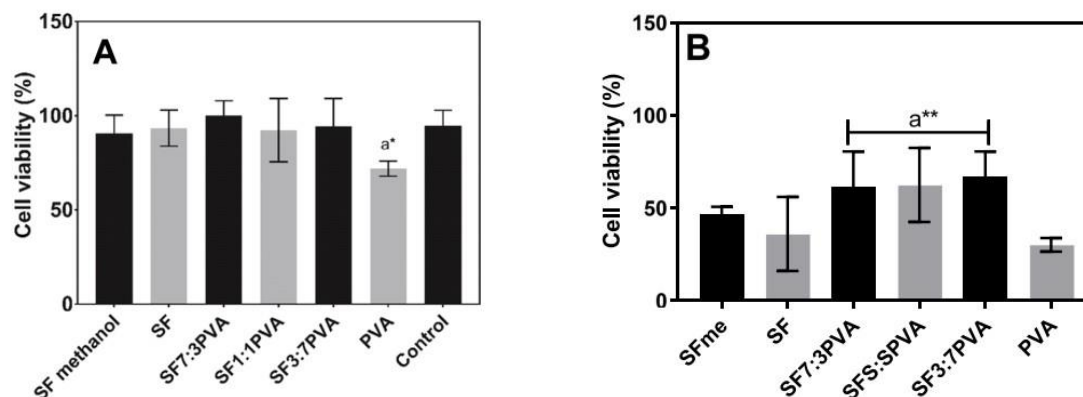
Any device designed for human or animal use must demonstrate low cytotoxicity or that the cytotoxicity is acceptable considering the benefit of the intended application. To satisfy regulatory requirements and be utilized in clinical applications, the prepared MNs were tested. After incubating SF/PVA microneedle patches with HaCaT cells for 24 h, the

cell viability was examined by MTT assays,^{74,75} and the results obtained are reported in Figure 39.

According to ISO 10993-5, materials that show percentages of cell viability above 80% are considered non-cytotoxic, and if the cell viability is 80–60%, the material is considered weakly cytotoxic; cell viability of 60–40% or below 40% are caused by materials with moderate and potent cytotoxicity, respectively. Cells viability assays were performed by using HaCat-keratinocytes and 3 T3-fibroblasts as models. Also, IL1- β and TNF- α levels were determined in 3 T3 cell cultures under the same conditions tested for the MTT reduction test.

Figure 39 displays the viability percentages for both cell lines. In general, the microneedles composed of the SF-PVA association presented above 75 and ~70% viability percentages for HaCat and 3 T3, respectively. Additionally, cytokine levels were lower than 31.5 pg/mL for TNF- α and 15.6 pg/mL for IL1- β , indicating that MNs are potential low-toxic materials for biomedical use. These results are in agreement with previous studies where SF and PVA microneedles and other materials like hydrogels and films are used for the delivery of drugs through the skin and demonstrate their low cytotoxicity (ALEXANDRE et al., 2014; GAO, Ya et al., 2019; KHALAJI; GOLSHAN EBRAHIMI; HOSSEINKHANI, 2021).

Figure 39- Effect of the MNs with a variable proportion of SF and PVA on (A) HaCaT keratinocytes and (B) 3 T3-fibroblasts viabilities after an incubation period of 24 h at 37 °C. Data are shown as mean \pm SD, n = 4. *p < 0.05 (unpaired t test)

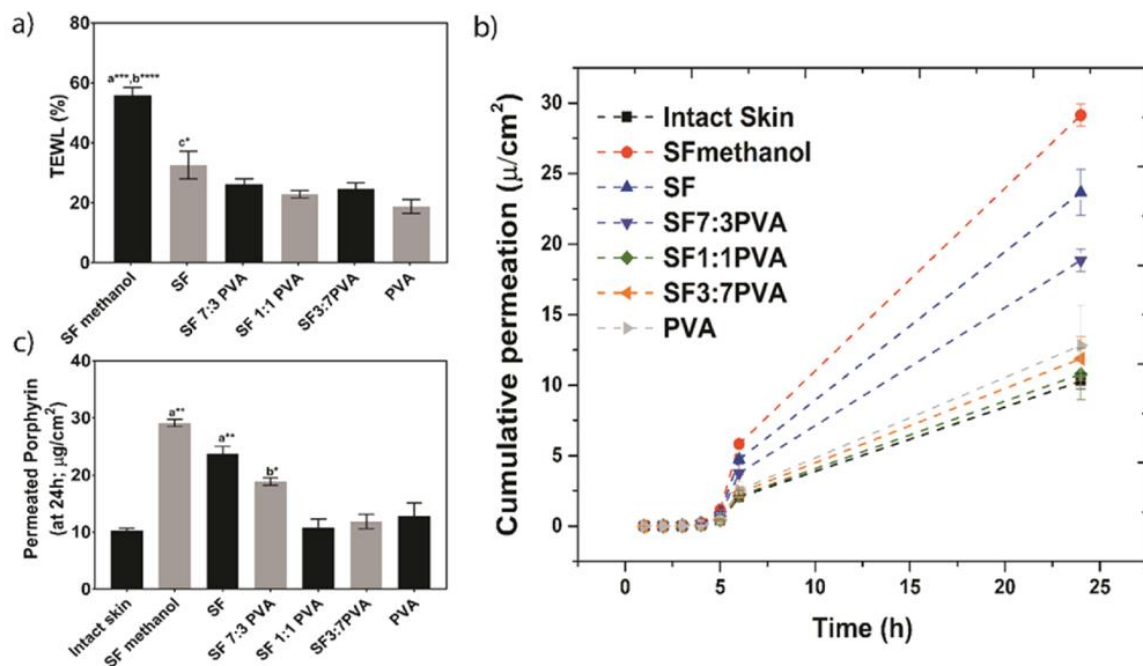


5.2.8. Porphyrin Cumulative Permeation across Porcine Ear Skin Treated with MNs

One of the main functions of the skin is to act as a protective barrier to the body. Its hydrophobic nature hinders the passage of large and hydrophilic molecules, reducing the effectiveness of treatments that depend on the transdermal route of administration.(AL SULAIMAN et al., 2019) To assess the potential of the SF/PVA microneedles as delivery vehicles for a large hydrophilic molecule, we studied the release profile of a water-soluble porphyrin across porcine skin. The transdermal delivery of porphyrins is of great interest for applications in photodynamic therapy as it would avoid the parenteral administration of photosensitizers.(KOU; DOU; YANG, 2017) In our study, 5- [4-(2-carboxyethanoyl) aminophenyl]-10,15,20-tris-(4-sulphonatophenyl) porphyrin trisodium was chosen for this study due to its water solubility and the aggregation properties displayed by porphyrins with a similar structure (ROJAS et al., 2019). The trans-epidermal water loss (TEWL) from porcine skin was measured before and after applying the microneedles to assess the skin barrier function. Ours results shows that the microneedles significantly increase the TEWL ($p < 0.01$ and $p < 0.05$), indicating that the pores formed can create drug permeation pathways across the skin, agreeing with the results reported here (Fifure 39a) (MAO et al., 2020; ZHOU et al., 2010).

These results agree with previous literature reports; for example, Liu et al. demonstrated that applying self-dissolving microneedle arrays fabricated from hyaluronic acid could pierce the skin, increasing the TEWL, turn to facilitate the delivery of relatively high molecular weight drugs.(CHEN, Mei Chin; LIN; LING, 2016; LIU, Shu et al., 2014) The porphyrin permeation with and without prior treatment with the microneedles was evaluated using full-thickness porcine skin in a Franz cell (Figure 41 b,c). The results show that the application of microneedles enhances the permeation compared with intact skin (Table 7).

Figure 40- Trans-epidermal water loss (TEWL) percentages and porphyrin permeation analyses. (a) Porcine skin TEWL before and after MN treatment and porphyrin permeation in untreated and treated full-thickness pork skin. Data were expressed as mean \pm SD ($n = 6$ /formulation). Statistical differences were a, intact skin vs SF methanol or SF, and b, intact skin vs SF 7:3 PVA. ** $p < 0.01$ and * $p < 0.05$. (b) Porphyrin cumulative permeation through full-thickness porcine skin after being treated with microneedle patches with different proportions of SF and PVA for 30 s. (c) Total amount of porphyrin permeated through pork skin at 24 h after being treated with microneedle patches with different proportions of SF and PVA



Notably, the high content of SF seems to be a crucial feature for the permeation enhancement, as skin treated with microneedles predominantly composed of PVA shows a permeation profile that is not too dissimilar from untreated skin (control). Those results can be explained by flow values obtained for intact skin ($0.99 \pm 0.38 \mu\text{g cm}^{-2} \text{ h}^{-1}$) and enhanced values after microneedle treatment with the different compositions of SF methanol ($2.8 \pm$

0.38 $\mu\text{g cm}^{-2} \text{ h}^{-1}$), SF ($2.3 \pm 0.88 \mu\text{g cm}^{-2} \text{ h}^{-1}$), and SF 7:3 PVA ($1.81 \pm 0.0.7 \mu\text{g cm}^2 \text{ h}1$) with $p < 0.01$ and $p < 0.05$, respectively. The permeation data align both with the results obtained in the mechanical strength and TEWL tests. The high content of SF in the needles leads to stronger needles and larger pores, which in turn causes higher TEWL and more efficient porphyrin penetration. Higher TEWL values are associated with damaged skin, while lower TEWL values indicate the integrity of the skin barrier or healthy skin.(LIU, Ting Ting; CHEN; WANG, 2018) This disturbance created by the application of the microneedles allows the porphyrin to penetrate the outer layers of the skin without interacting directly with them, thereby promoting a more efficient transdermal delivery regardless of its hydrophilic nature. Similar results have been reported in the literature where water-soluble molecules such as calcein and hydrophilic peptides have been delivered more efficiently using microneedles (OH et al., 2008; ZHANG, Suohui; QIU; GAO, 2014).

Table 7-Porphyrin Permeation Parameters across Intact and Microneedles treated Porcine Skin

microneedle compositions	flow ($\mu\text{g cm}^{-2} \text{ h}^{-1}$)
intact porcine skin	0.99 ± 0.38
SF methanol	2.8 ± 0.38
SF	2.3 ± 0.88
SF 7:3 PVA	$1.81 \pm 0.0.7$
SF 1:1 PVA	1.035 ± 0.3984
SF 3:7 PVA	1.141 ± 0.439
PVA	1.23 ± 0.4735

6. Conclusions

In this study, we developed two different scaffold formats for the controlled release of photosensitive molecules to improve their delivery for future applications in photodynamic therapy. We investigated the printability of 3D-printed hydrogels, which was found to depend on the choice of polymers and formulations used in their preparation. We studied eight formulations in total, four utilizing gelatin as the main component with varying concentrations of silk fibroin and four utilizing Pluronic F127 as the main component with different concentrations of silk fibroin incorporated within the structure. Our findings indicate that the gel behavior of the formulations is a critical factor in determining the printing parameters, and the addition of fibroin to the hydrogels significantly impacts their printability. Furthermore, the choice of the principal component of the hydrogel, whether it be gelatin or Pluronic, also affects the uniformity and printability of the resulting structures. Also, the addition of silk fibroin to the 3D scaffolds affects their compressive strength, with all hydrogel scaffolds showing decreased compression strength at higher SF concentrations.

The chosen scaffolds for the drug release assay were capable of releasing the photosensitive molecules within the structure after 30 minutes. We used different drug release models to explain the release dynamics of the hydrogels. The models that better explain the release of the photosensitive molecules from the hydrogel matrix were the first-order model for the Pluronic F127 (30%)/Alginate (2%)/SF(2%) and the Higuchi model for the gelatin (15%)/Alginate (2%)/SF(6%) hydrogels. This proves that the prepared 3D printed scaffolds can withstand compression forces and dissolve fast enough to deliver photosensitive molecules for future applications in photodynamic therapy.

Regarding the preparation and validation of silk fibroin microneedles, this study aimed to obtain SF microneedles with varying contents of PVA for transdermal delivery of porphyrins with potential applications in photodynamic therapy. The microneedles were characterized by their physicochemical and mechanical properties, as well as their

performance in terms of depth of penetration. The cytotoxicity of the material and its transdermal delivery were examined ex vivo using a Franz diffusion cell with porcine skin. The depth of penetration in a model membrane and full-thickness porcine skin was found to depend on the applied force rather than on the composition of the needles. In contrast, swelling and degradation were dictated by the relative content of SF/PVA. Finally, it was demonstrated that the application of the microneedles disturbs the skin barrier function enough to increase the TEWL and enhance the penetration of hydrophilic porphyrin through the skin. Overall, this study suggests that these hybrid SF and PVA microneedle arrays can potentially improve the transdermal delivery of photosensitizing molecules in future photodynamic therapy applications.

7. References

ABBASI, Asma Riaz et al. Bioinspired sodium alginate based thermosensitive hydrogel membranes for accelerated wound healing. **International Journal of Biological Macromolecules**, v. 155, p. 751–765, 2020. Disponível em: <<https://doi.org/10.1016/j.ijbiomac.2020.03.248>>.

ABDULLAH, Zainab Waheed; DONG, Yu. Biodegradable and water resistant poly(vinyl) alcohol (PVA)/starch (ST)/glycerol (GL)/halloysite nanotube (HNT) nanocomposite films for sustainable food packaging. **Frontiers in Materials**, v. 6, p. 1–17, 2019.

ABRAHAMSE, Heidi; HAMBLIN, Michael R. New photosensitizers for photodynamic therapy. **Biochemical Journal**, v. 473, n. 4, p. 347–364, 2017.

AHMED, Lina et al. Study the Using of Nanoparticles as Drug Delivery System Based on Mathematical Models for Controlled Release. **International Journal of Latest Technology in Engineering, Management & Applied Science**, v. 8, n. 5, p. 52–56, 2019. Disponível em: <www.ijltemas.in>.

AIRES-FERNANDES, Mariza et al. Development of Biotechnological Photosensitizers for Photodynamic Therapy: Cancer Research and Treatment—From Benchtop to Clinical Practice. **Molecules**, v. 27, n. 20, 2022.

AL SULAIMAN, Dana et al. Hydrogel-Coated Microneedle Arrays for Minimally Invasive Sampling and Sensing of Specific Circulating Nucleic Acids from Skin Interstitial Fluid. **ACS**

Nano, v. 13, n. 8, p. 9620–9628, 2019.

ALEXANDRE, Nuno et al. Biocompatibility and hemocompatibility of polyvinyl alcohol hydrogel used for vascular grafting - *In vitro* and *in vivo* studies. **Journal of Biomedical Materials Research - Part A**, v. 102, n. 12, p. 4262–4275, 2014.

ANDRONESCU, Ecaterina; GRUMEZESCU, Alexandru Mihai. **Nanostructures in Therapeutic Medicine Series Nanostructures for Drug Delivery**. [S.l.: s.n.], 2017.

ASAKURA, Tetsuo; OKUSHITA, Keiko; WILLIAMSON, Mike P. Analysis of the structure of Bombyx mori silk fibroin by NMR. **Macromolecules**, v. 48, n. 8, p. 2345–2357, 2015.

ASHAMMAKHI, N. et al. Bioinks and bioprinting technologies to make heterogeneous and biomimetic tissue constructs. **Materials Today Bio**, v. 1, n. May, 2019.

AVCIL, Muhammet et al. Efficacy of bioactive peptides loaded on hyaluronic acid microneedle patches: A monocentric clinical study. **Journal of Cosmetic Dermatology**, v. 19, n. 2, p. 328–337, 2020.

BADILLO-SANCHEZ, Diego et al. Understanding the structural degradation of South American historical silk: A Focal Plane Array (FPA) FTIR and multivariate analysis. **Scientific Reports**, v. 9, n. 1, p. 1–10, 2019.

BAILEY, Kevin. **Potential Applications of Silk Fibroin as a Biomaterial**. 2013. 2013.

BARBUGLI, Paula A. et al. **Photodynamic therapy utilizing liposomal CLALPc in human melanoma 3D cell cultures**. **Experimental Dermatology**. [S.l.: s.n.], 2015

BARIYA, Shital H et al. Microneedles : an emerging transdermal drug. p. 11–29, 2012.

BARRY, B. W. Novel mechanisms and devices to enable successful transdermal drug delivery. **European Journal of Pharmaceutical Sciences**, v. 14, n. 2, p. 101–114, 2001.

BITTNER, Sean M et al. Swelling Behaviors of 3D Printed Hydrogel and Hydrogel-Microcarrier Composite Scaffolds. **Tissue Engineering Part A**, v. 27, n. 11–12, p. 665–678, 20 jan. 2021. Disponível em: <<https://doi.org/10.1089/ten.tea.2020.0377>>.

BLOUT, Elkan R; KARPLUS, Robert. The Infrared Spectrum of Polyvinyl Alcohol. **Journal of the American Chemical Society**, v. 70, n. 2, p. 862–864, 1 fev. 1948. Disponível em: <<https://doi.org/10.1021/ja01182a504>>.

BORA, Pushpak; KUMAR, Lokesh; BANSAL, Arvind K. Microneedle Technology for Advanced Drug Delivery : Evolving vistas. **Crips**, v. 9, n. 1, p. 7–10, 2008.

BOULET-AUDET, Maxime; VOLLRATH, Fritz; HOLLAND, Chris. Identification and classification of silks using infrared spectroscopy. **Journal of Experimental Biology**, v. 218, n. 19, p. 3138–3149, 2015.

CAFFAREL-SALVADOR, Ester et al. Methylene blue-loaded dissolving microneedles: Potential use in photodynamic antimicrobial chemotherapy of infected wounds. **Pharmaceutics**, Analisis con lector de placa, v. 7, n. 4, p. 397–412, 2015.

- CALIARI, Steven R.; BURDICK, Jason A. A practical guide to hydrogels for cell culture. **Nature Methods**, v. 13, n. 5, p. 405–414, 2016.
- CALÓ, Enrica; KHUTORYANSKIY, Vitaliy V. Biomedical applications of hydrogels: A review of patents and commercial products. **European Polymer Journal**, v. 65, p. 252–267, 2015.
- CAO, Shi Lei; ZHANG, Qi Zhi; JIANG, Xin Guo. Preparation of ion-activated in situ gel systems of scopolamine hydrobromide and evaluation of its antinotion sickness efficacy. **Acta Pharmacologica Sinica**, v. 28, n. 4, p. 584–590, 2007.
- CAO, Yunteng et al. Precision Delivery of Multiscale Payloads to Tissue-Specific Targets in Plants. **Advanced Science**, v. 1903551, 2020.
- CARBINATTO, Fernanda M. et al. Insights into the swelling process and drug release mechanisms from cross-linked pectin/high amylose starch matrices. **Asian Journal of Pharmaceutical Sciences**, v. 9, n. 1, p. 27–34, 2014.
- CARVALHO, Cristiana R. et al. Tunable Enzymatically Cross-Linked Silk Fibroin Tubular Conduits for Guided Tissue Regeneration. **Advanced Healthcare Materials**, v. 7, n. 17, p. 1–15, 2018.
- CATOIRA, Marta Calvo et al. Overview of natural hydrogels for regenerative medicine applications. **Journal of Materials Science: Materials in Medicine**, v. 30, n. 10, 2019. Disponível em: <<http://dx.doi.org/10.1007/s10856-019-6318-7>>.
- CHANG, Hao et al. Advances in the Formulations of Microneedles for Manifold Biomedical Applications. **Advanced Materials Technologies**, v. 5, n. 4, p. 1–19, 2020.
- CHANG, Kai-Chi et al. Characterization of Genipin-Crosslinked Gelatin/Hyaluronic Acid-Based Hydrogel Membranes and Loaded with Hinokitiol: *In vitro* Evaluation of Antibacterial Activity and Biocompatibility. **Materials Science & Engineering. C, Materials for Biological Applications**, v. 105, p. 110074, dez. 2019.
- CHARU VEPARI; DAVID L. KAPLAN. Silk as Biomaterial. **Progress in Polymer Science**, v. 100, n. 2, p. 130–134, 2007.
- CHATTERJEE, Sudipta et al. Dual-responsive (pH/temperature) Pluronic F-127 hydrogel drug delivery system for textile-based transdermal therapy. **Scientific Reports**, v. 9, n. 1, p. 1–13, 2019.
- CHEN, Biao Qi et al. Investigation of silk fibroin nanoparticle-decorated poly(L-lactic acid) composite scaffolds for osteoblast growth and differentiation. **International Journal of Nanomedicine**, v. 12, p. 1877–1890, 2017.
- CHEN, Huabing et al. Polyion Complex Vesicles for Photoinduced Intracellular Delivery of Amphiphilic Photosensitizer. **Journal of the American Chemical Society**, v. 136, n. 1, p. 157–163, 8 jan. 2014. Disponível em: <<https://doi.org/10.1021/ja406992w>>.
- CHEN, Mei Chin; LIN, Zhi Wei; LING, Ming Hung. Near-infrared light-activatable microneedle system for treating superficial tumors by combination of chemotherapy and

photothermal therapy. **ACS Nano**, v. 10, n. 1, p. 93–101, 2016.

CHEN, Wei et al. Microneedle-array patches loaded with dual mineralized protein/peptide particles for type 2 diabetes therapy. **Nature Communications**, v. 8, n. 1, 2017. Disponível em: <<http://dx.doi.org/10.1038/s41467-017-01764-1>>.

CHENG, Baochang et al. Cooperative Assembly of a Peptide Gelator and Silk Fibroin Afford an Injectable Hydrogel for Tissue Engineering. **ACS Applied Materials and Interfaces**, v. 10, n. 15, p. 12474–12484, 2018.

CHENG, Yuan et al. On the strength of β -sheet crystallites of Bombyx mori silk fibroin. **Journal of The Royal Society Interface**, v. 11, n. 96, 2014.

CHIVERS, Phillip R A; SMITH, David K. Shaping and structuring supramolecular gels. **Nature Reviews Materials**, v. 4, n. 7, p. 463–478, 2019. Disponível em: <<https://doi.org/10.1038/s41578-019-0111-6>>.

CORREIA, José H. et al. Photodynamic therapy review: Principles, photosensitizers, applications, and future directions. **Pharmaceutics**, v. 13, n. 9, p. 1–16, 2021.

DAS, Merina Paul et al. Extraction and Characterization of Gelatin: a Functional Biopolymer. **International Journal of Pharmacy and Pharmaceutical Sciences**, v. 9, n. 9, p. 239, 2017.

DEBARI, Megan K. et al. Silk Fibroin as a Green Material. **ACS Biomaterials Science and Engineering**, v. 7, n. 8, p. 3530–3544, 2021.

DENG, Yan et al. Transdermal Delivery of siRNA through Microneedle Array. **Scientific Reports**, v. 6, n. October 2015, p. 1–8, 2016.

DERVISEVIC, Muamer et al. Skin in the diagnostics game: Wearable biosensor nano- and microsystems for medical diagnostics. **Nano Today**, v. 30, p. 100828, 2020. Disponível em: <<https://doi.org/10.1016/j.nantod.2019.100828>>.

DILLON, Colin et al. Formulation and characterisation of dissolving microneedles for the transdermal delivery of therapeutic peptides. **International Journal of Pharmaceutics**, v. 526, n. 1–2, p. 125–136, 2017. Disponível em: <<http://dx.doi.org/10.1016/j.ijpharm.2017.04.066>>.

DONDERWINKEL, Ilze; VAN HEST, Jan C M; CAMERON, Neil R. Bio-inks for 3D bioprinting: recent advances and future prospects. **Polymer Chemistry**, v. 8, n. 31, p. 4451–4471, 2017. Disponível em: <<http://dx.doi.org/10.1039/C7PY00826K>>.

DONNELLY, Ryan F. et al. Hydrogel-forming microneedles prepared from “super swelling” polymers combined with lyophilised wafers for transdermal drug delivery. **PLoS ONE**, v. 9, n. 10, 2014.

DOU, Qingqing; ABDUL KARIM, Anis; LOH, Xian Jun. Modification of Thermal and Mechanical Properties of PEG-PPG-PEG Copolymer (F127) with MA-POSS. **Polymers**, v. 8, n. 9, set. 2016.

DU, Guangsheng et al. Intradermal vaccination with hollow microneedles: A comparative study of various protein antigen and adjuvant encapsulated nanoparticles. **Journal of Controlled Release**, v. 266, n. September, p. 109–118, 2017. Disponível em: <<https://doi.org/10.1016/j.jconrel.2017.09.021>>.

DUNN, Alan M. et al. **Nanostructures for Drug Delivery. Proceedings of the 20th USENIX Security Symposium**. [S.l: s.n.], 2011

DUTTA, Sayan Deb et al. 3D-printed bioactive and biodegradable hydrogel scaffolds of alginate/gelatin/cellulose nanocrystals for tissue engineering. **International Journal of Biological Macromolecules**, v. 167, n. December 2020, p. 644–658, 2021.

ERIN C. DOWD, M.D.A, MICHAEL J. FRANK, PH.D.B, ANNE COLLINS, PH.D.C, JAMES M. GOLDD, AND DEANNA M. BARCH, Ph.D.e. A Microneedle Patch Containing Measles Vaccine is Immunogenic in Non-human Primates. **Physiology & Behavior**, v. 176, n. 12, p. 139–148, 2017.

ESTER-BRIDGED, Rheological Behavior et al. Effect of the Cross-Linking Density on the Swelling. 2021.

FEDIČ, Robert; ŽUROVEC, Michal; SEHNAL, František. Correlation between fibroin amino acid sequence and physical silk properties. **Journal of Biological Chemistry**, v. 278, n. 37, p. 35255–35264, 2003.

FU, Sai; YU, Hua. Redox-sensitive Pluronic F127-tocopherol micelles : synthesis , characterization , and cytotoxicity evaluation. p. 2635–2644, 2017.

GAO, Jie et al. Simultaneous detection of glucose, uric acid and cholesterol using flexible microneedle electrode array-based biosensor and multi-channel portable electrochemical analyzer. **Sensors and Actuators, B: Chemical**, v. 287, n. January, p. 102–110, 2019. Disponível em: <<https://doi.org/10.1016/j.snb.2019.02.020>>.

GAO, Ya et al. Highly Porous Silk Fibroin Scaffold Packed in PEGDA/Sucrose Microneedles for Controllable Transdermal Drug Delivery. **Biomacromolecules**, % porosity volumen displacement method, v. 20, n. 3, p. 1334–1345, 2019.

GHORBANI, Jaber et al. Photosensitizers in Antibacterial Photodynamic Therapy: An Overview. **Laser Therapy**, v. 27, n. 4, p. 293–302, dez. 2018.

GIOFFREDI, Emilia et al. Pluronic F127 Hydrogel Characterization and Biofabrication in Cellularized Constructs for Tissue Engineering Applications. **Procedia CIRP**, v. 49, n. iii, p. 125–132, 2016. Disponível em: <<http://dx.doi.org/10.1016/j.procir.2015.11.001>>.

GITTARD, Shaun D. et al. The effects of geometry on skin penetration and failure of polymer microneedles. **Journal of Adhesion Science and Technology**, v. 27, n. 3, p. 227–243, 2013.

GODIYA, Chirag B. et al. Silk fibroin/polyethylenimine functional hydrogel for metal ion adsorption and upcycling utilization. **Journal of Environmental Chemical Engineering**, v. 7,

n. 1, p. 102806, 2019. Disponível em: <<https://doi.org/10.1016/j.jece.2018.11.050>>.

GOUD, K. Yugender et al. Wearable Electrochemical Microneedle Sensor for Continuous Monitoring of Levodopa: Toward Parkinson Management. **ACS Sensors**, v. 4, n. 8, p. 2196–2204, 2019.

GU, Zeming et al. Development of 3D bioprinting: From printing methods to biomedical applications. **Asian Journal of Pharmaceutical Sciences**, v. 15, n. 5, p. 529–557, 2020. Disponível em: <<https://doi.org/10.1016/j.ajps.2019.11.003>>.

GUNAYDIN, Gurcan; GEDIK, M. Emre; AYAN, Seylan. Photodynamic Therapy—Current Limitations and Novel Approaches. **Frontiers in Chemistry**, v. 9, n. June, p. 1–25, 2021.

GYLES, Desireé Alesa et al. A review of the designs and prominent biomedical advances of natural and synthetic hydrogel formulations. **European Polymer Journal**, v. 88, p. 373–392, 2017. Disponível em: <<https://www.sciencedirect.com/science/article/pii/S0014305716312502>>.

HAN, Tae Y. et al. Facial skin barrier function recovery after microneedle transdermal delivery treatment. **Dermatologic Surgery**, Must read , for real, v. 38, n. 11, p. 1816–1822, 2012.

HARRIS, Adam G.; NAIDOO, Catherine; MURRELL, Dedee F. Skin needling as a treatment for acne scarring: An up-to-date review of the literature. **International Journal of Women's Dermatology**, v. 1, n. 2, p. 77–81, 2015. Disponível em: <<http://dx.doi.org/10.1016/j.ijwd.2015.03.004>>.

HENRY, Sebastien et al. Microfabricated microneedles: A novel approach to transdermal drug delivery. **Journal of Pharmaceutical Sciences**, v. 87, n. 8, p. 922–925, 1998.

HEREDIA, Nathaly S. et al. Comparative statistical analysis of the release kinetics models for nanoprecipitated drug delivery systems based on poly(lactic-co-glycolic acid). **PLoS ONE**, v. 17, n. 3 March, p. 1–28, 2022.

HO, Tzu-Chuan et al. Hydrogels: Properties and Applications in Biomedicine. **Molecules (Basel, Switzerland)**, v. 27, n. 9, maio 2022.

HONG, Ji Yeon et al. Efficacy and safety of a novel, soluble microneedle patch for the improvement of facial wrinkle. **Journal of Cosmetic Dermatology**, v. 17, n. 2, p. 235–241, 2018.

HUANG, Xing et al. A highly biocompatible bio-ink for 3D hydrogel scaffolds fabrication in the presence of living cells by two-photon polymerization. **European Polymer Journal**, v. 153, n. May, p. 110505, 2021. Disponível em: <<https://doi.org/10.1016/j.eurpolymj.2021.110505>>.

ILIESCU, Florina Silvia. A Review on Transdermal Drug Delivery Using Microneedles : Current Research and Perspective. n. November, 2014.

INDERMUN, Sunaina et al. Current advances in the fabrication of microneedles for

transdermal delivery. **Journal of Controlled Release**, v. 185, n. 1, p. 130–138, 2014. Disponível em: <<http://dx.doi.org/10.1016/j.jconrel.2014.04.052>>.

IOELE, Giuseppina et al. Photosensitive Drugs: A Review on Their Photoprotection by Liposomes and Cyclodextrins. **Drug Delivery**, v. 24, n. sup1, p. 33–44, dez. 2017.

JAIN, Naman; SINGH, Vinay Kumar; CHAUHAN, Sakshi. A review on mechanical and water absorption properties of polyvinyl alcohol based composites/films. **Journal of the Mechanical Behavior of Materials**, v. 26, n. 5–6, p. 213–222, 2017.

JANG, M. et al. Dissolving microneedle with high molecular weight hyaluronic acid to improve skin wrinkles, dermal density and elasticity. **International Journal of Cosmetic Science**, v. 42, n. 3, p. 302–309, 2020.

JAUZEIN, Vincent; COLOMBAN, Philippe. Types, structure and mechanical properties of silk. **Handbook of Tensile Properties of Textile and Technical Fibres**, p. 144–178, 2009.

JEON, Eun Young et al. Bio-inspired swellable hydrogel-forming double-layered adhesive microneedle protein patch for regenerative internal/external surgical closure. **Biomaterials**, v. 222, n. August, p. 119439, 2019. Disponível em: <<https://doi.org/10.1016/j.biomaterials.2019.119439>>.

JIANG, Teng; ZHOU, Ping. Environment-Induced Silk Fibroin Conformation Based on the Magnetic Resonance Spectroscopy. **On Biomimetics**, 2011.

JOHARI, Narges; MORONI, Lorenzo; SAMADIKUCHAKSARAEI, Ali. Tuning the conformation and mechanical properties of silk fibroin hydrogels. **European Polymer Journal**, v. 134, n. February, p. 109842, 2020. Disponível em: <<https://doi.org/10.1016/j.eurpolymj.2020.109842>>.

JOSEPH, Baby; RAJ, S Justin. Frontiers in Life Science Therapeutic applications and properties of silk proteins from Bombyx mori. v. 3769, 2013.

KAPUSTA, Oliwia et al. Antimicrobial Natural Hydrogels in Biomedicine: Properties, Applications, and Challenges—A Concise Review. **International Journal of Molecular Sciences**, v. 24, n. 3, 2023.

KEARNEY, Mary Carmel et al. Potential of microneedles in enhancing delivery of photosensitising agents for photodynamic therapy. **Photodiagnosis and Photodynamic Therapy**, v. 11, n. 4, p. 459–466, 2014. Disponível em: <<http://dx.doi.org/10.1016/j.pdpdt.2014.09.003>>.

KHALAJI, Saeideh; GOLSHAN EBRAHIMI, Nadereh; HOSSEINKHANI, Hossein. Enhancement of biocompatibility of PVA/HTCC blend polymer with collagen for skin care application. **International Journal of Polymeric Materials and Polymeric Biomaterials**, v. 70, n. 7, p. 459–468, 2021. Disponível em: <<https://doi.org/10.1080/00914037.2020.1725761>>.

KHAN, M.M.R.; TSUKADA, M. **Silk Biomater. Tissue Eng. Regen. Med.** [S.l: s.n.], 2014.

KIM, Hyun Ju et al. Effect of degumming methods on structural characteristics and

properties of regenerated silk. **International Journal of Biological Macromolecules**, v. 104, p. 294–302, 2017.

KIM, Min Hee et al. Silk fibroin/hydroxyapatite composite hydrogel induced by gamma-ray irradiation for bone tissue engineering. **Biomaterials Research**, v. 21, n. 1, p. 111–119, 2017.

KIM, Soon Hee et al. **3D bioprinted silk fibroin hydrogels for tissue engineering. Nature Protocols**. [S.l: s.n.], 2021

KIM, Yeu-chun; PARK, Jung-hwan; PRAUSNITZ, Mark R. Microneedles for drug and vaccine delivery ☆. **Advanced Drug Delivery Reviews**, v. 64, n. 14, p. 1547–1568, 2012.

KIM, Yujin et al. Fabrication and characterization of hyaluronic acid microneedles to enhance delivery of magnesium ascorbyl phosphate into skin. **Biomedical Microdevices**, v. 21, n. 4, p. 1–9, 2019.

KOCHHAR, Jaspreet Singh et al. simple method of microneedle array fabrication for transdermal drug delivery. v. 39, n. March 2012, p. 299–309, 2013.

KOH, Leng Duei et al. Advancing the frontiers of silk fibroin protein-based materials for futuristic electronics and clinical wound-healing (Invited review). **Materials Science and Engineering C**, v. 86, n. August 2017, p. 151–172, 2018. Disponível em: <<https://doi.org/10.1016/j.msec.2018.01.007>>.

_____. Structures, mechanical properties and applications of silk fibroin materials. **Progress in Polymer Science**, v. 46, p. 86–110, 2015. Disponível em: <<http://dx.doi.org/10.1016/j.progpolymsci.2015.02.001>>.

KOKOL, Vanja et al. Rheological properties of gelatine hydrogels affected by flow- and horizontally-induced cooling rates during 3D cryo-printing. **Colloids and Surfaces A: Physicochemical and Engineering Aspects**, v. 616, 2021.

KOU, Jiayuan; DOU, Dou; YANG, Liming. Porphyrin photosensitizers in photodynamic therapy and its applications. **Oncotarget**, v. 8, n. 46, p. 81591–81603, 2017.

KUNDU, Joydip et al. Silk fibroin/poly(vinyl alcohol) photocrosslinked hydrogels for delivery of macromolecular drugs. **Acta Biomaterialia**, v. 8, n. 5, p. 1720–1729, 2012.

KUO, Catherine K.; MA, Peter X. Ionically crosslinked alginate hydrogels as scaffolds for tissue engineering: Part 1. Structure, gelation rate and mechanical properties. **Biomaterials**, GDL for gelification, v. 22, n. 6, p. 511–521, 2001.

KWIATKOWSKI, Stanisław et al. Photodynamic therapy – mechanisms, photosensitizers and combinations. **Biomedicine & Pharmacotherapy**, v. 106, p. 1098–1107, 2018. Disponível em: <<https://www.sciencedirect.com/science/article/pii/S0753332218341611>>.

LANDA, R F et al. Microneedle arrays as transdermal and intradermal drug delivery systems : Materials science , manufacture and commercial development. 2016.

LANGER, Mark R Prausnitz & Robert. Transdermal drug delivery. **nature biotechnology**, v. 4, n. 10, p. 1235–1238, 2008.

LARRAÑETA, Eneko; RAGHU, Thakur; SINGH, Raj. Microneedle Manufacturing and Testing. 2018.

LAWRENCE, Brian D. et al. Effect of hydration on silk film material properties. **Macromolecular Bioscience**, Water aniling y trataminetos con metanol, v. 10, n. 4, p. 393–403, 2010.

LEE, I.-Chi et al. Fabrication of a novel partially dissolving polymer microneedle patch for transdermal drug delivery. **Journal of Materials Chemistry B**, v. 3, n. 2, p. 276–285, 2015. Disponível em: <<http://dx.doi.org/10.1039/C4TB01555J>>.

LEE, I. Chi et al. Fabrication of a novel partially dissolving polymer microneedle patch for transdermal drug delivery. **Journal of Materials Chemistry B**, v. 3, n. 2, p. 276–285, 2015. Disponível em: <<http://dx.doi.org/10.1039/C4TB01555J>>.

LEE, Jeong Woo; HAN, Mee Ree; PARK, Jung Hwan. Polymer microneedles for transdermal drug delivery. **Journal of Drug Targeting**, v. 21, n. 3, p. 211–223, 2013.

LEE, Ji Yong et al. Rapid and repeatable fabrication of high A/R silk fibroin microneedles using thermally-drawn micromolds. **European Journal of Pharmaceutics and Biopharmaceutics**, MEthanol treatment, v. 94, n. May, p. 11–19, 2015. Disponível em: <<http://dx.doi.org/10.1016/j.ejpb.2015.04.024>>.

LI, Qingtao et al. 3D printed silk-gelatin hydrogel scaffold with different porous structure and cell seeding strategy for cartilage regeneration. **Bioactive Materials**, Poropsity, v. 6, n. 10, p. 3396–3410, 2021. Disponível em: <<https://doi.org/10.1016/j.bioactmat.2021.03.013>>.

LI, Xiaomeng et al. Functional hydrogels with tunable structures and properties for tissue engineering applications. **Frontiers in Chemistry**, v. 6, n. OCT, p. 1–20, 2018.

LI, Yijie et al. Peptide-based supramolecular photodynamic therapy systems: From rational molecular design to effective cancer treatment. **Chemical Engineering Journal**, v. 436, p. 135240, 2022. Disponível em: <<https://www.sciencedirect.com/science/article/pii/S1385894722007458>>.

LIM, Seng Han et al. Enhanced Skin Permeation of Anti-wrinkle Peptides via Molecular Modification. **Scientific Reports**, v. 8, n. 1, p. 1–11, 2018. Disponível em: <<http://dx.doi.org/10.1038/s41598-017-18454-z>>.

LIN, Shiqi et al. Strategy for hypertrophic scar therapy: Improved delivery of triamcinolone acetonide using mechanically robust tip-concentrated dissolving microneedle array. **Journal of Controlled Release**, v. 306, n. May, p. 69–82, 2019. Disponível em: <<https://doi.org/10.1016/j.jconrel.2019.05.038>>.

LING, Shengjie et al. FTIR imaging, a useful method for studying the compatibility of silk

fibroin-based polymer blends. **Polymer Chemistry**, v. 4, n. 21, p. 5401–5406, 2013.

LISIK, Anna; MUSIAŁ, Witold. Conductometric evaluation of the release kinetics of active substances from pharmaceutical preparations containing iron ions. **Materials**, v. 12, n. 5, 2019.

LIU, Bin et al. Silk structure and degradation. **Colloids and Surfaces B: Biointerfaces**, v. 131, p. 122–128, 2015. Disponível em: <<http://dx.doi.org/10.1016/j.colsurfb.2015.04.040>>.

LIU, Li; ZHANG, Song; HUANG, Jun Yi. Progress in modification of silk fibroin fiber. **Science China Technological Sciences**, v. 62, n. 6, p. 919–930, 2019.

LIU, Qiang; LIU, Haifeng; FAN, Yubo. Preparation of silk fibroin carriers for controlled release. **Microscopy Research and Technique**, v. 80, n. 3, p. 312–320, 2017.

LIU, Shu et al. Transdermal delivery of relatively high molecular weight drugs using novel self-dissolving microneedle arrays fabricated from hyaluronic acid and their characteristics and safety after application to the skin. **European Journal of Pharmaceutics and Biopharmaceutics**, v. 86, n. 2, p. 267–276, 2014. Disponível em: <<http://dx.doi.org/10.1016/j.ejpb.2013.10.001>>.

LIU, Ting Ting; CHEN, Kai; WANG, Qiao. Skin drug permeability and safety through a vibrating solid micro-needle system. **Drug Delivery and Translational Research**, v. 8, n. 5, p. 1025–1033, 2018.

LUTTON, Rebecca E.M. et al. Microneedle characterisation: the need for universal acceptance criteria and GMP specifications when moving towards commercialisation. **Drug Delivery and Translational Research**, v. 5, n. 4, p. 313–331, 2015.

MADDUMA-BANDARAGE, Ujith S K; MADIHALLY, Sundararajan V. Synthetic hydrogels: Synthesis, novel trends, and applications. **Journal of Applied Polymer Science**, v. 138, n. 19, p. 50376, 15 maio 2021. Disponível em: <<https://doi.org/10.1002/app.50376>>.

MAKVANDI, Pooyan et al. Engineering Microneedle Patches for Improved Penetration: Analysis, Skin Models and Factors Affecting Needle Insertion. **Nano-Micro Letters**, v. 13, n. 1, 2021. Disponível em: <<https://doi.org/10.1007/s40820-021-00611-9>>.

MALEKMOHAMMADI, Samira et al. Smart and biomimetic 3d and 4d printed composite hydrogels: Opportunities for different biomedical applications. **Biomedicines**, v. 9, n. 11, p. 1–46, 2021.

MAO, Jinzhu et al. Transdermal delivery of rapamycin with poor water-solubility by dissolving polymeric microneedles for anti-angiogenesis. **Journal of Materials Chemistry B**, v. 8, n. 5, p. 928–934, 2020.

MEINEL, L. et al. Silk-based biomaterials. **Bone**, v. 24, n. 4, p. 401–416, 2003.

MEINEL, Lorenz et al. The inflammatory responses to silk films *in vitro* and *in vivo*. **Biomaterials**, v. 26, p. 147–155, 2005.

MFOUO-TYNGA, Ivan S et al. Features of third generation photosensitizers used in anticancer photodynamic therapy: Review. **Photodiagnosis and Photodynamic Therapy**, v. 34, p. 102091, 2021. Disponível em: <<https://www.sciencedirect.com/science/article/pii/S1572100020304452>>.

MIGDADI, Eman M. et al. Hydrogel-forming microneedles enhance transdermal delivery of metformin hydrochloride. **Journal of Controlled Release**, Importante diagrama, v. 285, n. February, p. 142–151, 2018. Disponível em: <<https://doi.org/10.1016/j.jconrel.2018.07.009>>.

MILLER, Philip R.; NARAYAN, Roger J.; POLSKY, Ronen. Microneedle-based sensors for medical diagnosis. **Journal of Materials Chemistry B**, v. 4, n. 8, p. 1379–1383, 2016.

MOHANKUMAR, B S et al. Hydrogels: potential aid in tissue engineering—a review. **Polymer Bulletin**, v. 79, n. 9, p. 7009–7039, 2022. Disponível em: <<https://doi.org/10.1007/s00289-021-03864-x>>.

MORE, S; GHADGE, T; DHOLE, S. Microneedle : an Advanced Technique in Transdermal Drug Delivery System. **Asian J. Res. Pharm. Sci**, v. 3, n. 3, p. 141–148, 2013.

MOREIRA, André F. et al. Microneedle-based delivery devices for cancer therapy: A review. **Pharmacological Research**, v. 148, n. August, p. 104438, 2019. Disponível em: <<https://doi.org/10.1016/j.phrs.2019.104438>>.

MÜLLER-HERRMANN, Susanne; SCHEIBEL, Thomas. Enzymatic Degradation of Films, Particles, and Nonwoven Meshes Made of a Recombinant Spider Silk Protein. **ACS Biomaterials Science and Engineering**, v. 1, n. 4, p. 247–259, 2015.

MURPHY, Amanda R.; KAPLAN, David L. Biomedical applications of chemically-modified silk fibroin. **Journal of Materials Chemistry**, v. 19, n. 36, p. 6443–6450, 2009.

MUYONGA, J H; COLE, C G B; DUODU, K G. Fourier transform infrared (FTIR) spectroscopic study of acid soluble collagen and gelatin from skins and bones of young and adult Nile perch (*Lates niloticus*). **Food Chemistry**, v. 86, n. 3, p. 325–332, 2004. Disponível em: <<https://www.sciencedirect.com/science/article/pii/S0308814603004588>>.

NAGHIEH, Saman; CHEN, Xiongbiao. Printability—A key issue in extrusion-based bioprinting. **Journal of Pharmaceutical Analysis**, v. 11, n. 5, p. 564–579, 2021. Disponível em: <<https://doi.org/10.1016/j.jpha.2021.02.001>>.

NAIDOO, Anushka et al. Impact of silk biomaterial structure on proteolysis. **Acta Biomaterialia**, v. 19, p. 161–169, 2015.

NGWULUKA, Ndidi et al. Comparative rheological characterization of two natural polymers from *Sesamum radiatum* and *bombax buonopozense* for application in drug delivery. **Macromolecular Symposia**, v. 345, n. 1, p. 51–58, 2014.

NISHIGUCHI, Akihiro et al. In Situ 3D-Printing using a Bio-ink of Protein–photosensitizer Conjugates for Single-cell Manipulation. **ACS Applied Bio Materials**, v. 3, n. 4, p. 2378–

2384, 20 abr. 2020. Disponível em: <<https://doi.org/10.1021/acsabm.0c00116>>.

NOGUEIRA, Grinia Michelle et al. Hydrogels from silk fibroin metastable solution: Formation and characterization from a biomaterial perspective. **Materials Science and Engineering C**, v. 31, n. 5, p. 997–1001, 2011. Disponível em: <<http://dx.doi.org/10.1016/j.msec.2011.02.019>>.

NORIOKA, Chisa et al. A universal method to easily design tough and stretchable hydrogels. **NPG Asia Materials**, v. 13, n. 1, 2021.

NULTSCH, Kira et al. Effects of Silk Degumming Process on Physicochemical, Tensile, and Optical Properties of Regenerated Silk Fibroin. **Macromolecular Materials and Engineering**, v. 303, n. 12, p. 1–10, 2018.

OGUNDELE, M; OKAFOR, H. Transdermal Drug Delivery: Microneedles, Their Fabrication and Current Trends in Delivery Methods. **Journal of Pharmaceutical Research International**, v. 18, n. 5, p. 1–14, 2017.

OH, Jae Ho et al. Influence of the delivery systems using a microneedle array on the permeation of a hydrophilic molecule, calcein. **European Journal of Pharmaceutics and Biopharmaceutics**, v. 69, n. 3, p. 1040–1045, 2008.

PAARAKH, M Padmaa et al. Release Kinetics – Concepts and Applications. **International Journal of Pharmacy Research & Technology**, v. 8, n. 1, p. 12–20, 2019.

PARRILLA, Marc et al. Wearable All-Solid-State Potentiometric Microneedle Patch for Intradermal Potassium Detection. **Analytical Chemistry**, v. 91, n. 2, p. 1578–1586, 2019.

PASCHE, Delphine et al. A new twist on sea silk: The peculiar protein ultrastructure of fan shell and pearl oyster byssus. **Soft Matter**, v. 14, n. 27, p. 5654–5664, 2018.

_____. Self-healing silk from the sea: role of helical hierarchical structure in: Pinna nobilis byssus mechanics. **Soft Matter**, v. 15, n. 47, p. 9654–9664, 2019.

PASTORE, Michael N. et al. Transdermal patches: History, development and pharmacology. **British Journal of Pharmacology**, v. 172, n. 9, p. 2179–2209, 2015.

PATRA, Jayanta Kumar et al. Nano based drug delivery systems: Recent developments and future prospects. **Journal of Nanobiotechnology**, v. 16, n. 1, p. 1–33, 2018. Disponível em: <<https://doi.org/10.1186/s12951-018-0392-8>>.

PATRAVALE, Vandana; DANDEKAR, Prajakta; JAIN, Ratnesh. Nanotoxicology: evaluating toxicity potential of drug-nanoparticles. **Nanoparticulate Drug Deliv.** [S.l: s.n.], 2012. p. 123–155.

PEARSON, Frances E. et al. Induction of CD8+ T cell responses and protective efficacy following microneedle-mediated delivery of a live adenovirus-vectored malaria vaccine. **Vaccine**, v. 33, n. 28, p. 3248–3255, 2015. Disponível em: <<http://dx.doi.org/10.1016/j.vaccine.2015.03.039>>.

- PENG, Zhiyuan; LI, Zhiping; SHEN, Yongqiang. Influence of Chemical Cross-Linking on Properties of Gelatin/Chitosan Microspheres. **Polymer-Plastics Technology and Engineering**, v. 51, n. 4, p. 381–385, 15 fev. 2012. Disponível em: <<https://doi.org/10.1080/03602559.2011.639830>>.
- PETRILLI, Raquel; LOPEZ, Renata Fonseca Vianna. Physical methods for topical skin drug delivery: Concepts and applications. **Brazilian Journal of Pharmaceutical Sciences**, v. 54, n. Special Issue, p. 1–19, 2018.
- PHAM, Thanh Chung et al. Recent Strategies to Develop Innovative Photosensitizers for Enhanced Photodynamic Therapy. **Chemical Reviews**, v. 121, n. 21, p. 13454–13619, 10 nov. 2021. Disponível em: <<https://doi.org/10.1021/acs.chemrev.1c00381>>.
- PHILIPP SEIB, F. Silk nanoparticles—an emerging anticancer nanomedicine. **AIMS Bioengineering**, v. 4, n. 2, p. 239–258, 2017.
- POLYAK, Fabian; REICH, Gabriele. Infrared spectroscopic study of the coil-helix transition of highly concentrated gelatin formulations. **European Journal of Pharmaceutics and Biopharmaceutics**, v. 140, p. 11–19, 2019. Disponível em: <<https://www.sciencedirect.com/science/article/pii/S0939641118316217>>.
- PORTER, David; VOLLRATH, Fritz. Silk as a biomimetic ideal for structural polymers. **Advanced Materials**, v. 21, n. 4, p. 487–492, 2009.
- PRAUSNITZ, Mark R; AVENUE, Andsbury; VIEW, Mountain. Microneedle-based vaccines. **Adeno Associated Virus Aav Vectors In Gene Therapy**, v. 333, n. August, p. 1–24, 2009. Disponível em: <<http://www.springerlink.com/index/10.1007/978-3-540-92165-3>>.
- PUZA, Fatih et al. Physical entanglement hydrogels: ultrahigh water content but good toughness and stretchability. **Polymer Chemistry**, v. 11, n. 13, p. 2339–2345, 2020. Disponível em: <<http://dx.doi.org/10.1039/D0PY00294A>>.
- QUINN, Helen L. et al. Design of a Dissolving Microneedle Platform for Transdermal Delivery of a Fixed-Dose Combination of Cardiovascular Drugs. **Journal of Pharmaceutical Sciences**, v. 104, n. 10, p. 3490–3500, 2015. Disponível em: <<http://dx.doi.org/10.1002/jps.24563>>.
- RAJA, Waseem K. et al. Transdermal delivery devices: Fabrication, mechanics and drug release from silk. **Small**, v. 9, n. 21, p. 3704–3713, 2013a.
- _____. Transdermal delivery devices: Fabrication, mechanics and drug release from silk. **Small**, v. 9, n. 21, p. 3704–3713, 2013b.
- RAPE, Andrew D. et al. A synthetic hydrogel for the high-throughput study of cell-ECM interactions. **Nature Communications**, v. 6, n. May, 2015.
- REJINOLD, N. Sanoj et al. Biomedical applications of microneedles in therapeutics: Recent advancements and implications in drug delivery. **Expert Opinion on Drug Delivery**, v. 13, n. 1, p. 109–131, 2016.

- RIPOLIN, Anastasia et al. Successful application of large microneedle patches by human volunteers. **International Journal of Pharmaceutics**, v. 521, n. 1–2, p. 92–101, 2017. Disponível em: <<http://dx.doi.org/10.1016/j.ijpharm.2017.02.011>>.
- ROCKWOOD, Danielle N. et al. Materials fabrication from Bombyx mori silk fibroin. **Nature Protocols**, v. 6, n. 10, p. 1612–1631, 2011.
- RODGERS, Aoife M. et al. Design and characterisation of a dissolving microneedle patch for intradermal vaccination with heat-inactivated bacteria: A proof of concept study. **International Journal of Pharmaceutics**, v. 549, n. 1–2, p. 87–95, 2018. Disponível em: <<https://doi.org/10.1016/j.ijpharm.2018.07.049>>.
- ROJAS, Jose Eduardo U. et al. Silk fibroin hydrogels for potential applications in photodynamic therapy. **Biopolymers**, v. 110, n. 2, p. e23245, 2019.
- RUBIO-HERNÁNDEZ, Francisco José et al. **Perspectives in Fundamental and Applied Rheology**. [S.l: s.n.], 2013.
- RZHEVSKIY, Alexey S et al. Microneedles as the technique of drug delivery enhancement in diverse organs and tissues. **Journal of Controlled Release**, v. 270, p. 184–202, 2018.
- SARAVANAKUMAR, K. et al. Transdermal drug delivery system: A review. **Journal of Global Trends in Pharmaceutical Sciences**, v. 6, n. 1, p. 2485–2490, 2015.
- SAROIA, Jabran et al. A review on biocompatibility nature of hydrogels with 3D printing techniques, tissue engineering application and its future prospective. **Bio-Design and Manufacturing**, v. 1, n. 4, p. 265–279, 2018. Disponível em: <<https://doi.org/10.1007/s42242-018-0029-7>>.
- SATRIALDI et al. The optimization of cancer photodynamic therapy by utilization of a pi-extended porphyrin-type photosensitizer in combination with MITO-Porter. **Chemical Communications**, v. 56, n. 7, p. 1145–1148, 2020.
- SENEL, Mehmet; DERVISEVIC, Muamer; VOELCKER, Nicolas H. Gold microneedles fabricated by casting of gold ink used for urea sensing. **Materials Letters**, v. 243, p. 50–53, 2019. Disponível em: <<https://doi.org/10.1016/j.matlet.2019.02.014>>.
- SHABBIR, Maryam et al. Influence of different formulation variables on the performance of transdermal drug delivery system containing tizanidine hydrochloride: *In vitro* and ex vivo evaluations. **Brazilian Journal of Pharmaceutical Sciences**, v. 54, n. 4, p. 1–12, 2018.
- SHAHBAZI, Mahdiyar et al. Physico-mechanical and structural characteristics of blend film of poly (vinyl alcohol) with biodegradable polymers as affected by disorder-to-order conformational transition. **Food Hydrocolloids**, v. 71, p. 259–269, 2017. Disponível em: <<https://www.sciencedirect.com/science/article/pii/S0268005X17306549>>.
- SHAOUL, Esther et al. Transdermal delivery of scopolamine by natural submicron injectors: In-vivo study in pig. **PLoS ONE**, v. 7, n. 2, p. 1–6, 2012.
- SHARMA, Sanjiv et al. A pilot study in humans of microneedle sensor arrays for continuous

glucose monitoring. **Analytical Methods**, v. 10, n. 18, p. 2088–2095, 2018.

SHARMAN, Wesley M.; ALLEN, Cynthia M.; VAN LIER, Johan E. Photodynamic therapeutics: Basic principles and clinical applications. **Drug Discovery Today**, v. 4, n. 11, p. 507–517, 1999.

SHIN, Chong In et al. Microneedles for vaccine delivery: Challenges and future perspectives. **Therapeutic Delivery**, v. 8, n. 6, p. 447–460, 2017.

SHRIKY, Bana et al. Pluronic F127 thermosensitive injectable smart hydrogels for controlled drug delivery system development. **Journal of Colloid and Interface Science**, v. 565, p. 119–130, 2020. Disponível em: <<https://doi.org/10.1016/j.jcis.2019.12.096>>.

SILVA, Simone S. et al. Fabrication and characterization of Eri silk fibers-based sponges for biomedical application. **Acta Biomaterialia**, v. 32, p. 178–189, 2016.

SINGH, Parbeen et al. Polymeric microneedles for controlled transdermal drug delivery. **Journal of Controlled Release**, v. 315, p. 97–113, 2019. Disponível em: <<https://doi.org/10.1016/j.jconrel.2019.10.022>>.

SRIHANAM, Prasong et al. Silk fibroin microspheres prepared by the water-in-oil emulsion solvent diffusion method for protein delivery. **Korean Journal of Chemical Engineering**, v. 28, n. 1, p. 293–297, 2011.

STINSON, Jordan A. et al. Silk Fibroin Microneedles for Transdermal Vaccine Delivery. **ACS Biomaterials Science and Engineering**, v. 3, n. 3, p. 360–369, 2017.

SUN, Lixin et al. Assembled small organic molecules for photodynamic therapy and photothermal therapy. **RSC Advances**, v. 11, n. 17, p. 10061–10074, 2021.

SUN, Mingyue et al. Synthesis and properties of gelatin methacryloyl (GelMA) hydrogels and their recent applications in load-bearing tissue. **Polymers**, v. 10, n. 11, 2018.

TAVSANLI, Burak; OKAY, Oguz. Mechanically robust and stretchable silk/hyaluronic acid hydrogels. **Carbohydrate Polymers**, v. 208, n. October 2018, p. 413–420, 2019. Disponível em: <<https://doi.org/10.1016/j.carbpol.2018.12.088>>.

TEO, Ai Ling et al. Transdermal microneedles for drug delivery applications. **Materials Science and Engineering B: Solid-State Materials for Advanced Technology**, v. 132, n. 1–2, p. 151–154, 2006.

THONG, H.-Y.; ZHAI, H; MAIBACH, H I. Percutaneous Penetration Enhancers: An Overview. **Skin Pharmacology and Physiology**, v. 20, n. 6, p. 272–282, 2007. Disponível em: <<https://www.karger.com/DOI/10.1159/000107575>>.

TRUCCO, Diego et al. Modeling and Fabrication of Silk Fibroin–Gelatin-Based Constructs Using Extrusion-Based Three-Dimensional Bioprinting. **ACS Biomaterials Science & Engineering**, v. 7, n. 7, p. 3306–3320, 12 jul. 2021. Disponível em: <<https://doi.org/10.1021/acsbiomaterials.1c00410>>.

- TRUCILLO, Paolo. Drug Carriers: A Review on the Most Used Mathematical Models for Drug Release. **Processes**, v. 10, n. 6, 2022.
- TSIORIS, Konstantinos et al. Fabrication of silk microneedles for controlled-release drug delivery. **Advanced Functional Materials**, v. 22, n. 2, p. 330–335, 2012.
- TSUCHIYA, Kousuke; MASUNAGA, Hiroyasu; NUMATA, Keiji. Tensile Reinforcement of Silk Films by the Addition of Telechelic-Type Polyalanine. **Biomacromolecules**, v. 18, n. 3, p. 1002–1009, 2017.
- TURNER, Joseph G. et al. Hydrogel-Forming Microneedles: Current Advancements and Future Trends. **Macromolecular Bioscience**, v. 21, n. 2, p. 1–18, 2021.
- UMUHOZA, Diane et al. Strategies for Tuning the Biodegradation of Silk Fibroin-Based Materials for Tissue Engineering Applications. **ACS Biomaterials Science and Engineering**, v. 6, n. 3, p. 1290–1310, 2020.
- VAN DER MAADEN, Koen et al. Hollow microneedle-mediated micro-injections of a liposomal HPV E743–63 synthetic long peptide vaccine for efficient induction of cytotoxic and T-helper responses. **Journal of Controlled Release**, v. 269, n. September 2017, p. 347–354, 2018. Disponível em: <<https://doi.org/10.1016/j.jconrel.2017.11.035>>.
- VARELAS, Charalambos G.; DIXON, David G.; STEINER, Carol A. Zero-order release from biphasic polymer hydrogels. **Journal of Controlled Release**, v. 34, n. 3, p. 185–192, 1995.
- VITORINO, Carla et al. Passive and active strategies for transdermal delivery using co-encapsulating nanostructured lipid carriers: *In vitro* vs. *in vivo* studies. **European Journal of Pharmaceutics and Biopharmaceutics**, v. 86, n. 2, p. 133–144, 2014. Disponível em: <<http://dx.doi.org/10.1016/j.ejpb.2013.12.004>>.
- WAGHULE, Tejashree et al. Microneedles: A smart approach and increasing potential for transdermal drug delivery system. **Biomedicine and Pharmacotherapy**, v. 109, n. July 2018, p. 1249–1258, 2019. Disponível em: <<https://doi.org/10.1016/j.biopha.2018.10.078>>.
- WANG, Hai Yan; ZHANG, Yu Qing. Processing silk hydrogel and its applications in biomedical materials. **Biotechnology Progress**, v. 31, n. 3, p. 630–640, 2015.
- WANG, Ke et al. Preparation of bacterial cellulose/silk fibroin double-network hydrogel with high mechanical strength and biocompatibility for artificial cartilage. **Cellulose**, v. 27, n. 4, p. 1845–1852, 2020. Disponível em: <<https://doi.org/10.1007/s10570-019-02869-0>>.
- WANG, Min et al. Inorganic Nanoparticles for Transdermal Drug Delivery and Topical Application. **Nanoscience in Dermatology**, p. 57–72, 2016.
- WANG, Qi Lei et al. Microneedles with controlled bubble sizes and drug distributions for efficient transdermal drug delivery. **Scientific Reports**, v. 6, p. 1–11, 2016. Disponível em: <<http://dx.doi.org/10.1038/srep38755>>.
- WANG, Shiyi et al. Insulin-Loaded Silk Fibroin Microneedles as Sustained Release System.

ACS Biomaterials Science and Engineering, v. 5, n. 4, p. 1887–1894, 2019.

WANG, Yuzhen et al. Tailoring bioinks of extrusion-based bioprinting for cutaneous wound healing. **Bioactive Materials**, v. 17, n. January, p. 178–194, 2022. Disponível em: <<https://doi.org/10.1016/j.bioactmat.2022.01.024>>.

WEI, Liang et al. 3D printing of silk fibroin-based hybrid scaffold treated with platelet rich plasma for bone tissue engineering. **Bioactive Materials**, v. 4, n. September 2019, p. 256–260, 2019.

WENK, Esther; MERKLE, Hans P.; MEINEL, Lorenz. Silk fibroin as a vehicle for drug delivery applications. **Journal of Controlled Release**, v. 150, n. 2, p. 128–141, 2011.

WILSON, Donna; VALLUZZI, Regina; KAPLAN, David. Conformational transitions model silk peptides. **Biophysical Journal**, v. 78, n. 5, p. 2690–2701, 2000.

WISOTZKI, Emilia I et al. Influence of high energy electron irradiation on the network structure of gelatin hydrogels as investigated by small-angle X-ray scattering (SAXS). **Physical Chemistry Chemical Physics**, v. 19, n. 19, p. 12064–12074, 2017. Disponível em: <<http://dx.doi.org/10.1039/C7CP00195A>>.

WRAY, Lindsay S et al. Effect of processing on silk-based biomaterials: reproducibility and biocompatibility. **Journal of biomedical materials research. Part B, Applied biomaterials**, v. 99, n. 1, p. 89–101, out. 2011.

WU, Iren Yeeling et al. Interpreting non-linear drug diffusion data: Utilizing Korsmeyer-Peppas model to study drug release from liposomes. **European Journal of Pharmaceutical Sciences**, v. 138, p. 105026, 2019. Disponível em: <<https://www.sciencedirect.com/science/article/pii/S0928098719302908>>.

WU, Puyuan et al. Novel silk fibroin nanoparticles incorporated silk fibroin hydrogel for inhibition of cancer stem cells and tumor growth. **International Journal of Nanomedicine**, v. 13, p. 5405–5418, 2018.

XIE, Huixu et al. Biocompatibility and safety evaluation of a silk fibroin-doped calcium polyphosphate scaffold copolymer: *In vitro* and *in vivo*. **RSC Advances**, v. 7, n. 73, p. 46036–46044, 2017.

XING, Jin-Feng; ZHENG, Mei-Ling; DUAN, Xuan-Ming. Two-photon polymerization microfabrication of hydrogels: an advanced 3D printing technology for tissue engineering and drug delivery. **Chemical Society Reviews**, v. 44, n. 15, p. 5031–5039, 2015. Disponível em: <<http://dx.doi.org/10.1039/C5CS00278H>>.

XU, Long et al. A Reactive Oxygen Species (ROS)-Responsive Low Molecular Weight Gel Co-Loaded with Doxorubicin and Zn(II) Phthalocyanine Tetrasulfonic Acid for Combined Chemo-Photodynamic Therapy. **Journal of Materials Chemistry. B**, v. 5, n. 46, p. 9157–9164, dez. 2017.

XU, Zongpu et al. Preparation and biomedical applications of silk fibroin-nanoparticles

composites with enhanced properties - A review. **Materials Science and Engineering C**, v. 95, n. November 2018, p. 302–311, 2019. Disponível em: <<https://doi.org/10.1016/j.msec.2018.11.010>>.

YANG, Jian et al. Recent advances of microneedles for biomedical applications: drug delivery and beyond. **Acta Pharmaceutica Sinica B**, v. 9, n. 3, p. 469–483, 2019. Disponível em: <<https://doi.org/10.1016/j.apsb.2019.03.007>>.

YANG, Sixing et al. A scalable fabrication process of polymer microneedles. **International Journal of Nanomedicine**, v. 7, p. 1415–1422, 2012.

YANG, Zhe et al. Rheological Behaviors of PVA/H₂O Solutions of High-Polymer Concentration. **Journal of Applied Polymer Science**, v. 116, n. 5, p. 2658–2667, 2010.

YEH, Mei Yu et al. Reverse thermo-responsive hydrogels prepared from Pluronic F127 and gelatin composite materials. **RSC Advances**, v. 7, n. 34, p. 21252–21257, 2017.

YOU, Sung Kyun et al. Effect of applying modes of the polymer microneedle-roller on the permeation of L-ascorbic acid in rats. **Journal of Drug Targeting**, v. 18, n. 1, p. 15–20, 2010.

YOU, Xueqiu; PAK, James Jungho; CHANG, Jong Hyeon. Rapidly dissolving silk protein microneedles for transdermal drug delivery. **2010 IEEE International Conference on Nano/Molecular Medicine and Engineering, IEEE NANOMED 2010**, p. 144–147, 2010.

YOU, Zhengying et al. Extraordinary Mechanical Properties of Composite Silk Through Hereditary Transgenic Silkworm Expressing Recombinant Major Ampullate Spidroin. **Scientific Reports**, v. 8, n. 1, p. 1–14, 2018. Disponível em: <<http://dx.doi.org/10.1038/s41598-018-34150-y>>.

YOUN, Jina et al. Pluronic f-127/silk fibroin for enhanced mechanical property and sustained release drug for tissue engineering biomaterial. **Materials**, v. 14, n. 5, p. 1–11, 2021.

YU, Jicheng et al. Glucose-responsive insulin patch for the regulation of blood glucose in mice and minipigs. **Nature Biomedical Engineering**, 2020. Disponível em: <<http://dx.doi.org/10.1038/s41551-019-0508-y>>.

YU, Weijiang et al. Fabrication of biodegradable composite microneedles based on calcium sulfate and gelatin for transdermal delivery of insulin. **Materials Science and Engineering C**, v. 71, p. 725–734, 2017. Disponível em: <<http://dx.doi.org/10.1016/j.msec.2016.10.063>>.

Z.Z. ZHENG, M. LIUB, S.Z. GUOA, J.B. WUA, D.S. LUD, G. LIA, S.S. LIUA, X.Q. WANGA, and D. L. Kaplan. Incorporation of quantum dots in silk biomaterials for fluorescence imaging. **Physiology & behavior**, v. 21, n. 3, p. 6509–6519, 2016.

ZAHARIA, C. et al. Silk fibroin films for tissue bioengineering applications. **Journal of Optoelectronics and Advanced Materials**, v. 14, n. 1–2, p. 163–168, 2012.

ZHANG, Junmei et al. Facile fabrication of tough photocrosslinked polyvinyl alcohol hydrogels with cellulose nanofibrils reinforcement. **Polymer**, v. 173, n. April, p. 103–109, 2019. Disponível em: <<https://doi.org/10.1016/j.polymer.2019.04.028>>.

ZHANG, Suohui; QIU, Yuqin; GAO, Yunhua. Enhanced delivery of hydrophilic peptides *in vitro* by transdermal microneedle pretreatment. **Acta Pharmaceutica Sinica B**, v. 4, n. 1, p. 100–104, 2014. Disponível em: <<http://dx.doi.org/10.1016/j.apsb.2013.12.011>>.

ZHANG, Xin; PAN, Zhijuan. Rheological behavior of regenerated silk fibroin / polyvinyl alcohol blended solutions in steady and dynamic state and the effect of temperature. **Journal of Materials Science**, v. 55, n. 31, p. 15350–15363, 2020. Disponível em: <<https://doi.org/10.1007/s10853-020-05086-4>>.

ZHAO, Liang et al. Silk/polyols/GOD microneedle based electrochemical biosensor for continuous glucose monitoring. **RSC Advances**, v. 10, n. 11, p. 6163–6171, 2020.

ZHAO, Xueze et al. Recent progress in photosensitizers for overcoming the challenges of photodynamic therapy: from molecular design to application. **Chemical Society Reviews**, v. 50, n. 6, p. 4185–4219, 2021. Disponível em: <<http://dx.doi.org/10.1039/D0CS00173B>>.

ZHOU, Cui Ping et al. Transdermal delivery of insulin using microneedle rollers *in vivo*. **International Journal of Pharmaceutics**, v. 392, n. 1–2, p. 127–133, 2010. Disponível em: <<http://dx.doi.org/10.1016/j.ijpharm.2010.03.041>>.

ZHU, Mingmei et al. Combined Silk Fibroin Microneedles for Insulin Delivery. **ACS Biomaterials Science & Engineering**, v. 6, n. 6, p. 3422–3429, 2020.

ZOREC, Barbara et al. Active enhancement methods for intra- and transdermal drug delivery: A review. **Zdravniški Vestnik**, v. 82, n. 5, p. 339–356, 2013.